ANISOTROPIC FRACTURE ANALYSIS OF THE BX-265 FOAM INSULATION MATERIAL UNDER MIXED-MODE LOADING

By

ERIK KNUDSEN

A DISSERTATION PRESENTED TO THE GRADUATE SCHOOL
OF THE UNIVERSITY OF FLORIDA IN PARTIAL FULFILLMENT
OF THE REQUIREMENTS FOR THE DEGREE OF
DOCTOR OF PHILOSOPHY

UNIVERSITY OF FLORIDA

2006

This thesis is dedicated to my parents, friends, family, lab mates and everyone else who was there for me when I needed them the most. I will never forget you!

ACKNOWLEDGMENTS

First and foremost I would like to thank my parents for their unwavering love and support. My advisor, Dr. Nagaraj Arakere, has been in my corner since I first came to graduate school and his contacts at NASA paved the way for the two degrees I now hold in engineering. In the summer of 2002 I accompanied Dr. Arakere to Huntsville as part of the Summer Faculty Fellowship Program. During our ten week stay, I met many experts and scientists who work at Marshall, particularly Dr. Greg Swanson, Jeff Rayburn, Greg Duke, Dr. Gilda Battista, Stan Oliver, Preston McGill, Doug Wells, Dr. Eric Poole, Dr. Philip Allen and Denise Duncan (in a later trip), and many, many others. They have helped me grow as a student and a person, and I am forever indebted.

After my trip to NASA, approximately one year later, I earned a NASA Fellowship to sponsor this work. Ed Adams of the Education Directorate at Marshall deserves special praise here, and I thank him for blessing me with the opportunity to, once more, work with NASA. I shared an on office Dr. Philip Allen and one could not ask for a more pleasant person to work with and learn from.

The Cornell Fracture Group was also a tremendous help in my quest to better understand and learn the principles of fracture mechanics. Drs. Paul "Wash" Wawryznek and Bruce Carter are two of the nicest and most patient people I have ever known and I owe them many thanks for taking the time to help me.

Last, but certainly not least, I wish to thank my labmates over the years: Srikant, Sangeet, Shadab, Niraj, Shannon, Yogen, Jeff, TJ, and George. Without their insight,

jokes, and patience I would not be where I am today. I now consider many of them to be my best friends and I hope we can stay in touch.

TABLE OF CONTENTS

LIST OF TABLES

LIST OF FIGURES

Abstract of Dissertation Presented to the Graduate School
of the University of Florida in Partial Fulfillment of the
Requirements for the Degree of Doctor of Philosophy

ANISOTROPIC FRACTURE ANALYSIS OF THE BX-265 FOAM INSULATION MATERIAL UNDER MIXED-MODE LOADING

By

Erik Knudsen

August 2006

Chair: Nagaraj K. Arakere
Major Department: Mechanical and Aerospace Engineering

The National Aeronautics and Space Administration (NASA) uses a closed-cell polyurethane foam to insulate the external tank (ET) which contains the liquid oxygen and hydrogen for the Space Shuttle main engines. This is a type of spray-on foam insulation (SOFI), similar to the material used to insulate attics in residential construction. In February of 2003, the Shuttle *Columbia* suffered a catastrophic accident during re-entry. Debris from the ET impacting the Shuttle's thermal protection tiles during liftoff is believed to have caused the Space Shuttle *Columbia* failure during re-entry.

NASA engineers are very interested in understanding the processes that govern the breakup/fracture of this complex material from the shuttle ET. The foam is anisotropic in nature and the required stress and fracture mechanics analysis must include the effects of the direction dependence on material properties. Over smooth, flat areas of the ET the foam can be sprayed down in a very uniform fashion. However, near bolts and fitting

points it is possible for voids and other defects to be present after the foam is applied. Also, the orientation of the foam, as it rises from non-uniform surfaces, can be significantly different from the orientation over typical acreage sprays. NASA believes that air present in these small voids is liquefied and then turned into a gas during liftoff. While the Shuttle is ascending to space, the pressure in these cavities can become large enough to force a subsurface crack toward the exterior of the tank, thus freeing portions of foam insulation.

As a first step toward understanding the fracture mechanics of this complex material, a general theoretical and numerical framework is presented for computing stress intensity factors (SIFs), under mixed-mode loading conditions, taking into account the material anisotropy. The effects of material orientation and mode mixity on the anisotropic SIF solution are analyzed. Crack turning predictions under mixed mode loading are presented. Furthermore, the influence of temperature gradients on the SIF solution is studied, in view of the thermal gradient present through the foam thickness on the ET. The results presented represent a quantitative basis for evaluating the strength and fracture properties of anisotropic BX-265 foam insulation material.

CHAPTER 1
BACKGROUND

Problem Motivation

On February 1st, 2003, the Space Shuttle *Columbia* suffered a catastrophic failure during re-entry. NASA has conducted an exhaustive investigation of the failure and the consensus now is the breakup was caused by a segment of BX-265 foam insulation, roughly the size of a suitcase, striking the wing during liftoff. The foam impact, in prior Shuttle launches, has been known to cause impact damage to the thermal protection tiles, but was not considered to be a serious problem until the Columbia disaster. The damage to the thermal protection tiles on the leading edge of the wing is thought to have allowed gases to penetrate the wing during re-entry, triggering a cascading series of catastrophic events that led to the loss of the Shuttle.

It is believed that when the foam insulation is applied to the external tank (ET) that voids are created in certain areas where geometric discontinuities such as bolts, flanges, and fittings are encountered. Since the tank is filled with liquid oxygen and hydrogen the foam is exposed to cryogenic temperatures at the ET's surface. The air inside these voids can be liquefied and nitrogen can condense into these small cavities. During liftoff the outer surface of the foam is exposed to aerodynamic heating. This heating raises the temperature of the liquid nitrogen, turning it into a gas. The pressure difference associated with the formation of the gas can cause pieces of foam to be blown out during liftoff(see Figure1-1).

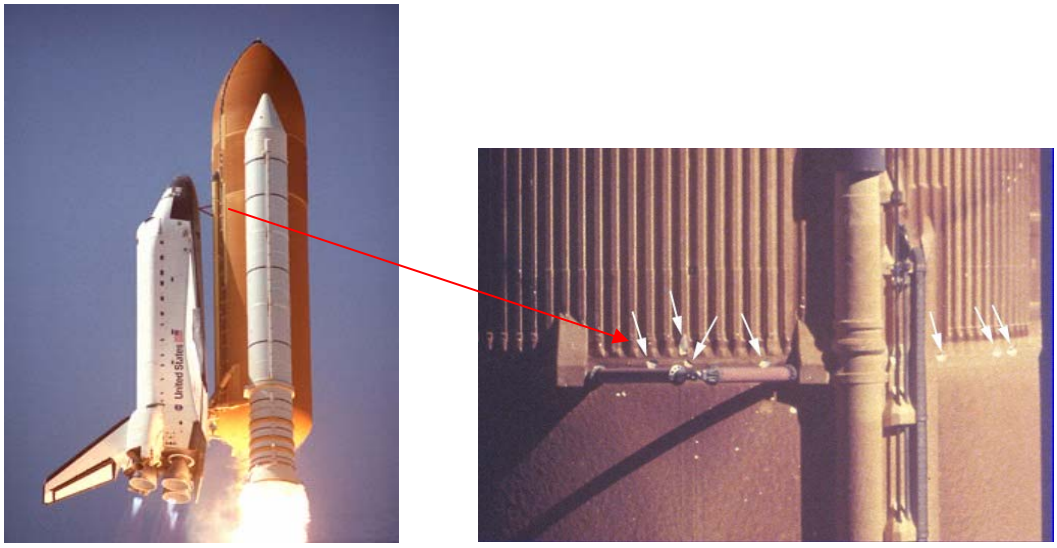

Figure1-1. Foam loss during Shuttle ascension

Program Scope and Focus

Prior to the Columbia disaster, the foam that insulates the tank was not understood at a fundamental level. Quantities like the elastic moduli, and thermal properties such as coefficient of thermal expansion are needed for a meaningful failure analysis of this material. This prompted NASA to initiate an intensive testing program to ascertain various properties at cryogenic, room, and elevated temperatures. The pictures in Figure 1-1 show the foam breaking off areas near fitting points. At these locations, insulation is sprayed around various parts, such as bolts, and it is here that the foam's orientation, relative to the tank, can change by quite a bit. For typical acreage sprays, there is very little difference between the local coordinate axes of the foam and those of the substrate (Figure 1-2).

Pictures of the Shuttle during liftoff, such as those shown in Figure 1-1, show us that large pieces of foam are not really breaking away over smooth, open, areas of the tank. The problem seems to be confined to areas where the foam is applied over fitting points, bolts, and other areas where various parts can protrude the surface of the ET.

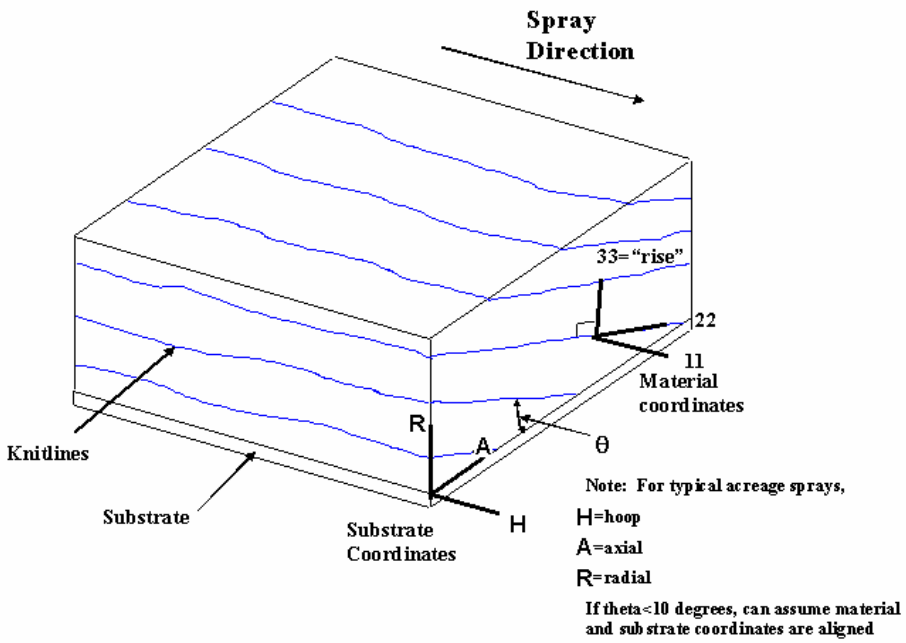

Figure 1-2. Spray-on foam insulation (SOFI)

Right away we notice that two potential problems come to mind at these locations: it is possible for voids to be created when the foam is being laid down, and the orientation of the foam can change by a large degree.

The material tests conducted by NASA have shown that this type of foam is brittle. Perhaps the best way to analyze sharp, crack-like, defects for this sort of material is through linear elastic fracture mechanics (LEFM). For isotropic materials, the near-tip stresses are completely characterized by K—the stress intensity factor (SIF). The analytical K-solutions for anisotropic materials take a similar form, but have additional terms that come from the various elastic moduli. The formulations of near-tip stresses for isotropic materials are well established and are now incorporated in many finite element (FE) software packages. Some K-solutions for certain kinds of direction-dependent materials started appearing in the 1960s and more generalized solutions were presented in the 1980s. Since many engineering materials are not isotropic (such as rolled aluminum

in aircraft fuselages and single-crystal superalloys used in high performance gas turbine engines), more attention is being paid toward the implementation of anisotropic K-solutions in various FE schemes. Still, many of the most popular FE software packages do not allow accurate computations of SIFs for simulations involving anisotropic materials.

Foams are inherently anisotropic, and NASA, after extensive testing, has classified this material as transversely isotropic. Such materials also have fracture characteristics that are direction dependent and both of these traits must be accounted for in the analytical and numerical analyses. Although anisotropic K-solutions are not readily available, the Cornell Fracture Group has developed a software package, FRANC3D, that simplifies the meshing process necessary for FE modeling of crack-like defects in elastic solids and also computes a K-solution for anisotropic materials. Concurrently, an alternative method for computing the SIFs, based on the work of Hoenig (1982), for anisotropic materials has been employed and extended to account for thermal stresses and strains.

It is hoped that the present study will enhance NASA's understanding of this material, since the K-solutions used in this analysis account for both the direction-dependent properties and the impact of thermal stresses and strains. The following points summarize the scope of this study in a broad sense:

1. Through the use of the middle tension, M(T), specimen and the FE method a systematic rotation of material properties and its impact on the K-solution is examined
2. The impact of mode mixity on the K-solution is studied
3. Crack turning predictions that take into account both the anisotropic stiffness and fracture properties are presented

4. The effect of a thermal gradient through the M(T) specimen and its impact on the K-solution are presented

CHAPTER 2
FOAM TESTING AND MATERIAL CLASSIFICATION

Cellular Solid Background Information

Cellular solids are generally comprised into two sets of structural categories: 1) honeycomb layouts where the microstructure is comprised of two-dimensional arrays of polygons that fill a planar area and 2) foams, the three-dimensional counterpart to honeycombs where the cells take the form of polyhedra. Within Gibson and Ashby's (1988) definitive text on cellular solids, we see how many types of materials can be foamed: metals, glasses, and ceramics can be fabricated into cells that take on a variety of shapes and sizes. Among the most common types of foam are polymers which are used for many applications including insulation for residential homes or disposable coffee cups. Polymer foams are usually very light and they are popular in industries where weight is of prime importance, such as in the aerospace industry.

Foams are typically made by bubbling a gas into the liquid monomer or hot polymer. The gas can be introduced mechanically by stirring or by using a blowing agent. Physical blowing agents are normally gases like nitrogen or carbon dioxide. Chemical blowing agents are special additives that decompose when they are heated or react in such a fashion where gas is released. The bubbles grow and eventually settle and then, as the liquid is cooling down, become solid.

In general, polymer foams have considerably lower strength and density than solid metals. However, their low thermal conductivity coupled with their much lighter weight

make them an ideal insulator for the ET. Table 2-1 (Gibson and Ashby, 1988) lists several properties of polymer foams and true solids (solid metals and ceramics).

Table 2-1. Properties of solids and polymer foams

	Density (lb/in^3)	Conductivity (BTU/hr in F)	Young's modulus (psi)
Solids	$3.6 \times 10^{-2} – 3.6 \times 10^{-1}$	$4.8 \times 10^{-3} – 48$	$3 – 30 \times 10^{6}$
Polymer foams	3.6×10^{-4}	4.8×10^{-3}	3×10^{3}

Initial Foam Material Testing

The Columbia disaster forced NASA and all those associated with the application of the foam insulation material to the ET to see it in an entirely different light. Numerous tests were conducted at cryogenic, room, and elevated temperatures to ascertain the properties of this material. In addition to standard torsion and tension tests to obtain the elastic moduli, various tests were performed to evaluate the failure characteristics, such as the plane strain fracture toughness, KI_c. While these tests are an important first step in understanding how the foam behaves on a fundamental level, NASA also took extra steps to examine how the foam sheds from the tank through a specialized test covered in a later section.

Determination of Elastic Constants and Material Classification

Some of the initial work toward understanding the mechanical properties of foams took places in the 1960s and 1970s. Gent and Thomas (1959), and Patel and Finnie (1970) among others were among the first to explore the properties of cellular materials. The model developed by Gibson and Ashby (1982), however, is perhaps the most widely accepted way to analyze the properties of cellular solids. Their analysis is rooted in a unit cell comprised of a network of interconnected struts (Figure 2-1) The equations that arise from this mathematical treatment are in terms of the strut dimensions, which in turn

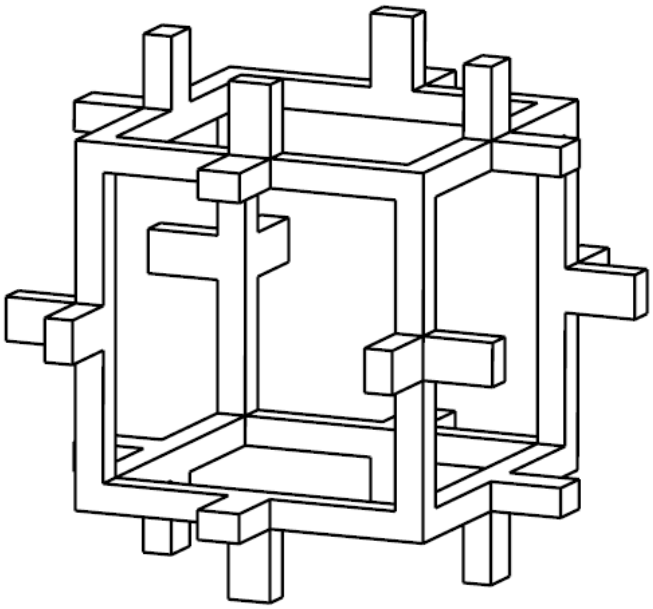

Figure 2-1: Idealized foam microstructure

allow some material properties to be related to the *relative density*. The relative density is the density of cellular material, ρ^*, divided by the density of the solid from which the cell walls are made, ρ_s.

Generally, foams can be divided into two main categories: those with *open* or *closed* cells. By closed we mean materials where each cell is partitioned from its neighbor by membrane-like faces. Within open-celled structures the individual members, struts say, are individually connected. With Gibson and Ashby's (1982) model, many of the equations that determine various properties, such as the elastic moduli or the fracture toughness are derived considering the configuration of the cell walls.

Understanding the mechanical and metallurgical aspects of these struts at a microscopic level is very important. After all, it is these struts that transmit the applied mechanical loads and transfer heat energy. But from a practical standpoint, models that contain these microscopic parameters are not very useful to the engineering community. The engineer may not have access to the equipment and facilities necessary to measure

things like cell wall thickness. Generally, the analyst, or engineer, may only be privy to a quantity like the relative density. This parameter is one of the most important, and useful, concepts that help define and understand the properties of cellular materials. The relative density can be related to the dimensions of the cell walls. For honeycombs we have

$$\frac{\rho^*}{\rho_s} = C_1 \frac{t}{l} \tag{2-1}$$

where t is the cell wall thickness and the l is the edge-length. For open-cell foams

$$\frac{\rho^*}{\rho_s} = C_2 \left(\frac{t}{l} \right)^2 \tag{2-2}$$

Finally, for the foams of the closed-cell variety we have

$$\frac{\rho^*}{\rho_s} = C_3 \frac{t}{l} \tag{2-3}$$

The *C* terms are numerical constants that depend on the cell shape, normally taking a value of unity.

As mentioned beforehand, certain open-celled foams can be modeled as a network of beams. Using an idealized array of connected beams, the theory in many solid mechanics texts such as Timoshenko and Goodier (1982) is adequate to determine the deflections, strains, and stresses. It can be shown that the Young's modulus for the open-celled foam is given by

$$E^* = \frac{\sigma}{\varepsilon} = \frac{C_1 E_s I}{l^4} \tag{2-4}$$

where E^* is the modulus of the foam material. The relative density is related to the dimensions, t and l as shown in (2-2). The second moment of the area, *I*, can also be related to the cell wall dimensions

$$I \propto t^4 \tag{2-5}$$

Now (2-4) can be re-written as

$$\frac{E^*}{E_s} = C_1 \left(\frac{\rho^*}{\rho_s} \right)^2 \tag{2-6}$$

Using the same reasoning, we can write down the relationship for the shear moduli

$$\frac{\mu^*}{E_s} = C_2 \left(\frac{\rho^*}{\rho_s} \right)^2 \tag{2-7}$$

Lastly, we need ν*, the Poisson ratio, which is defined as the ratio between the lateral and axial strains. The strains are proportional to the bending deflection and their ratio is constant. Thus, ν* depends only on the cell wall geometry. We can show this for isotropic foams where μ_s, the shear modulus is

$$\mu_s = \frac{E}{2(1+\nu)} \tag{2-8}$$

Using (2-8) along with (2-6) and (2-7) we have

$$\nu^* = \frac{C_1}{2C_2} - 1 = C_3 \tag{2-9}$$

The above analysis is for open-celled foams. When examining closed-cell foams, the derivations are more complex because most foams are made from a liquid and surface tension draws the material to the edges which might leave only thin membrane across the cell. For sufficiently thin membranes, the open-celled formulas can be applied. But if an appreciable quantity of foam is present in these membranes, the amount, or fraction, of this material contributes to the stiffness. There are three potential contributions that sum to the total stiffness of a closed-cell material. The aforementioned cell walls make a contribution when they are stretched. The second contribution is present due to a fluid,

usually air, trapped within the cells, and finally the cell walls, and beams, can also be bent when a load is applied.

The contribution from the stretching is derived by considering how the applied load bends and stretches the cell face. The cell edge bending is proportional to $\frac{1}{2}S\delta^2$ where S is the stiffness of the cell edge, and $S \propto E_s I/l^3$, and δ is the displacement that arises from the applied load. The contribution from the stretching of the face is proportional to $\frac{1}{2}E_s\varepsilon 2V_f$. The V_f term is the volume of solid in the cell face and $\varepsilon \propto \delta/l$ and $V_f \propto l^2 t_f$. The thickness of the edges and faces are denoted as t_e and t_f, respectively. In the linear-elastic regime, we can define the work done by the applied force as

$$\frac{1}{2}F\delta = \frac{\alpha E_s I \delta^2}{l^3} + \beta E_s \left(\frac{\delta}{l}\right) l^2 t_f \tag{2-10}$$

Equation (2-10) can be re-written when we note that $I \propto t_e^4$ and $E^* \propto (F/l^2)/(\delta/l)$ which yields

$$\frac{E^*}{E_s} = \alpha' \frac{t_e^{\,4}}{l^4} + \beta' \frac{t_f}{l} \tag{2-11}$$

For many foams the edge and face thickness is related to the relative density by the following empirical relations

$$\frac{t_f}{l} = 1.4(1-\phi)\frac{\rho^*}{\rho_s}$$
$$\frac{t_e}{l} = 0.93\phi^{1/2}\left(\frac{\rho^*}{\rho_s}\right)^{1/2} \tag{2-12}$$

If we substitute (2-12) into (2-11) we obtain the ratio of the elastic moduli in terms of the relative density and volume fraction of material in the cell edges is ϕ

$$\frac{E^*}{E_s} = C_1\phi^2\left(\frac{\rho^*}{\rho_s}\right) + C_1'(1-\phi)\frac{\rho^*}{\rho_s} \tag{2-13}$$

where α, β, α', β', C_1, and C_1'are all constants of proportionality. The above equations take care of the contribution from the stretching of the cell walls. The next contribution comes from accounting for the fluid trapped in the cell walls, E^*_g. From Gent and Thomas (1963) we have

$$E^*_g = \frac{p_0(1-2\nu^*)}{\left(1-\frac{\rho^*}{\rho_s}\right)} \tag{2-14}$$

where p_0 is the initial gas pressure. Gibson and Ashby (1988) note that if this pressure happens to be equal to the atmospheric pressure, this contribution is small. Lastly, shear modulus for the closed-cell foam is shown below

$$\frac{G^*}{E_s} = C_2\phi^2\left(\frac{\rho^*}{\rho_s}\right) + C_2'(1-\phi)\frac{\rho^*}{\rho_s} \tag{2-15}$$

Finally the last contribution to consider comes from the bending on the cell struts, and that analysis is identical to the open-celled formulation presented earlier.

We note that the above relations are for foams where the cell walls are equiaxed. Most man-made foams are anisotropic. When this particular foam is sprayed down, foaming agents cause it to rise and the cells are stretched in the rise direction. Cell shape, then, can significantly impact the material properties. The shape anisotropy ratio, R, is

$$R_{12} = \frac{\bar{L}_1}{\bar{L}_2}$$
$$R_{13} = \frac{\bar{L}_1}{\bar{L}_3} \tag{2-16}$$

where $\bar{L}_1$, $\bar{L}_2$, and, $\bar{L}_3$ are the lengths of principal cell dimensions and $\bar{L}_1$ is the largest of the three. Following a similar analysis for the bending stresses within the beams for the isotropic lattice Gibson and Ashby (1988) go onto define a quantity called the Young's modulus anisotropy ratio for open-celled foams as

$$\frac{E^*_3}{E^*_1} = \frac{2R^2}{(1+(1/R)^3)} \tag{2-17}$$

For closed cells an additional term $(1-\phi)\frac{2R}{1+(1/R)}$ appears in (2-17). For the anisotropic shear modulus, we have

$$\frac{G^*_{31}}{G^*_{12}} = \frac{2}{1+R} \tag{2-18}$$

The Poisson ratio is once again the ratio of lateral and normal strains and, just like in the equiaxed case, is independent of the relative density. As such this elastic constant is dependent solely on the cell geometry. Unfortunately, for the anisotropic foams, employing the same type of dimensional analysis used to determine the elastic moduli for the Poisson ratio will not offer any insight into its dependence on cell wall geometry and Gibson and Ashby (1988) do not discuss this in their text.

So there appear to be two ways to try and determine the properties of the foam insulation material. The properties can be estimated using the relative density and shape anisotropy ratio or they can be experimentally evaluated. The BX-265 foam contains closed cells, so the equations presented earlier for this particular cell wall geometry along with corrections necessary to account for the anisotropy could be utilized for evaluating various material properties in terms of the relative density.

Evaluating the all-important relative density, though, may not be as straightforward as it seems. While it is not difficult to measure the density of the foamed material (one simply weighs the sample and divide it by the measured volume), getting a handle on the un-foamed density for this particular kind of polyurethane foam is not so simple unless the exact same foam is available in the literature somewhere. Also, when NASA was preparing various foam test panels (from which the test specimens are machined) they determined the density could vary within the specimen. Also, there are several ways in which the insulation can be sprayed down. The foam can be applied via a mechanical process where a machine sprays it down, or it is laid down by hand using special equipment that delivers the insulation to the testing surface (normally an aluminum plate).

Thus, since the density could change throughout the test panel, and even vary depending on the process by which it is sprayed, NASA developed a test program where a vast database of information was to be established for this particular foam material. It was decided that standard test procedures for evaluating both elastic properties and fracture response were to be employed, instead of estimating the properties based on relations that require the relative density to be known beforehand.

Figures 2-2 and 2-3 display some of the various test specimens used in various tension and torsion tests. A summary of typical stress-strain data is shown in Figure 2-4. Within this chart the results of several tests performed with different foam orientations (denoted as local rise, spray, and axial) at a few temperatures (RT denotes room temperature and LN2 is the temperature of liquid nitrogen).

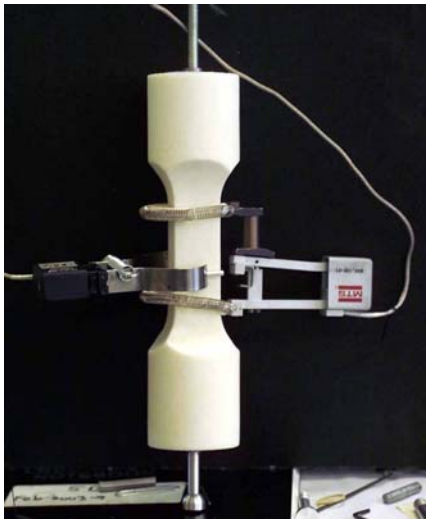

Figure 2-2. Square specimen tensile test used to determine the Poisson ratio

As expected the colder the temperature, the more ‘stiff’ the foam becomes and in general the foam fractures with little deformation. It should be pointed out that the foam is not a material that behaves exactly like a generic isotropic steel alloy. Most engineering

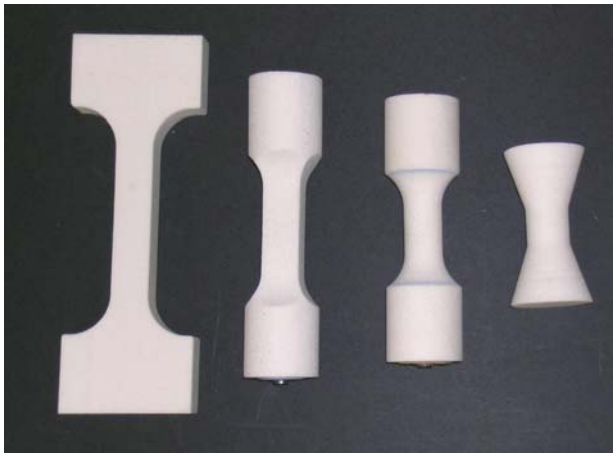

Figure 2-3. Foam test specimens

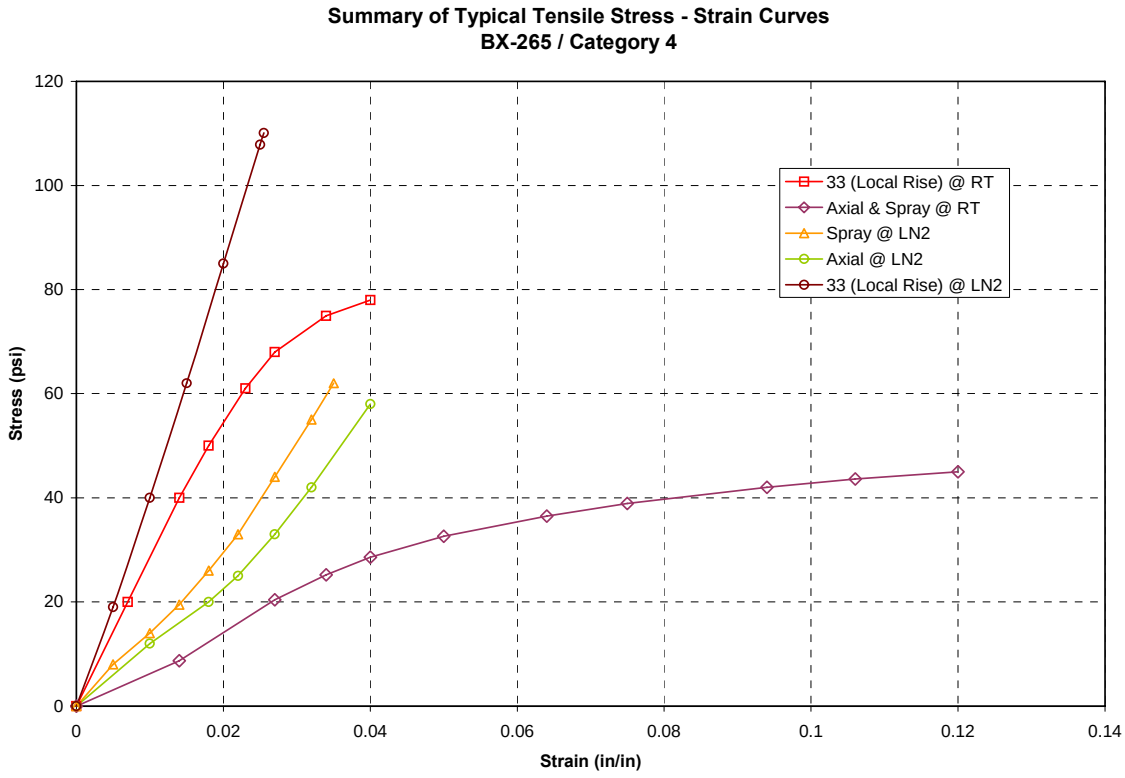

Figure 2-4. Summary of stress-strain data †

metals, when placed in a uniaxial tension test, have a linear relationship between stress and strain up until the yield point. Cellular materials generally have a non-linear relationship between stress and strain and the constitutive relations defined in this chapter assume that this material has a linear stress strain relationship because a model that accurately describes the response for foam has not yet been developed.

The aforementioned tension and torsion tests have led NASA to classify the foam as a transversely isotropic material. These materials are sometimes called hexagonal materials and five independent elastic constants relate the stresses to the strains in the constitutive matrix. The 11-22 plane in Figure 2-5 is a plane of isotropy.

† Source: personal communication, Doug Wells (MSFC)

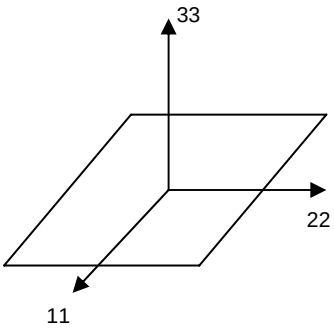

Figure 2-5. Coordinate system for the transversely isotropic material

Using the coordinate axes from Figure 2-4 we can define the constitutive relations for a transversely isotropic material. The Young's moduli in the 11 and 22 directions are defined as being equal as are the shear moduli in the 33, or rise, direction. The other shear modulus, G_{12}, is determined through a relation with E_{11} and ν_{12}: $G_{12} = 2(1+\nu_{12})/E_{11}$. Table 2-1 lists the room temperature values of the elastic constants for the orientation shown in Figure 2-5.

Since one of the objectives of this study is to analyze the effect of temperature, or thermal loads, on the K-solution the material properties at various temperatures are needed for a meaningful analysis. NASA evaluated the foam's elastic moduli, thermal conductivity, and coefficient of thermal expansion.

$$\begin{Bmatrix} \varepsilon_{11} \\ \varepsilon_{22} \\ \varepsilon_{33} \\ \gamma_{23} \\ \gamma_{13} \\ \gamma_{12} \end{Bmatrix} = \begin{bmatrix} \frac{1}{E_1} & \frac{-\nu_{12}}{E_2} & \frac{-\nu_{13}}{E_3} & 0 & 0 & 0 \\ \frac{-\nu_{21}}{E_1} & \frac{1}{E_2} & \frac{-\nu_{23}}{E_3} & 0 & 0 & 0 \\ \frac{-\nu_{31}}{E_1} & \frac{-\nu_{32}}{E_2} & \frac{1}{E_3} & 0 & 0 & 0 \\ 0 & 0 & 0 & \frac{1}{G_{23}} & 0 & 0 \\ 0 & 0 & 0 & 0 & \frac{1}{G_{13}} & 0 \\ 0 & 0 & 0 & 0 & 0 & \frac{1}{G_{12}} \end{bmatrix} \begin{Bmatrix} \sigma_{11} \\ \sigma_{22} \\ \sigma_{33} \\ \sigma_{23} \\ \sigma_{13} \\ \sigma_{12} \end{Bmatrix} \tag{2-19}$$

where the five independent elastic constants are

$$E_{11} = E_{22}; E_{33}$$
$$G_{23} = G_{13} \qquad (2\text{-}20)$$
$$\frac{\nu_{13}}{E_3} = \frac{\nu_{31}}{E_1}, \nu_{12} = \nu_{21}$$

Table 2-1. Measured material property values from experiment

E_{11} = 950 psi	ν_{12} = 0.45	G_{12} = 328 psi
E_{22} = 950 psi	ν_{31} = 0.3	G_{23} = 231 psi
E_{33} = 2400 psi	ν_{13} = 0.3	G_{31} = 231 psi

These values are plotted in Figures 2-6 through 2-9. The tests performed by NASA indicated that the Poisson ratios did not vary substantially with temperature. As of this writing, only one value for k, the thermal conductivity, is available. It is possible for that value to vary with direction as well as temperature. It will be assumed, however, that k is 'isotropic,' or has no direction dependency.

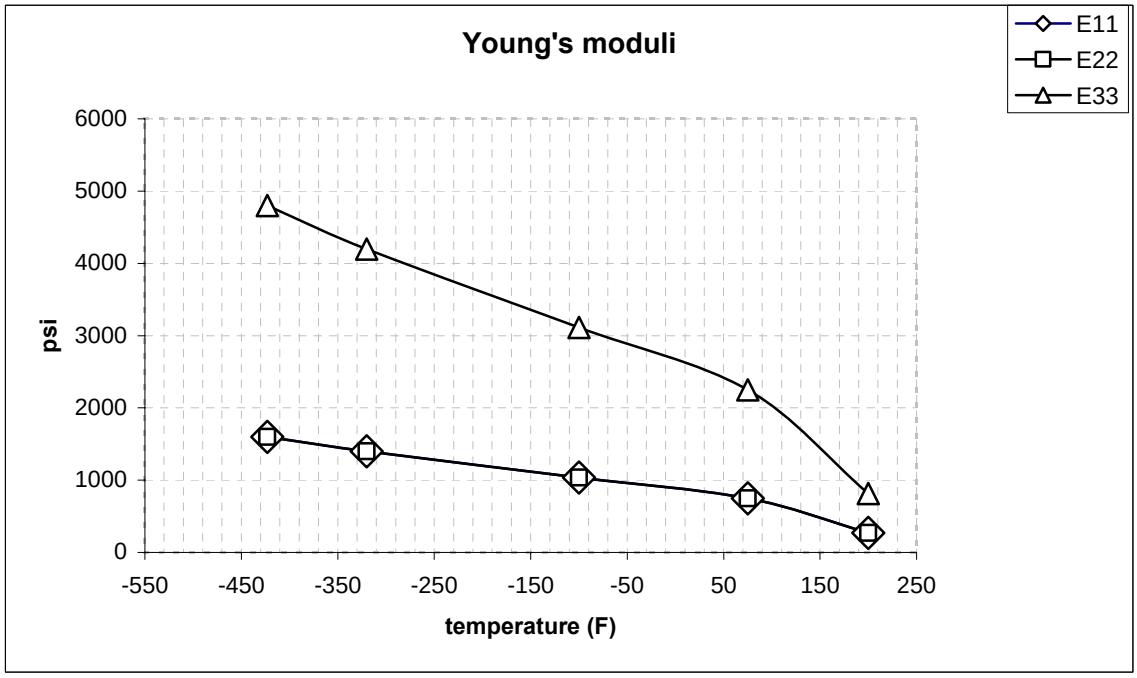

Figure 2-6. Young's moduli vs. temperature[†]

[†]Source: personal communication, Doug Wells (MSFC)

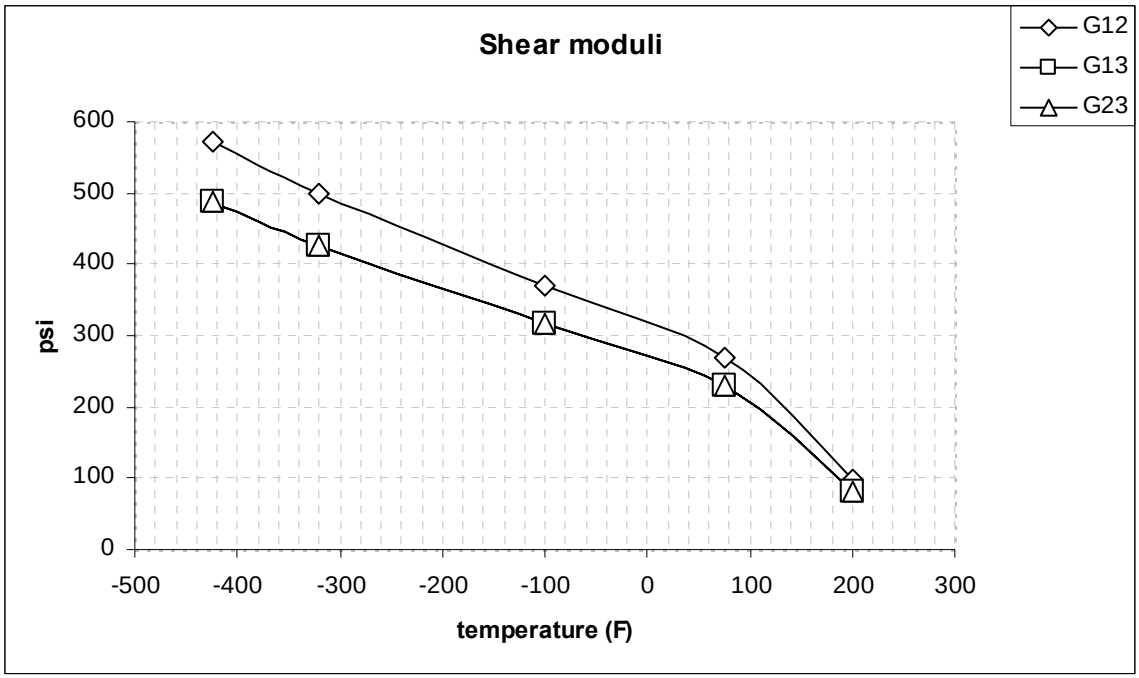

Figure 2-7. Shear moduli vs. temperature†

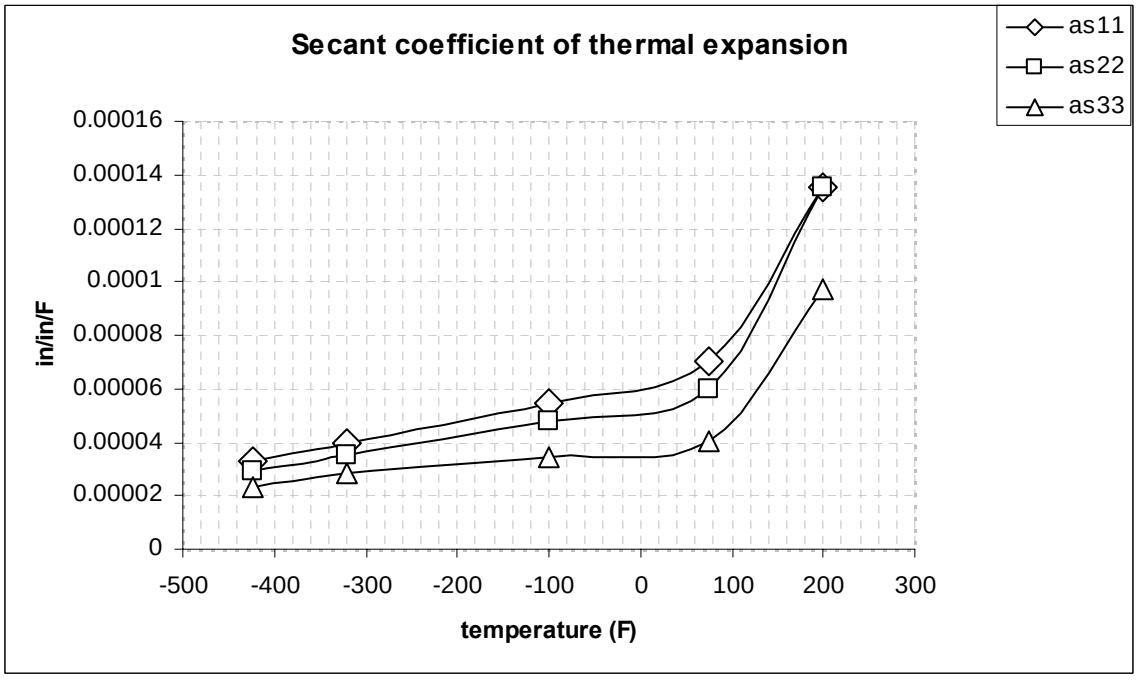

Figure 2-8. Coefficient of thermal expansion vs. temperature†

†Source: personal communication, Doug Wells (MSFC)

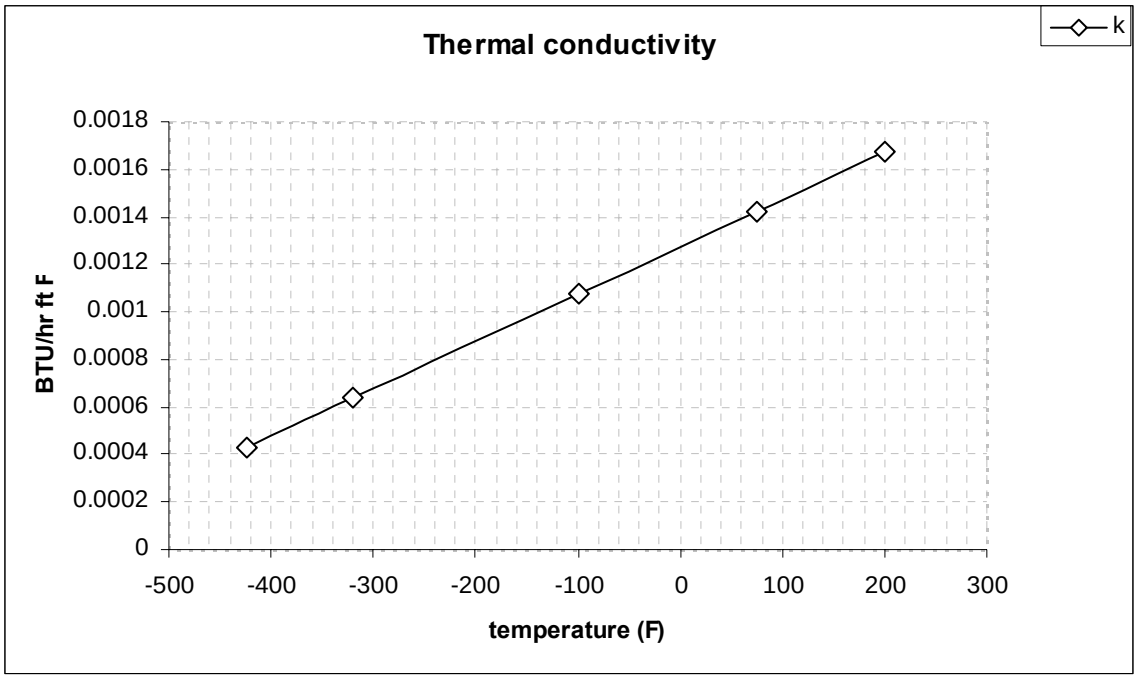

Figure 2-9. Thermal conductivity vs. temperature†

Fracture Testing for the BX-265 Foam Material

While many foam materials do not exhibit linear-elastic response before yielding, brittle foams normally exhibit linear-elastic behavior (while in tension) up until fracture takes place. Thus, we would like to use LEFM concepts to compute the near-tip stresses. These analytical expressions assume that we are dealing with a continuum. So if the crack is very small, cell size could influence these computations. Brittle fracture of foams has been studied by Fowlkes (1974), McIntyre and Anderton (1978), Morgan *et al.* (1981), Maiti *et al.* (1984), and Huang and Gibson (1991) among others. Perhaps the most widely accepted theory for the brittle facture of foam is the Maiti *et al.* (1984) study. They present a relation to compute the toughness for brittle foams as

$$KI_c = C_8 \sigma_{fs} (\pi l)^{1/2} (\rho^* / \rho_s)^{3/2} \qquad (2\text{-}21)$$

where C_8 is a constant of proportionality and σ_{fs} is the failure strength of the struts. Equation (2-21) can also be re-written as

$$KI_c = C'_8 \, KI_{Cs} \left(\rho^* / \rho_s \right)^{3/2} \tag{2-22}$$

where KI_{Cs} is the toughness of the solid material. Equation (2-22) assumes that KI_{Cs} is proportional to $\sigma_{fs} l^{1/2}$ and once more the desired property is related to the relative density. The concern, now, is at what length scale is such an equation valid.

Huang and Gibson (1991) analyze the fracture toughness of brittle honeycombs. The primary aim of their paper is to examine the effect of short cracks and determine some sort of correction factor for (2-21). They go on to show that cell size does indeed impact the fracture toughness calculations. Using fractographic analysis, Brezny and Green (1991) study short cracks in oxidized carbon foams. Their results dovetail with Huang and Gibson's (1991) in that cell size can influence the fracture response.

However, in both studies short cracks are used in the various experiments. By short, we mean crack lengths less than an order of magnitude greater than the average cell size. But in Huang and Gibson's (1991) paper, the well-known relations based on continuum assumptions seem to be valid as long as the crack length is an order of magnitude larger than the cell size. Thus, if one is considering cracks much greater than the size of the cell lattice, it seams reasonable to model the foam as a continuum.

To that end NASA conducted numerous single-edge bending SEN(B), compact tension C(T), and middle tension M(T) tests to examine how the foam fractures under load and used the regular, continuum-based relations to determine fracture properties, such as the plane strain toughness. Pictures of these test specimens are shown in Figure 2-10. Since this material is anisotropic, each time the fracture toughness is calculated,

the material's orientation is supposed to be reported along with it. Figure 2-11 summarizes some of the tested geometries at various temperatures (left and right sides of the vertical lines), for a few orientations, denoted by the labels along the bottommost horizontal axis.

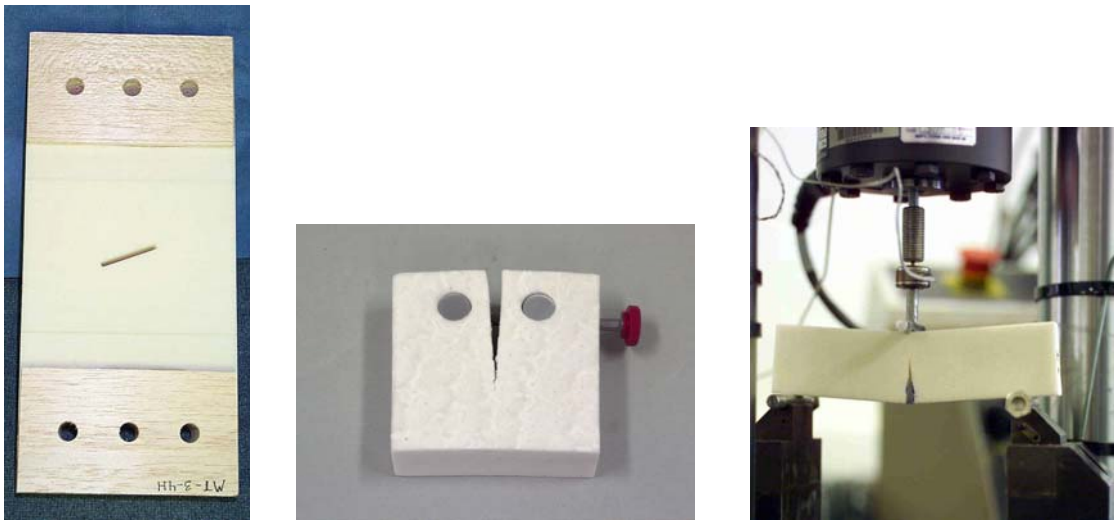

Figure 2-10. From left to right: M(T), C(T), and SNE(B) fracture test specimens

While NASA utilized many geometries to test the fracture toughness, the C(T) test was the most extensively tested specimen used to estimate a toughness. The plane strain fracture toughness is usually obtained with slow loading rates (Barsom and Rolfe, 1999). By plane strain, we mean thick plates, or test specimens, with deep cracks. The foam is brittle and fracture is sudden with little or no stable crack growth. Wells (1966) suggested that the fracture behavior near the crack tip can be characterized by crack tip opening displacement (CTOD). He showed that CTOD is analogous to the crack extension force (sometimes referred to as G_c in the literature) and CTOD could be related to the plain strain fracture toughness-KI_c.

If the material is brittle and the subsequent load vs crack mouth opening displacement (CMOD) curve (Figure 2-12) is linear-elastic and the C(T) specimen meets

the standards mandated by the ASTM, KI_c can be calculated from this test method and this approach is that NASA used to calculate the fracture toughness for the foam. In order to determine KI_c, a preliminary fracture toughness, K_Q, is determined by the following relationship (Anderson, 1991).

Where P_Q (Figure 2-13) is maximum load applied to the C(T) specimen before failure, B is the specimen thickness, W is the width of the specimen measured from the centerline of the pin holes to the rear of the specimen, and f(a/W) is a dimensionless polynomial function. The ASTM E399 standard denotes which function to use depending on what specimen one is using. If the a/W ratio and B (thickness) are correct per ASTM procedure and as long as P_{max} is $\leq 1.10P_Q$ then $K_Q = KI_c$.

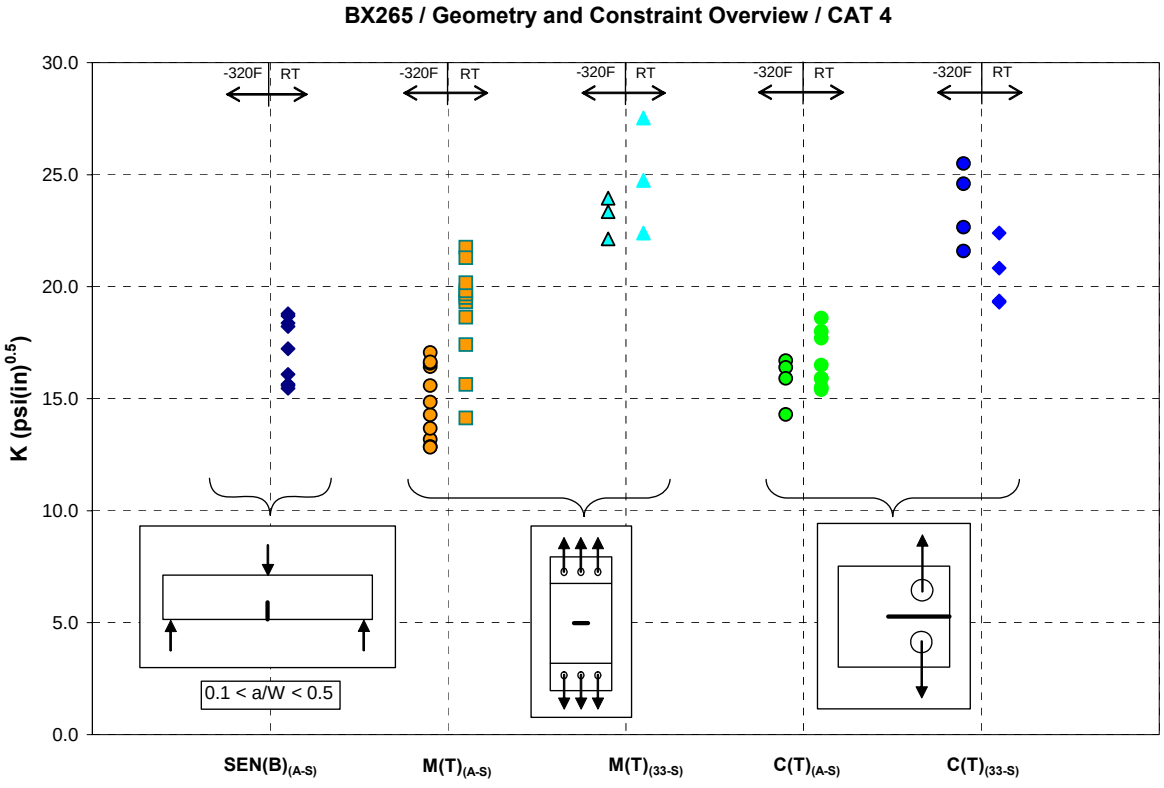

Figure 2-11. Summary K-values for various fracture specimens

$$K_Q = \frac{P_Q}{B\sqrt{W}} f(a/W) \tag{2-5}$$

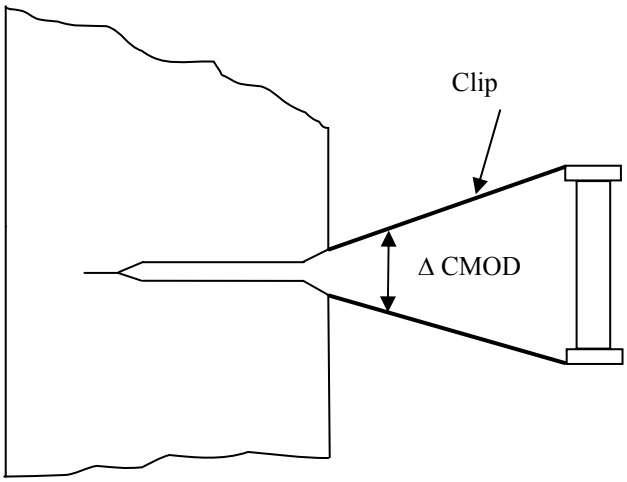

Figure 2-12. Clip gauge on C(T) specimen used to measure CMOD

Additional Testing: Divot Test Specimens

While NASA was conducting tests to evaluate the material properties at various temperatures, additional experiments were devised to examine how and why the foam becomes detached from the tank. Gibson and Ashby (1988) discuss the design of sandwich panels with foam cores. These types of structural members are normally comprised of two, stiff, skins separated by a lightweight core. These parts are utilized heavily by the aircraft industry, particularly in applications where resistance to bending and buckling loads are important, such as helicopter rotor blades. One mode of failure for these types of structural members is decohesion of the adhesive bond between the skin and the core.

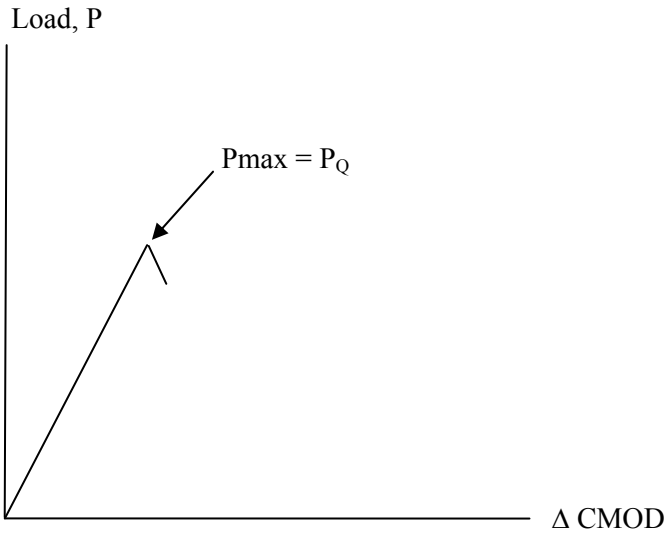

Figure 2-13. Typical load vs CMOD curve for a brittle material

Often the epoxy bond is stronger than the core material itself. So if the interface between the skin and core is defect-free, delamination is usually not a concern. The situation changes if there are defects within the interface, however. This type of analysis is complicated by the difference in elastic constants between skin, adhesives and core. The delamination described by Gibson and Ashby can be likened to 'weakening' the bond between the core and the outer skin. When the strength of the bond becomes too weak, the foam core and skin can peal apart. The failure mode that NASA is encountering, however, is more of an explosive and sudden 'blowout' of foam from the ET.

Since the foam loss seems to be the greatest near areas where the surface of the tank is somewhat uneven (from bolts and fittings), NASA believes that voids created when the foam is first being sprayed down are the primary reason why the foam is able to break off. These are indeed defects between the ET, or skin, and the foam, or core material. To model this phenomenon, NASA devised an experiment to examine how

various voids within foam test panels could contribute to large pieces of foam being blown out under certain conditions. Rectangular test panels like the one shown in Figure 2-14 are used for the 'divot testing.'

Figure 2-14. Divot test panel

In this experiment a cylindrical bore is machined into the panel. At the top of that bore, a sharp notch is created to simulate a crack, or defect, near this void. Liquid nitrogen is then pumped into the bored hole and a heat flux is applied across the other side of the foam panel. Two-dimensional schematics of this process are shown in Figures 2-15 and 2-16.

The applied flux warms the liquid nitrogen and eventually a phase change takes place. The experiment takes place in a thermo-vacuum chamber to simulate the environment the foam is exposed to during liftoff. As the Shuttle ascends to space, the atmospheric pressure is dropping, but the gaseous N_2 applies pressure on the walls of the void and the crack faces. With enough force, the flaw turns and propagates toward the surface.

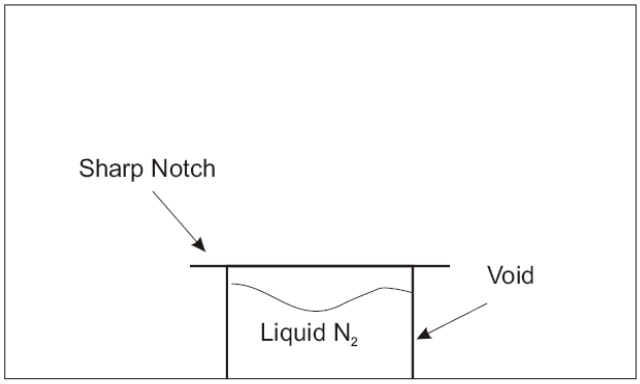

Figure 2-15. 2-D view of divot test

In Figure 2-17, we see the aftermath of one of these experiments. A frustum shaped piece of foam has been blown out and the crater left behind resembles a 'divot,' similar to the removal of a small piece of turf after a golf shot has been played. It is here that predicting the crack turning angle could have a practical application.

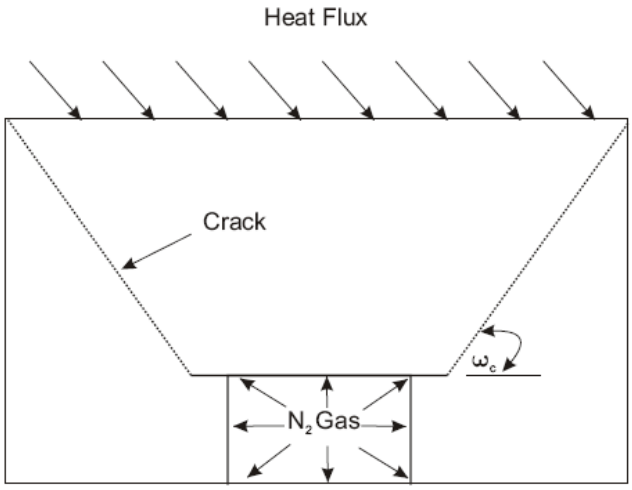

Figure 2-16. 2-D view of test panel after heat flux has been applied

For a given void and flaw size, along with the applied tractions, it might be possible to calculate this angle, denoted as ω_c in Figure 2-16, by calculating near-tip stresses and applying a turning theory such as the maximum tangential stress criterion. The concept of the crack turning angle and methods to compute it will be covered in a later chapter.

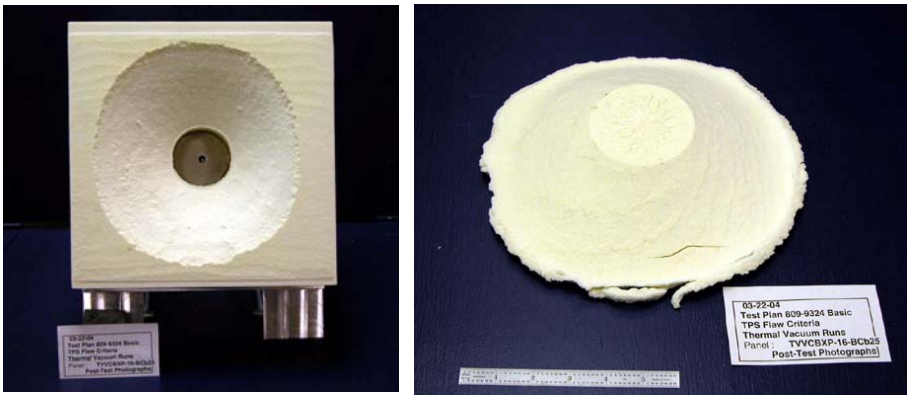

Figure 2-17. Foam blow out from divot test

Summary

The pertinent theory (Gibson and Ashby, 1988) regarding cellular solids is presented and various formulas are available depending on what type (open or close-celled) of foam one is analyzing. Formulae for anisotropic foams are presented as well. The elastic constants, for both isotropic and anisotropic constants can be estimated through the relations presented in the early sections of this chapter or via experiment. While there is extensive literature available on foams, NASA decided to perform tests to evaluate the elastic constants and fracture properties at various temperatures. This enabled NASA to have a large collection of experimental data for several material orientations, over a wide range of geometries.

Once the tests were conducted, determining the fracture properties can be done using the well-known empirical relations for standard test specimens. One of the main assumptions behind these equations is that they are to be applied to a continuum. The foam is a porous material and it has been shown that cell size can impact fracture properties if one is conducting analyses with short cracks. However, continuum

assumptions are acceptable as long as the crack is an order of magnitude longer than the cell length.

Lastly, additional and highly specialized tests were performed to investigate how the foam is able to free itself from the tank. NASA believes that voids near fittings and bolts allow liquefied air to collect in these cavities prior to liftoff. During liftoff, the air rushing over the outside surface of the insulation warms the liquid nitrogen which converts it into a gas. The pressure, while small, appears to be sufficient to drive a crack toward the exterior and this seems to account for the foam loss outlined in chapter one.

An idealized case of this process is examined through the divot test. These experiments entail machining oval or cylindrical-shaped voids into a foam test panel and pumping in liquid nitrogen. The cryogen is heated when a flux is applied to the top part of the foam panel. At the top of the void, a sharp notch is inserted and when the nitrogen is turned into a gas, the pressures exerted on the void walls and crack faces are sufficient to drive a crack toward the surface. It is here that a determination of the crack turning angle could be of some use to NASA and there a few theories prevalent in the literature on this topic. Most of them require the evaluation of near-tip stresses and/or strains. Since this an anisotropic material, the general equations for isotropic materials are not applicable in most cases. In the next chapter a detailed discussion covering linear, elastic, anisotropic fracture mechanics is covered and these concepts are applied in chapter four when crack turning theory is presented.

CHAPTER 3
AN INTRODUCTION TO FRACTURE MECHANICS

Material Definitions

For local crack tip calculations there are material definitions, or classifications, that need to be defined before moving on with discussions on how to compute near-tip stresses for materials that are anisotropic, or have direction-dependent properties. In general, most texts on fracture mechanics focus on materials that are isotropic. Here the constitutive matrix contains three elastic constants, two of which are independent, E and ν. For isotropic materials, there are an infinite number of planes of material symmetry and the strains and stresses are related to each other via equation (3-1).

$$\begin{Bmatrix} \varepsilon_{xx} \\ \varepsilon_{yy} \\ \varepsilon_{zz} \\ \gamma_{yz} \\ \gamma_{xz} \\ \gamma_{xy} \end{Bmatrix} = \begin{bmatrix} 1/E & -\nu/E & -\nu/E & 0 & 0 & 0 \\ & 1/E & -\nu/E & 0 & 0 & 0 \\ & & 1/E & 0 & 0 & 0 \\ & & & 2(1+\nu)/E & 0 & 0 \\ & & & & 2(1+\nu)/E & 0 \\ sym & & & & & 2(1+\nu)/E \end{bmatrix} \begin{Bmatrix} \sigma_{xx} \\ \sigma_{yy} \\ \sigma_{zz} \\ \sigma_{yz} \\ \sigma_{xz} \\ \sigma_{xy} \end{Bmatrix} \tag{3-1}$$

Many other types of materials can be characterized by the number of planes of internal symmetry (Dieter 1976). Cubic materials, for example, have three independent material parameters and nine planes of symmetry. Materials with three internal planes of symmetry are known as orthotropic materials and many engineering metals fall into this category, such as rolled aluminum. A special class of orthotropic materials has a single plane of symmetry that is also isotropic. These are known as transversely isotropic materials and the constitutive relations for this material were defined in the previous

chapter. Monoclinic materials possess a single plane of material symmetry, but the behavior in that plane is not isotropic.

Being cognizant of the constitutive relations for the particular material in question (be it isotropic or fully anisotropic) is important because many of the initial derivations of near-tip stress fields for anisotropic materials tried to take advantage of material symmetry to decouple 'in-plane,' and 'out-of-plane' displacements, which, in turn, makes the mathematical formulation a little less complicated.

Isotropic Fracture Mechanics

For isotropic materials, the near-tip stress fields have been analyzed by Westergaard (1939), Sneddon (1946), Williams (1957), and Irwin (1960) among others. These solutions pertain to specific cracked configurations with applied far-field loads and are governed by a single parameter, *K,* the stress intensity factor (Anderson, 1991).

$$\sigma_{ij}(r,\omega) = \frac{K}{\sqrt{2\pi r}} f_{ij}(\omega) + \text{higher order terms} \qquad (3\text{-}1)$$

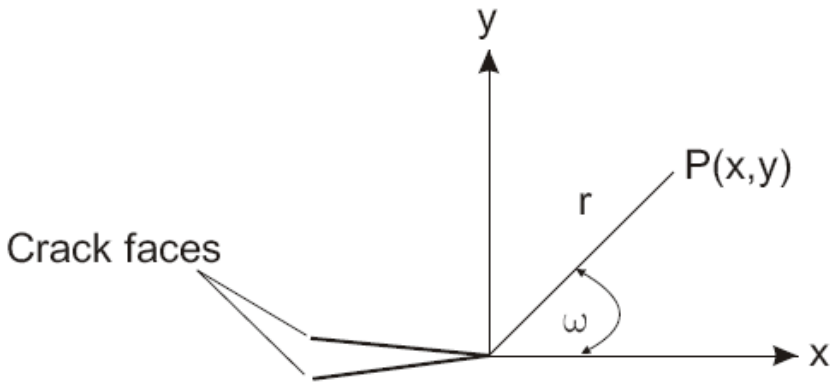

Figure 3-1. Coordinate system used in equation (3-1)

The coordinate system for equation (3-1) is shown in Figure 3-1, where the f_{ij} term is a trigonometric function. We note the Greek letter, theta, is normally used to define the angle with the horizontal in the polar coordinate system presented above, but theta will be

used later on to define the material orientation. A different variable name is selected to avoid confusion. The key points about (3-1) are that the near-tip stresses have no dependence on the elastic constants and the first term is proportional to $1/\sqrt{r}$ and, therefore, the stresses approach infinity as r is made smaller and smaller. Also, as r approaches zero the 'higher order terms' in (3-1) get smaller or remain at some finite value. Thus, in many texts and papers the analysis is restricted to small values of r such that the higher order terms are neglected.

There is typically a roman numeral written next to the stress intensity factor to denote the mode of loading and Figure 3-2 displays the three modes of deformation.

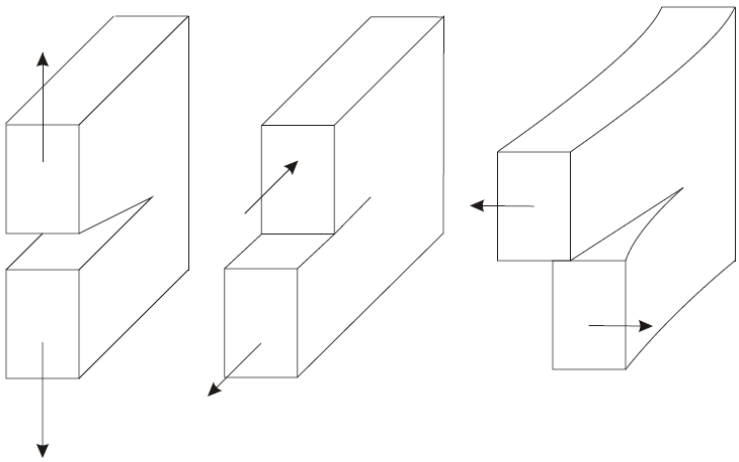

Figure 3-2. From left to right: mode I (opening), mode II (shearing), mode III (tearing)
While the stresses are proportional to $1/\sqrt{r}$, the displacements are related to $\sqrt{r}$-equation (3-2).

$$\begin{Bmatrix} u_x \\ u_y \\ u_z \end{Bmatrix} = \frac{1}{2\mu_s}\sqrt{\frac{r}{2\pi}} \begin{bmatrix} \cos\frac{\omega}{2}\left(\kappa\text{-}1+2\sin^2\frac{\omega}{2}\right) & \sin\frac{\omega}{2}\left(\kappa+1+2\cos^2\frac{\omega}{2}\right) & 0 \\ \sin\frac{\omega}{2}\left(\kappa+1\text{-}2\cos^2\frac{\omega}{2}\right) & -\cos\frac{\omega}{2}\left(\kappa\text{-}1\text{-}2\sin^2\frac{\omega}{2}\right) & 0 \\ 0 & 0 & \sin\frac{\omega}{2} \end{bmatrix} \begin{Bmatrix} KI \\ KII \\ KIII \end{Bmatrix} \quad (3\text{-}2)$$

where $\kappa = 3\text{-}4\nu$ for plane strain and $\kappa = (3\text{-}\nu)/(1+\nu)$ for plane stress and μ_s is the shear modulus.

Linear Elastic Fracture Mechanics for Anisotropic Materials

In general, the equations in the previous section cannot be applied to this problem directly because the material properties are direction-dependent. The analytical work geared at developing the near-tip stress fields for elastic anisotropic materials has been examined by Sih *et al.* (1965), Bowie and Freese (1972), Barnett and Asaro (1972), Bogy (1972), Tupholme (1974), Kuo and Bogy (1974), Rathod (1979), Hoenig (1982), and Dhondt (2002) among other researchers.

The important work of Sih *et al.* is one of the most cited references for determining the stress fields near the crack tip for anisotropic materials. Following Westergaard's use of stress functions and complex variables to determine near-tip stresses for isotropic materials, Sih *et al.* use a similar approach for materials with direction-dependent properties. Whenever stress functions are utilized to solve this kind of problem, there is normally a corresponding characteristic equation (a detailed explanation of the characteristic equation can be found in Appendix A). For the most general case, the order of the characteristic equation is six. In Sih *et al.*'s paper the material in question is monoclinic and the crack is resting in the symmetry plane. The constitutive relations for monoclinic materials are shown in equation (3-3).

$$\begin{Bmatrix} \varepsilon_x \\ \varepsilon_y \\ \varepsilon_z \\ \gamma_{yz} \\ \gamma_{xz} \\ \gamma_{xy} \end{Bmatrix} = \begin{bmatrix} S_{11} & S_{12} & S_{13} & 0 & 0 & S_{16} \\ & S_{22} & S_{23} & 0 & 0 & S_{26} \\ & & S_{33} & 0 & 0 & S_{36} \\ & & & S_{44} & S_{45} & 0 \\ & & & & S_{55} & 0 \\ sym & & & & & S_{66} \end{bmatrix} \begin{Bmatrix} \sigma_x \\ \sigma_y \\ \sigma_z \\ \sigma_{yz} \\ \sigma_{xz} \\ \sigma_{xy} \end{Bmatrix} \tag{3-3}$$

This configuration is advantageous because the in-plane and out-of-plane displacements become decoupled, which in turn reduces the order of the characteristic equation to four.

$$\begin{Bmatrix} \sigma_{xx} \\ \sigma_{yy} \\ \sigma_{xy} \\ \sigma_{xz} \\ \sigma_{yz} \end{Bmatrix} = \frac{1}{\sqrt{2\pi r}} \begin{bmatrix} \mathrm{Re}\left[\left(\frac{\mu_1\mu_2}{\mu_1-\mu_2}\right)\left(\frac{\mu_2}{Q_2}-\frac{\mu_1}{Q_1}\right)\right] & \mathrm{Re}\left[\left(\frac{1}{\mu_1-\mu_2}\right)\left(\frac{\mu_2^2}{Q_2}-\frac{\mu_1^2}{Q_1}\right)\right] & 0 \\ \mathrm{Re}\left[\left(\frac{1}{\mu_1-\mu_2}\right)\left(\frac{\mu_1}{Q_2}-\frac{\mu_2}{Q_1}\right)\right] & \mathrm{Re}\left[\left(\frac{1}{\mu_1-\mu_2}\right)\left(\frac{1}{Q_2}-\frac{1}{Q_1}\right)\right] & 0 \\ \mathrm{Re}\left[\left(\frac{\mu_1\mu_2}{\mu_1-\mu_2}\right)\left(\frac{1}{Q_1}-\frac{1}{Q_2}\right)\right] & \mathrm{Re}\left[\left(\frac{1}{\mu_1-\mu_2}\right)\left(\frac{\mu_1}{Q_1}-\frac{\mu_2}{Q_2}\right)\right] & 0 \\ 0 & 0 & -\mathrm{Re}\left[\frac{\mu_3}{Q_3}\right] \\ 0 & 0 & \mathrm{Re}\left[\frac{1}{Q_3}\right] \end{bmatrix} \begin{Bmatrix} KI \\ KII \\ KIII \end{Bmatrix} \tag{3-4}$$

$$\sigma_{zz} = -\left(S_{31}\sigma_{xx} + S_{32}\sigma_{yy} + S_{36}\sigma_{xy}\right)\Big/ S_{33} \tag{3-5}$$

where the elastic constants in compliance form are defined as

$$\varepsilon_i = S_{ij}\sigma_j \tag{3-6}$$

$$\begin{Bmatrix} u_x \\ u_y \\ u_z \end{Bmatrix} = \sqrt{\frac{2r}{\pi}} \begin{bmatrix} \mathrm{Re}\left[\left(\frac{1}{\mu_1-\mu_2}\right)\left(\mu_1 p_2 Q_2 - \mu_2 p_1 Q_1\right)\right] & \mathrm{Re}\left[\left(\frac{1}{\mu_1-\mu_2}\right)\left(p_2 Q_2 - p_1 Q_1\right)\right] & 0 \\ \mathrm{Re}\left[\left(\frac{1}{\mu_1-\mu_2}\right)\left(\mu_1 q_2 Q_2 - \mu_2 q_1 Q_1\right)\right] & \mathrm{Re}\left[\left(\frac{1}{\mu_1-\mu_2}\right)\left(q_2 Q_2 - q_1 Q_1\right)\right] & 0 \\ 0 & 0 & \mathrm{Re}\left[\frac{Q_3}{C_{45}+\mu_3 C_{44}}\right] \end{bmatrix} \begin{Bmatrix} KI \\ KII \\ KIII \end{Bmatrix} \tag{3-7}$$

The roots μ_1, μ_2, and μ_3 for this particular formulation come from the special case for monoclinic materials listed in Appendix A.

$$p_j = S'_{11}\mu_j^2 - S'_{16}\mu_j + S'_{12} \tag{3-8}$$

$$q_j = S'_{12}\mu_j - S'_{26} + S'_{22}/\mu_j \tag{3-9}$$

Sih *et al.* enforce a plane strain condition and the reduced compliance matrix becomes

$$S'_{ij} = S_{ij} - \frac{S_{i3}S_{3j}}{S_{33}} \tag{3-10}$$

$$Q_i = \sqrt{\cos\omega + \mu_i \sin\omega} \tag{3-11}$$

The C_{45} and C_{44} terms in (3-7) are the elastic constants which are in stiffness form

$$\sigma_i = C_{ij}\varepsilon_j \tag{3-12}$$

where

$$C_{ij} = S_{ij}^{-1} \tag{3-13}$$

The aforementioned 'decoupling' of the anti-plane displacement is now evident in equation (3-7). The u_z displacement does not depend on KI and KII. This is similar to the isotropic case in equation (3-2); the z component of displacement only depends on KIII.

When analyzing the foam problem for NASA, a crack, or defect, can be at any orientation relative to the insulation. In that sense, it does not seem very practical to employ the Sih *et al.* solution unless we know the crack always lies in the symmetry plane. More general solutions, ones that do not require a decoupling of the anti-plane displacements, will be used instead.

The asymptotic solution derived by Hoenig is the one we will adopt to get the near-tip stress fields. Materials with virtually any orientation, irrespective of the location of the crack front, can be modeled with this method. Hoenig uses the pioneering work of Lekhnitksii (1963) to derive the stresses and displacements given below by using complex variables and stress functions to derive a coupled set of differential equations whose solution entails determining the roots of the ensuing sixth order characteristic

equation. We notice that K once again arises as a scalar multiplier just as it did for the isotropic solution.

$$\sigma_x = \frac{1}{\sqrt{2\pi r}} \mathrm{Re} \sum_{i=1}^{3} \frac{\mu_i^{\,2} N_{ij}^{\,-1} K_j}{\sqrt{\cos\omega + \mu_i \sin\omega}}$$

$$\sigma_y = \frac{1}{\sqrt{2\pi r}} \mathrm{Re} \sum_{i=1}^{3} \frac{N_{ij}^{\,-1} K_j}{\sqrt{\cos\omega + \mu_i \sin\omega}}$$

$$\tau_{xz} = \frac{1}{\sqrt{2\pi r}} \mathrm{Re} \sum_{i=1}^{3} \frac{\mu_i \lambda_i N_{ij}^{\,-1} K_j}{\sqrt{\cos\omega + \mu_i \sin\omega}} \tag{3-14}$$

$$\tau_{yz} = \frac{-1}{\sqrt{2\pi r}} \mathrm{Re} \sum_{i=1}^{3} \frac{\lambda_i N_{ij}^{\,-1} K_j}{\sqrt{\cos\omega + \mu_i \sin\omega}}$$

$$\tau_{xy} = \frac{-1}{\sqrt{2\pi r}} \mathrm{Re} \sum_{i=1}^{3} \frac{\mu_i N_{ij}^{\,-1} K_j}{\sqrt{\cos\omega + \mu_i \sin\omega}}$$

$$\sigma_{zz} = -\left(S_{31}\sigma_{xx} + S_{32}\sigma_{yy} + S_{34}\sigma_{yz} + S_{35}\sigma_{xz} + S_{36}\sigma_{xy} \right) \Big/ S_{33} \tag{3-15}$$

$$u_i = \sqrt{\frac{2r}{\pi}} \mathrm{Re} \left(\sum_{j=1}^{3} m_{ij} N_{jl}^{-1} K_l \left(\cos\omega + \mu_j \sin\omega \right) \right) \tag{3-16}$$

Here an important distinction is made between the general case and Sih et al's formulation. Notice in (3-16) how the mode I-III SIFs are to be summed over all three modes of displacement. Thus, all three components of displacement are dependent on KI-KIII.

$$\begin{aligned} m_{1i} &= S'_{11}\,\mu_i^{\,2} - S'_{16} + S'_{12} + \lambda_i \left(S'_{15}\,\mu_i - S'_{14} \right) \\ m_{2i} &= S'_{21}\,\mu_i - S'_{26} + \frac{S'_{22}}{\mu_i} + \lambda_i \left(S'_{25} - \frac{S'_{24}}{\mu_i} \right) \\ m_{3i} &= S'_{41}\,\mu_i - S'_{46} + \frac{S'_{42}}{\mu_i} + \lambda_i \left(S'_{45} - \frac{S'_{44}}{\mu_i} \right) \end{aligned} \tag{3-17}$$

The μ_i are the roots that occur in conjugate pairs and they arise from the sixth order polynomial, equation (3-18). The coordinate system used in equations (3-14) and (3-16) is the same as the one used in (3-1).

$$l_4(\mu)l_2(\mu)-l_3^2(\mu)=0 \tag{3-18}$$

Where

$$l_2(\mu)=S'_{55}\mu^2-2S'_{45}\mu+S'_{44}$$
$$l_3(\mu)=S'_{15}\mu^3-\left(S'_{14}+S'_{56}\right)\mu^2+\left(S'_{25}+S'_{46}\right)\mu-S'_{24}$$
$$l_4(\mu)=S'_{11}\mu^4-2S'_{16}\mu^3+\left(2S'_{12}+S'_{66}\right)\mu^2-2S'_{26}\mu+S'_{22}$$

The N matrix in equation (3-14) is defined as

$$N_{ij}=\begin{bmatrix}1 & 1 & 1\\ -\mu_1 & -\mu_2 & -\mu_3\\ -\lambda_1 & -\lambda_2 & -\lambda_3\end{bmatrix} \tag{3-20}$$

Where λ_i is defined as $l_3(\mu_i)/\, l_2(\mu_i)$.

There are two situations, also called degenerate cases, where this solution is invalid, however. If anti-plane shear and plane strain displacements becomes decoupled-for monoclinic materials, say-Hoenig's formulation falls apart. He does present an alternate solution for monoclinic materials which turns out to be consistent with the Sih et al solution mentioned earlier. His solution also encounters difficulties if the crack is lying in a plane that is isotropic. The N-matrix, equation (3-20), becomes singular because μ_1 and μ_2 = i. However, we have near-tip solutions for the isotropic cases. These are shown in equations (3-1) and (3-2).

Determining the Stress Intensity Factor—*K*

In the above sections, it is necessary to develop solutions for determining the stress intensity factor, *K*. Over the past 50 years, numerous methods have been developed to

determine this parameter. For simple geometries, a handbook (Tada et al, 1973) of K-solutions could be consulted. Alaibadi and Rooke (1991) present an excellent summary of the literature on the subject of numerical evaluations of SIFs. They divide many of the available methods into three main categories, denoted as stages in Table 3-1.

Table 3-1. Various methods for determining the SIF

Stage 1	Stage 2	Stage 3
Handbooks	Superposition	Collocating, or mapping
	Stress concentration	Integral transform
	Stress distribution	Body force method
	Green's function	Method of lines
	Approximate weight function	Finite element method
	Compounding	Boundary element
		Alternating technique

As one might have guessed, the procedures listed in the Stage 3 category are the most accurate. Since computers have become less expensive and more powerful in recent years, many of the current studies geared toward K-solutions incorporate the use of the finite element (FE) method or boundary element (BE) techniques. Boundary element methods are particularly attractive because the dimensionality of the numerical problem is reduced, i.e. 2-D problems involve discretizing the line-boundary of the domain and for 3-D problems, just the surface of the domain is discretized.

This analysis will call on the FE method to help compute K, and there are a few ways of determining it with this method, such as: extrapolation of near-tip stress and displacement fields, Rice's J-integral (1968), strain energy, and the virtual crack extension method.

FRANC3D Next Generation Software

The Cornell Fracture Group has developed software capable of creating crack meshes and computing an anisotropic K-solution. This particular method of solution would fall under Stage 3 in Table 3-1, and in this case Rice's J-contour integral along

with displacements output from FE software will be used to determine K along the crack front. This software is very versatile in that it is not restricted to analyzing any one kind of material; K-solutions can be generated for isotropic and fully anisotropic materials alike.

Since many FE models were built and the subsequent K-solutions computed with this software, it would be prudent to discuss the pertinent theory (Banks-Sills et al, 2005) that governs this particular way of calculating K. Rice's J integral, a conservation integral that measures the energy flux into the crack tip, is equivalent to the strain energy release rate (denoted as *G*) for small scale yielding. Furthermore, it can be shown for a plane problem that only has KI and KII that

$$G = J = \alpha(KI^2 + KII^2) \tag{3-21}$$

Where $\alpha = (1-\nu^2)/E$ for plane strain and $\alpha = 1/E$ for plane stress. One can see that the J-integral equation, as is, cannot give us the SIFs on an individual basis.

$$J = \int_{\Gamma}\left(W dy - T_i \frac{\partial u_i}{\partial x} ds \right) \tag{3-22}$$

with $W = (1/2)\sigma_{ij}\varepsilon_{ij}$, also known as the strain energy density, $T = \sigma_{ij}n_j$ and u_i is the displacement vector.

The path, Γ, is defined in Figure 3-3

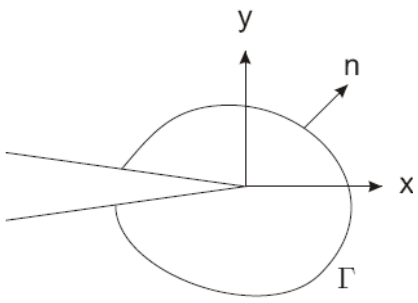

Figure 3-3. Path of the J-integral

The J-integral was initially formulated for 2-D problems, however since this material has properties that are direction dependent, our analysis requires the use of 3-D FE models. The J-integral, then, needs to be modified so it can be used in integrations that take place over volumes. Following Li et al (1985), the J-integral can be rewritten as

$$J = \left[\int_{\Gamma} \sigma_{ij} \frac{\partial u_i}{\partial x_1} - W\delta_{1j} \right] \frac{\partial q}{\partial x_j} ds \tag{3-23}$$

In this formulation, the crack is undergoing a 'virtual extension,' and only a small portion of the crack front is being advanced. When using the formulation from the Li et al paper, the J-integral is now evaluated in a cylindrical domain centered over the crack front.

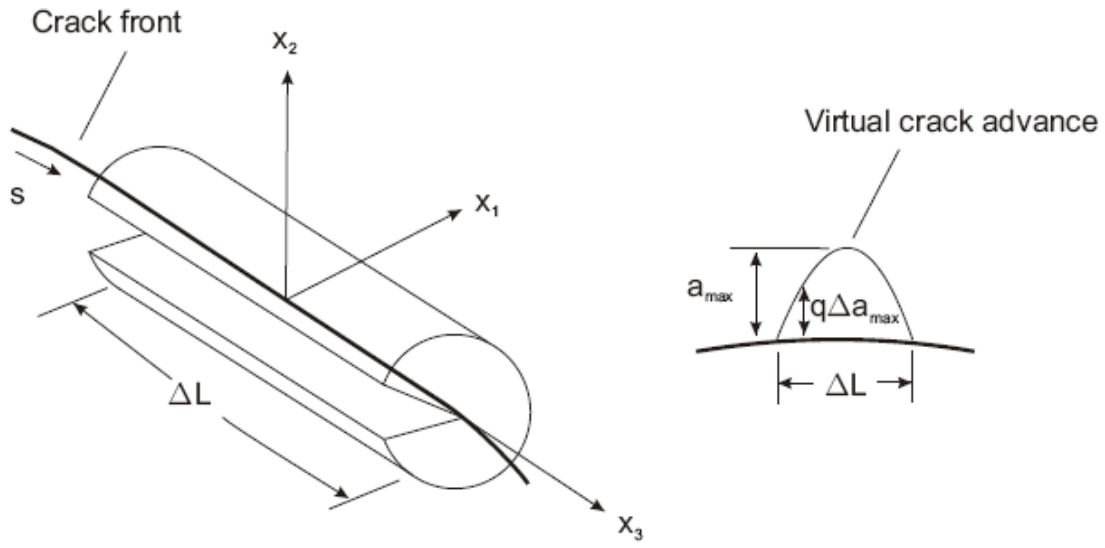

Figure 3-4. Cylindrical domain and virtual crack advance for a 3-D crack front

Following Figure 3-4 we can define incremental area of virtual crack advance as

$$A_q = \Delta a_{\max} \int_{\Delta L} q(s)\, ds \tag{3-24}$$

The definition of J in equation (3-22) requires Γ to be very small. It is difficult to compute stresses and strains about a vanishingly small path about the crack tip. Instead,

area integrals (Moran and Shih, 1987) are used (for 2-D problems) because they are easier to implement numerically. So, the q term in (3-23) is simply a mathematical tool that enables us to recast the J-integral into a slightly more usable form.

This virtual extension method is the modern-day approach to solve computational fracture mechanics problems. One of the main advantages of such a method is the ability to compute the energy release rates across the crack front for 3-D problems. Since the energy release rates can vary over the front that implies K can also change with respect to crack front position as well

$$J = \frac{\int J(s) q_t(s) ds}{\int q_t(s) ds} = \frac{\overline{J}}{A_q} \tag{3-25}$$

where $q_t(s)$ is the crack tip perturbation.

Rice's J-integral does not allow us to look at the SIFs on an individual basis for a mixed mode crack problem. This hurdle was first surpassed by Ishikawa (1980) where he decomposes the stress, strain, and displacement fields into symmetric and anti-symmetric parts. This allows him to use the J-integral to compute the Ks individually. Ishikawa's method, though, has not been extended for anisotropic materials. Yau *et al.* (1980) uses the M-integral developed by Freund (1978) to determine KI and KII, individually, by using the idea that two separate and independent equilibrium states (denoted by superscripts (1) and (2)) for a linear elastic, isotropic material can be related to a third equilibrium state, denoted with no superscript. That is to say the stresses, strains, displacements, and SIFs from these separate equilibrium states can be superposed

$$\begin{aligned} \sigma_{ij} &= \sigma_{ij}^{(1)} + \sigma_{ij}^{(2)} \qquad & KI &= KI^{(1)} + KI^{(2)} \\ \varepsilon_{ij} &= \varepsilon_{ij}^{(1)} + \varepsilon_{ij}^{(2)} \qquad & KII &= KII^{(1)} + KII^{(2)} \\ u_i &= u_i^{(1)} + u_i^{(2)} \qquad & KIII &= KIII^{(1)} + KIII^{(2)} \end{aligned} \tag{3-26}$$

The J-integral can now take the form

$$\overline{J} = \overline{J^{(1)}} + \overline{J^{(2)}} + \overline{M^{(1,2)}} \tag{3-27}$$

The $M^{(1,2)}$ term is known as the M-integral initially derived by Freund and it can be recast in terms of the aforementioned equilibrium states

$$\overline{M^{(1,2)}} = \left(\int_{\Gamma} \sigma_{ij}^{(1,2)} \frac{\partial u_i^{(2)}}{\partial x_1} + \sigma_{ij}^{(2)} \frac{\partial u_i^{(1)}}{\partial x_1} - W^{(1,2)} \delta_{1,j} \right) \frac{\partial q}{\partial x_j} \tag{3-28}$$

This integral describes the interaction between the two equilibrium states, and sometimes the M-integral is called the 'interaction' integral in the literature.

The first step in the procedure to determine the SIFs is to define the strain energy release rate using Irwin's (1957) crack closure integral. Consider the crack in Figure 3-5. Now a compressive, or closure stress, is applied in such a fashion to clamp the crack faces down along the length δ-r. The work it takes to perform this closure can be related to the energy release rate, *G*. Irwin goes on to use the force displacement curve and equate that to the work required to close the crack. Substitutions are made for near-tip displacements and stresses and eventually an integral expression is obtained that relates the energy release rate to the stress intensity factor.

In a similar manner, Hoenig (via Equation 3-30) provides us an analytical expression for the energy release for general anisotropy in terms of the SIFs and material constants. Irwin's work was initially developed for brittle, isotropic materials; his expression for the energy release rate includes the isotropic Poisson ratio and the Young and shear moduli.

$$G = \lim_{\delta \to 0} \frac{1}{\delta} \int_0^{\delta} \sigma_j(\delta - r, 0) \cdot u_j(r, \pi) dr \tag{3-29}$$

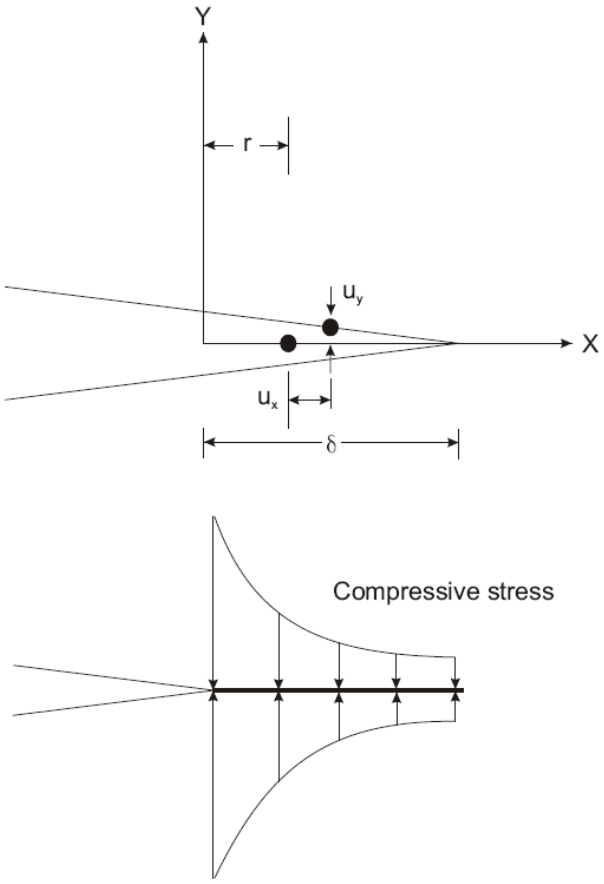

Figure 3-5. Definition of Irwin's crack closure integral

Now, if the stress and displacement fields are substituted in (3-29), we have

$$G = J = -\frac{1}{2}\left[KI\ \mathrm{Im}(m_{2i} N_{ij}^{-1} K_j) + KII\ \mathrm{Im}(m_{1i} N_{ij}^{-1} K_j) + KIII\ \mathrm{Im}(m_{3i} N_{ij}^{-1} K_j) \right] \tag{3-30}$$

When we use the relations for SIFs in (3-26), we get

$$G = J = -\frac{1}{2}\left[\begin{array}{l} (KI^{(1)} + KI^{(2)})\ \mathrm{Im}(m_{2i} N_{ij}^{-1} K_j) + (KII^{(1)} + KII^{(2)})\ \mathrm{Im}(m_{1i} N_{ij}^{-1} K_j) \\ +(KIII^{(1)} + KIII^{(2)})\ \mathrm{Im}(m_{3i} N_{ij}^{-1} K_j) \end{array} \right] \tag{3-31}$$

The terms in (3-27) have bars over them because a certain definition of J is used in (3-23). Let us define an alternate form of (3-27) where J is not normalized with respect to the extended area as

$$J = J^{(1)} + J^{(2)} + M^{(1,2)} \tag{3-32}$$

Now we substitute (3-31) into (3-32) and for clarity the individual terms of that equation are listed below

$$J^{(1)} = -\frac{1}{2}\left[KI^{(1)}\,\mathrm{Im}(m_{2i}N_{ij}{}^{-1}K_j{}^{(1)}) + KII^{(1)}\,\mathrm{Im}(m_{1i}N_{ij}{}^{-1}K_j{}^{(1)}) + KIII^{(1)}\,\mathrm{Im}(m_{3i}N_{ij}{}^{-1}K_j{}^{(1)})\right]$$
$$J^{(2)} = -\frac{1}{2}\left[KI^{(2)}\,\mathrm{Im}(m_{2i}N_{ij}{}^{-1}K_j{}^{(2)}) + KII^{(2)}\,\mathrm{Im}(m_{1i}N_{ij}{}^{-1}K_j{}^{(2)}) + KIII^{(1)}\,\mathrm{Im}(m_{3i}N_{ij}{}^{-1}K_j{}^{(2)})\right] \tag{3-33}$$

$$\begin{aligned} M^{(1,2)} = -\tfrac{1}{2}\Big[& KI^{(1)}\,\mathrm{Im}\left(m_{2i}N_{ij}^{-1}K_j^{(2)}\right) + KI^{(2)}\,\mathrm{Im}\left(m_{2i}N_{ij}^{-1}K_j^{(1)}\right) \\ & + KII^{(1)}\,\mathrm{Im}\left(m_{1i}N_{ij}^{-1}K_j^{(2)}\right) + KII^{(2)}\,\mathrm{Im}\left(m_{1i}N_{ij}^{-1}K_j^{(1)}\right) \\ & + KIII^{(1)}\,\mathrm{Im}\left(m_{3i}N_{ij}^{-1}K_j^{(2)}\right) + KIII^{(2)}\,\mathrm{Im}\left(m_{3i}N_{ij}^{-1}K_j^{(2)}\right)\Big] \end{aligned} \tag{3-34}$$

It is now evident how the decomposition of displacements, strains, and stresses into separate equilibrium states is helpful. One can see that we have two definitions of the M-integral, equations (3-28) and (3-34). If they are equated, the individual SIFs ($KI^{(1)}$, $KII^{(1)}$, $KIII^{(1)}$) can be computed. But before that step, we must define 'auxiliary' solutions for the second equilibrium state, denoted by superscripts (2a, 2b, 2c). The terms with the (1) superscript are going be computed numerically via FE software.

The three auxiliary solutions are defined as: 2a, 2b, and 2c. For case 2a, $KI^{(2a)} = 1$ and $KII^{(2a)} = KIII^{(2a)} = 0$. For case 2b, $KII^{(2b)} = 1$ and $KI^{(2b)} = KIII^{(2b)} = 0$, and for case 2c, $KIII^{(2c)} = 1$ and $KI^{(2c)} = KII^{(2c)} = 0$. Since the SIFs are being prescribed beforehand, the stresses, for those equilibrium states, can be computed from (3-14). Now the two relations for the M-integral are equated

$$\frac{\displaystyle\int_{\Gamma}\left(\sigma_{ij}{}^{(1)}\frac{\partial u_i{}^{(2)}}{\partial x_1} + \sigma_{ij}{}^{(2)}\frac{\partial u_i{}^{(1)}}{\partial x_1} - W^{(1,2)}\delta_{1j}\right)\frac{\partial q}{\partial x_j}\,ds}{A_q} = -\frac{1}{2}\begin{bmatrix} KI^{(1)}\,\mathrm{Im}(m_{2i}N_{ij}{}^{-1}K_j{}^{(2)}) + \\ KI^{(2)}\,\mathrm{Im}(m_{2i}N_{ij}{}^{-1}K_j{}^{(1)}) + \\ KII^{(1)}\,\mathrm{Im}(m_{1i}N_{ij}{}^{-1}K_j{}^{(2)}) + \\ KII^{(2)}\,\mathrm{Im}(m_{1i}N_{ij}{}^{-1}K_j{}^{(1)}) + \\ KIII^{(1)}\,\mathrm{Im}(m_{3i}N_{ij}{}^{-1}K_j{}^{(2)}) + \\ KIII^{(2)}\,\mathrm{Im}(m_{3i}N_{ij}{}^{-1}K_j{}^{(2)}) \end{bmatrix} \tag{3-35}$$

From (3-35) we can assemble a system of equations that contain the three unknown SIFs we are after

$$\begin{bmatrix} 2\,\mathrm{Im}\left(m_{2i}N_{i1}^{-1}\right) & \mathrm{Im}\left(m_{1i}N_{i1}^{-1}+m_{2i}N_{i2}^{-1}\right) & \mathrm{Im}\left(m_{3i}N_{i1}^{-1}+m_{2i}N_{i3}^{-1}\right) \\ \mathrm{Im}\left(m_{2i}N_{i2}^{-1}+m_{1i}N_{i1}^{-1}\right) & 2\,\mathrm{Im}\left(m_{1i}N_{i2}^{-1}\right) & \mathrm{Im}\left(m_{3i}N_{i2}^{-1}+m_{1i}N_{i3}^{-1}\right) \\ \mathrm{Im}\left(m_{2i}N_{i3}^{-1}+m_{3i}N_{i1}^{-1}\right) & \mathrm{Im}\left(m_{1i}N_{i3}^{-1}+m_{3i}N_{i2}^{-1}\right) & 2\,\mathrm{Im}\left(m_{3i}N_{i3}^{-1}\right) \end{bmatrix} \begin{Bmatrix} KI^{(1)} \\ KII^{(1)} \\ KIII^{(1)} \end{Bmatrix} = \begin{Bmatrix} M^{(1,2a)}/A_q \\ M^{(1,2b)}/A_q \\ M^{(1,2c)}/A_q \end{Bmatrix} \tag{3-36}$$

Finally, we note that (3-36) involved the extraction of stresses near the crack tip. These stresses are taken from the Gauss point locations within the elements that encompass the crack front. Also, the integral in (3-36) is evaluated numerically using Gauss quadrature.

Computing SIFs Using Displacement Correlation

Displacement correlation (DC) is perhaps the oldest and simplest method to compute SIFs via FE displacements. Chan et al (1970) were among the first group of researchers to employ such a method to obtain SIFs this way. In general, the correlation point is selected where the crack tip displacements are the largest so the relative error in displacements is small. Another advantage in using such a method is the SIFs are separated into the three modes defined in Figure 3-2. In its most basic form, crack tip opening displacement (CTOD) can be used to determine the SIF by equating the displacements at the points in question to some analytical solution.

From equation (3-2) with $\omega = \pi$ and Figure 3-6 for a plane strain problem dealing with an isotropic material, we have

$$KI = \frac{\left(u_{yb} - u_{ya}\right)2\mu_s}{\kappa + 1}\sqrt{\frac{2\pi}{r}} \tag{3-37}$$

$$KII = \frac{\left(u_{xb} - u_{xa}\right)2\mu_s}{\kappa + 1}\sqrt{\frac{2\pi}{r}} \tag{3-38}$$

where μ_s, again, is the shear modulus determined by $E/2(1+\nu)$ and $\kappa = 3-4\nu$ for plane strain . We note that u_y and u_x are the opening and sliding modes of displacement. The above method is sometimes called a 'one-point' matching technique since it involves extracting displacements from one point near the crack tip. The downside of such a

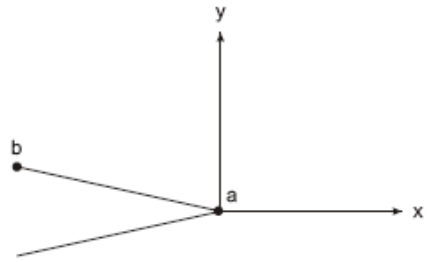

Figure 3-6. Correlation points typically used for displacement correlation

method is that very refined meshes are needed for accurate results. Improved accuracy is obtained through the use of a special element specifically designed to capture the singularity present at the crack tip.

From equation (3-1), we see how the stresses have a $1/\sqrt{r}$ singularity at the crack tip. For accurate computations, we would like our FE models to also have this singularity. Quarter point elements are one way to do this. The first attempts at modeling cracks were done so using quadrilateral elements with the mid-side nodes moved to quarter point locations (Barsoum, 1976) When this is done the desired strain singularity is achieved. However, one downside of using this type of element is that the singularity is only present on the edges that contain the quarter point. If triangular-shaped elements are used instead, the singularity exists both along the edges and within the element (Anderson, 1991).

In Figure 3-7, we see how an eight node quadrilateral element can be transformed to a triangle and then certain nodes are moved to the quarter point locations. Let us

derive how the required strain singularity is obtained along the edge of the quadrilateral element with the mid-side nodes moved to the quarter point locations. Consider the bottom edge of the element on the right in Figure 3-8. Nodes one, five, and two lie along this boundary. In order to show how the strain singularity comes about, we will need to list the shape functions for this particular element. The shape functions (Logan, 2002) for the isoparametric element at the corner nodes are

$$N_i = \frac{1}{4}\left(1+\xi\xi_i\right)\left(1+\eta\eta_i\right)\left(\xi\xi_i+\eta\eta_i-1\right) \tag{3-39}$$

where i is the number of the shape functions at the corresponding node (i.e. N_1 is the shape function for node 1) and

$$\begin{aligned} \xi_i &= -1,1,1,-1 \qquad (i=1,2,3,4) \\ \eta_i &= -1,-1,1,1 \qquad (i=1,2,3,4) \end{aligned} \tag{3-40}$$

We also have shape functions for the mid-side nodes

$$\begin{aligned} N_i &= \frac{1}{2}\left(1-\xi^2\right)\left(1+\eta\eta_i\right) \qquad t_i=-1,1 \qquad (i=5,7) \\ N_i &= \frac{1}{2}\left(1-\xi\xi_i\right)\left(1+\eta^2\right) \qquad \xi_i=-1,1 \qquad (i=6,8) \end{aligned} \tag{3-41}$$

The global origin is placed at the corner of the element. We will need the shape functions at nodes one, two, and five. Setting $\eta = -1$ we have

$$\begin{aligned} N_1 &= -\frac{1}{2}\xi\left(1-\xi\right) \\ N_2 &= \frac{1}{2}\xi\left(1+\xi\right) \\ N_5 &= \left(1-\xi^2\right) \end{aligned} \tag{3-42}$$

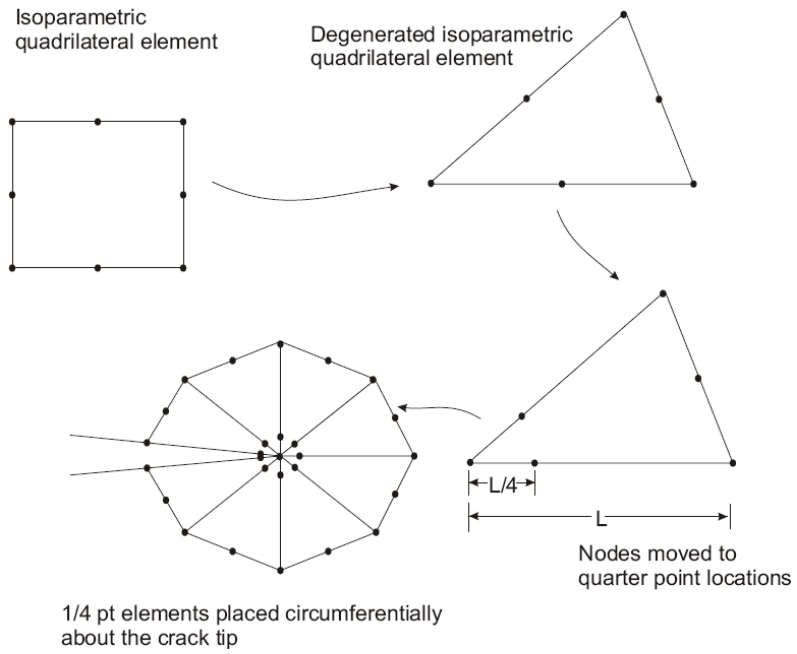

Figure 3-7. Triangular quarter point elements

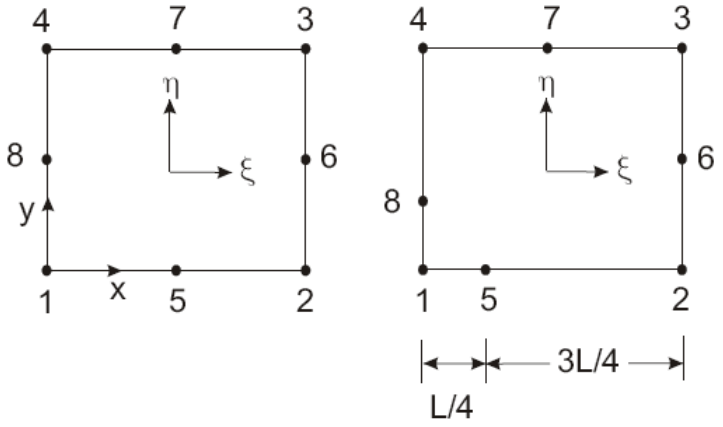

Figure 3-8. Isoparametric element and degenerated element with mid-side nodes moved to quarter point locations

The global x coordinate is related to the isoparametric coordinate system via

$$x = N_i x_i \tag{3-43}$$

where the repeated index is an implied summation. Setting $x_1 = 0$, $x_2 = L$, and $x_5 = L/4$ we have

$$x = \frac{1}{2}\xi(1+\xi)L + (1-\xi^2)\frac{L}{4} \tag{3-44}$$

We can now solve for ξ

$$\xi = 2\sqrt{\frac{x}{L}} - 1 \tag{3-45}$$

In the same way that we can relate the global x coordinate to the shape functions, we can also determine the displacements using the shape functions

$$u = N_i u_i \tag{3-46}$$

Again determining the displacements along the edge containing nodes one, two, and five we write

$$u = -\frac{1}{2}\xi(1-\xi)u_1 + \frac{1}{2}\xi(1+\xi)u_2 + (1-\xi^2)u_5 \tag{3-47}$$

Now we can substitute (3-45) into (3-47) to obtain

$$u = -\frac{1}{2}\left(-1+2\sqrt{\frac{x}{L}}\right)\left(2-2\sqrt{\frac{x}{L}}\right)u_1 + \left(-1+2\sqrt{\frac{x}{L}}\right)\left(2\sqrt{\frac{x}{L}}\right)u_2 + 4\left(\sqrt{\frac{x}{L}} - \frac{x}{L}\right)u_5 \tag{3-48}$$

We note that the displacement shown in (3-48) has a √x term present. This is consistent with equation (3-2) where the displacements vary with √r. We need to differentiate equation (3-48) to obtain the strain in the x direction

$$\varepsilon_x = \frac{\partial u}{\partial x} = -\frac{1}{2}\left(\frac{3}{\sqrt{xL}} - \frac{4}{L}\right)u_1 + \frac{1}{2}\left(-\frac{1}{\sqrt{xL}} + \frac{4}{L}\right)u_2 + \left(\frac{2}{\sqrt{xL}} - \frac{4}{L}\right)u_5 \tag{3-49}$$

Finally, it is shown in (3-49) how the strain displays the desired singularity (x-1/2). One can see why the quarter point element has been the standard for modeling cracks for the past 30 years. No special programming, or internal tampering, with the FE code is required. Any FE program that carries quadratic, or higher order, elements can support these special ones with the nodes moved to the quarter points.

Let us now return to our discussion of using displacement correlation to extract SIFs from FE models. If quarter point elements are used, equations (3-37) and (3-38) are modified because r = L/4

$$KI = \frac{\left(u_{yb} - u_{ya}\right)4\mu_s}{\kappa + 1}\sqrt{\frac{2\pi}{L}} \tag{3-50}$$

$$KII = \frac{\left(u_{xb} - u_{xa}\right)4\mu_s}{\kappa + 1}\sqrt{\frac{2\pi}{L}} \tag{3-51}$$

The SIFs extraction via the DC method need not be restricted to just one set of nodes, or correlation points. One can also consider the displacements over the whole element. The form of these equations depends on the shape functions of the elements. Ingraffea and Manu (1980) derive a DC extraction method using 3-D elements. This formulation is particularly useful to the present study since 3-D simulations are used to model the fracture response of the foam material. Ingraffea and Manu use a special labeling convention shown in Figure 3-10 for a collapsed 20 node brick element (Figure 3-9), also known as a 15 node wedge.

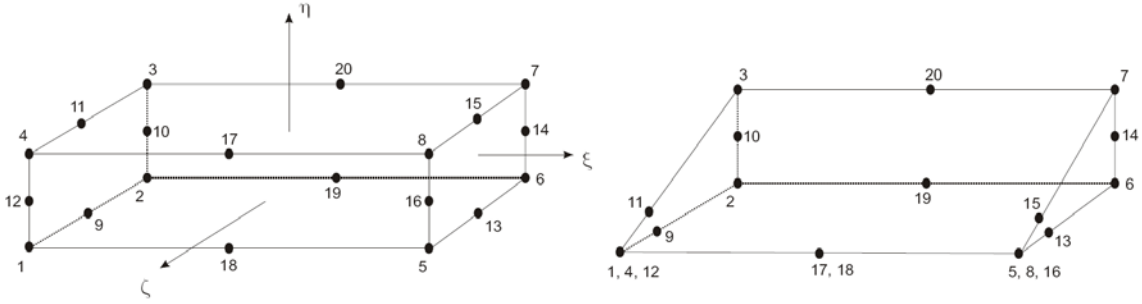

Figure 3-9. 20 node brick and 15 node wedge elements

The shape functions for a 20 node brick element are listed below. The local (ξ,η,ζ) coordinate system is placed at the center of the brick element. For the corner nodes at positions i = 1,2…8 and ξi, ηi, ζi = ±1

$$N_i = \frac{(1+\xi\xi_i)(1+\eta\eta_i)(1+\zeta\zeta_i)}{8}(\xi\xi_i + \eta\eta_i + \zeta\zeta_i - 2) \tag{3-52}$$

For the nodes at positions i = 17, 18, 19, 20 and $\xi_i = 0$, $\eta_i = \pm 1$, $\zeta_i = \pm 1$

$$N_i = \frac{(1-\xi^2)(1+\eta\eta_i)(1+\zeta\zeta_i)}{4} \tag{3-53}$$

At i = 10, 12, 14, 16 and $\xi_i = \pm 1$, $\eta_i = 0$, $\zeta_i = \pm 1$

$$N_i = \frac{(1+\xi\xi_i)(1-\eta^2)(1+\zeta\zeta_i)}{4} \tag{3-54}$$

Finally, for the nodes at positions i = 9, 11, 13, 15 and $\xi_i = \pm 1$, $\eta_i = \pm 1$, $\zeta_i = 0$

$$N_i = \frac{(1+\xi\xi_i)(1+\eta\eta_i)(1+\zeta^2)}{4} \tag{3-55}$$

For anisotropic materials, Saouma and Sikiotis (1986) extend Ingraffea's work for anisotropic materials. They use the displacement relations developed by Sih *et al*. A similar procedure is followed in this study, but instead of using displacement equations from Sih et al's paper, the relations in (3-16) are to be employed. The equations to determine the anisotropic Ks, using Hoenig's displacement equations, are as follows

$$\begin{Bmatrix} KI \\ KII \\ KIII \end{Bmatrix} = [B]^{-1}\sqrt{\frac{\pi}{2L}}[A] \tag{3-58}$$

where [B] is

$$[B] = \mathrm{Re}\begin{bmatrix} m_{1j}N^{-1}{}_{jl}\left(\cos\omega + \mu_j \sin\omega\right) \\ m_{2j}N^{-1}{}_{jl}\left(\cos\omega + \mu_j \sin\omega\right) \\ m_{3j}N^{-1}{}_{jl}\left(\cos\omega + \mu_j \sin\omega\right) \end{bmatrix} \tag{3-59}$$

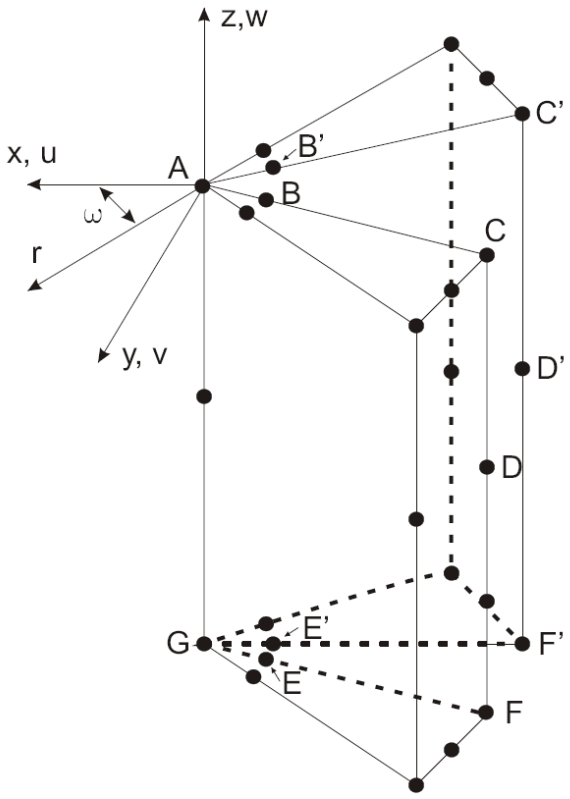

Figure 3-10. Collapsed 20-node brick element

$$\begin{bmatrix} 2v_B - v_C + 2v_E + v_F - 2v_{B'} + v_{C'} - 2v_{E'} + v_{F'} - v_{D'} + \frac{1}{2}\xi\left(-4v_B + v_C + 4v_E - v_F + 4v_{B'} - v_{c'} - 4v_{E'} + v_{F'}\right) \\ + \frac{1}{2}\xi^2\left(v_F + v_C - 2v_D - v_{F'} - v_{C'} - 2v_{D'}\right) \\ 2u_B - u_C + 2u_E + u_F - 2u_{B'} + u_{C'} - 2u_{E'} + u_{F'} - u_{D'} + \frac{1}{2}\xi\left(-4u_B + u_C + 4u_E - u_F + 4u_{B'} - u_{c'} - 4u_{E'} + u_{F'}\right) \\ + \frac{1}{2}\xi^2\left(u_F + u_C - 2u_D - u_{F'} - u_{C'} - 2u_{D'}\right) \\ 2w_B - w_C + 2w_E + w_F - 2w_{B'} + w_{C'} - 2w_{E'} + w_{F'} - w_{D'} + \frac{1}{2}\xi\left(-4w_B + w_C + 4w_E - w_F + 4w_{B'} - w_{c'} - 4w_{E'} + w_{F'}\right) \\ + \frac{1}{2}\xi^2\left(w_F + w_C - 2w_D - w_{F'} - w_{C'} - 2w_{D'}\right) \end{bmatrix} \quad (3\text{-}57)$$

Once again, the repeated indices are an implied summation. The terms in the B matrix only depend on the roots of the sixth order characteristic equation.

Effects of Temperature on the SIF Solution

In chapter two it is pointed out that temperature plays no small role in causing the foam to break off from the ET. For example, when Shuttle is resting on the launching

pad, one side of the foam is exposed to the temperature of liquid hydrogen and oxygen; roughly -300^{o}F. The other side of the foam is exposed to air, perhaps at 75 ^{o}F prior to liftoff. Over typical acreage sprays, the foam is approximately three inches thick. This small thickness coupled with a large thermal gradient suggests that thermal strains could be significant. As shown with the divot testing in chapter two, even though there are no applied far-field mechanical loads, the thermal gradient seems to be sufficient enough to impart stresses capable of driving a crack toward the surface of the ET resulting in a loss of material.

To account for thermal strains, we simply add this term to our constitutive matrix. Following Hyer (1998), the stress-strain relations can be written as

$$\begin{Bmatrix} \varepsilon_{11} - \varepsilon^{Th}{}_{11}(T, T_{ref}) \\ \varepsilon_{22} - \varepsilon^{Th}{}_{22}(T, T_{ref}) \\ \varepsilon_{33} - \varepsilon^{Th}{}_{33}(T, T_{ref}) \\ \gamma_{23} \\ \gamma_{13} \\ \gamma_{12} \end{Bmatrix} = \begin{bmatrix} S_{11} & S_{12} & S_{13} & 0 & 0 & 0 \\ S_{21} & S_{22} & S_{23} & 0 & 0 & 0 \\ S_{31} & S_{32} & S_{33} & 0 & 0 & 0 \\ & & & S_{44} & 0 & 0 \\ & & & & S_{55} & 0 \\ sym & & & & & S_{66} \end{bmatrix} \begin{Bmatrix} \sigma_{11} \\ \sigma_{22} \\ \sigma_{33} \\ \sigma_{23} \\ \sigma_{13} \\ \sigma_{12} \end{Bmatrix} \tag{3-60}$$

where the total strain is $\{\varepsilon_{11}\, \varepsilon_{22}\, \varepsilon_{33}\, \gamma_{23}\, \gamma_{13}\, \gamma_{12}\}^{T}$, $\varepsilon^{Th}{}_{11}(T, T_{ref})$ is the free thermal strain in the 11-direction, and T_{ref} is the reference temperature. The mechanical strains are

$$\begin{Bmatrix} \varepsilon_{11}{}^{mech} \\ \varepsilon_{22}{}^{mech} \\ \varepsilon_{33}{}^{mech} \\ \gamma_{23}{}^{mech} \\ \gamma_{13}{}^{mech} \\ \gamma_{12}{}^{mech} \end{Bmatrix} = \begin{Bmatrix} \varepsilon_{11} - \varepsilon^{Th}{}_{11}(T, T_{ref}) \\ \varepsilon_{22} - \varepsilon^{Th}{}_{22}(T, T_{ref}) \\ \varepsilon_{33} - \varepsilon^{Th}{}_{33}(T, T_{ref}) \\ \gamma_{23} \\ \gamma_{13} \\ \gamma_{12} \end{Bmatrix} \tag{3-61}$$

or, stated more concisely the total strain is

$$\boldsymbol{\varepsilon}_{total} = \boldsymbol{\varepsilon}^{mech} + \boldsymbol{\varepsilon}^{thermal} \tag{3-62}$$

If the thermal expansion is linear with the temperature change, we can rewrite (3-60) as

$$\begin{Bmatrix} \varepsilon_{11}-\alpha_1\Delta T \\ \varepsilon_{22}-\alpha_2\Delta T \\ \varepsilon_{33}-\alpha_3\Delta T \\ \gamma_{23} \\ \gamma_{13} \\ \gamma_{12} \end{Bmatrix} = \begin{bmatrix} S_{11} & S_{12} & S_{13} & 0 & 0 & 0 \\ S_{21} & S_{22} & S_{23} & 0 & 0 & 0 \\ S_{31} & S_{32} & S_{33} & 0 & 0 & 0 \\ & & & S_{44} & 0 & 0 \\ & & & & S_{55} & 0 \\ sym & & & & & S_{66} \end{bmatrix} \begin{Bmatrix} \sigma_{11} \\ \sigma_{22} \\ \sigma_{33} \\ \sigma_{23} \\ \sigma_{13} \\ \sigma_{12} \end{Bmatrix} \tag{3-63}$$

The α_i term is the coefficient of thermal expansion and ΔT is the difference of temperature between the state of interest and the reference state.

The above equations allow us to compute thermal strains in the numerical models. Incorporating thermal and mechanical loads will involve two separate steps because a thermal gradient implies that a temperature distribution must be obtained before solving the model that contains both the thermal and mechanical boundary conditions. The first step is to solve the conduction problem using the thermal conductivity coefficient listed in chapter two. The nodal temperature distribution is saved for later use. In a subsequent run, now with mechanical loads, the nodal temperatures are carried over as body forces along with any applied mechanical loads.

Summary

Summing up, the analytical expressions from Hoenig's near-tip solution is presented. His equations depend solely on the roots of the characteristic equation and the stress intensity factor, *K*. Hoenig's solution is not as well known as Sih et al's paper and as such the vast majority of studies dealing with near-tip solutions for cracked anisotropic bodies use the Sih et al formulae to compute the stresses. This is acceptable as long as one realizes those particular equations are valid for certain configurations where a decoupling of in-plane and out-of-plane displacements takes place. Hoenig's solution is

more general and his formulation of the energy release rate is the one chosen to compute the SIFs within the FRANC3D software. The DC technique presented also uses Hoenig's equations, but only the ones that pertain to displacements.

These two methods, interaction integral and DC, are presented to show how the mode I-III SIFs can be computed. These formulations are different in a few ways. Computing K with the J-integral is inherently more accurate because only a moderate level of mesh refinement is needed for the solution. However, the implementation of such a method is very involved. Alternatively, the DC approach is much easier to apply but the accuracy of the solution does depend on the level of mesh refinement.

Finally, the relations dealing with handling thermal strains are presented. These equations assume an expansion that is linear with temperature change. Handling thermal loads is straightforward by first solving the conduction problem to obtain the nodal temperature distribution. With that, those values are forwarded as body forces that are applied alongside the mechanical loads.

CHAPTER 4
CRACK TURNING THEORY AND FINITE ELEMENT MODELING

Crack Turning Theory

There are three theories prevalent in the literature to predict incipient crack turning angles for isotropic materials: maximum energy release rate, minimum strain energy density, and maximum hoop stress. All of these theories are based on LEFM concepts and were initially developed from experiments involving brittle plates.

The turning theory proposed by Hussain *et al.* (1974) seeks the direction where the energy release rate, G, will be a maximum. The minimum strain energy density theory (Sih, 1974) postulates crack turning in the direction where the strain energy density is at a minimum. The maximum hoop stress theory proposed by Erdogan and Sih (1963) predicts crack propagation in the direction where σ_{ω}, defined in equation (4-1), is a maximum relative to the crack tip. Crack turning, in this study, denotes the incipient turning angle. We define the crack turning angle, ω_c, below in Figure 4-1.

For isotropic materials, the near-tip stresses (in the r, ω polar coordinate system) have been derived by Williams (1957). If the derivative with respect to theta of equation (4-1) is taken and set to zero, the critical angle, ω_c, can be determined; equation (4-4).

$$\sigma_{\omega} = \frac{1}{\sqrt{2\pi r}} \cos\frac{\omega}{2}\left[KI\cos^2\frac{\omega}{2} - \frac{3}{2} KII \sin\omega \right] \tag{4-1}$$

$$\sigma_{r} = \frac{1}{\sqrt{2\pi r}} \cos\frac{\omega}{2}\left[KI\left(1+\sin^2\frac{\omega}{2}\right) + \frac{3}{2} KII \sin\omega - 2KII\tan\frac{\omega}{2} \right] \tag{4-2}$$

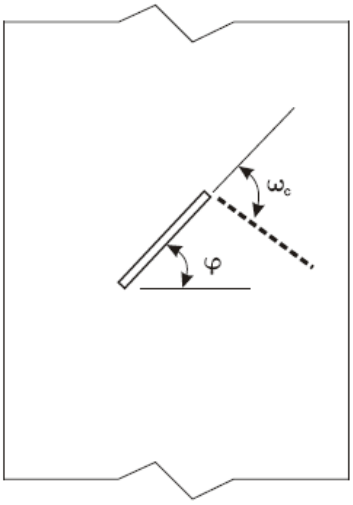

Figure 4-1. Definition of crack turning angle

$$\sigma_{r\omega} = \frac{1}{2\sqrt{2\pi r}} \cos\frac{\omega}{2}\left[KI \sin\omega + KII\left(3\cos\omega - 1\right)\right] \tag{4-3}$$

$$\omega_c = 2\tan^{-1}\left(\frac{1-\sqrt{1+8(KII/KI)^2}}{4(KII/KI)}\right) \tag{4-4}$$

The maximum hoop stress theory is the easiest to implement and that is perhaps the main reason why it is widely used for turning angle predictions. The minimum strain energy density criterion is also very popular and there is some debate (Gdoutos, 1984) as to which one is superior. Some might argue that it is not correct to use just a single component of stress to predict the incipient turning angle, whereas a quantity such as strain energy density seems to be more comprehensive as all components of stress and strain are included. Maccagno and Knott (1989, 1992) study mixed-mode facture behavior of PMMA and lightly tempered steel alloys and in both cases the crack turning angles are well approximated by the maximum tangential stress theory.

There have been some topical investigations for crack turning within materials that have direction dependent properties. Buzcek and Herakovich (1985) predict the crack

extension angle for orthotropic materials and some of the recent work in this area mirrors their ideas. They assume the tensile strength, *T*, of the orthotropic material varies with direction, η. Since it is difficult to measure the strength of a material in all possible orientations, they assume that $T = f(\eta, \theta, X_T, Y_T)$ where η is the angle in a polar coordinate system, θ is the material orientation and X_T and Y_T are the strengths of the material in the axial and fiber directions respectively (they are analyzing orthotropic composites). The equation for T, also denoted as a fracture resistance parameter, must be independent of η if the material is isotropic. The lowest order function that satisfies these requirements is an ellipse. This function is plotted in Figure 4-2 in ($T_{\eta\eta}$, η) polar coordinates. Now $T_{\eta\eta}$ can be expressed as

$$T_{\eta\eta} = X_T \sin^2 \eta + Y_T \cos^2 \eta \tag{4-5}$$

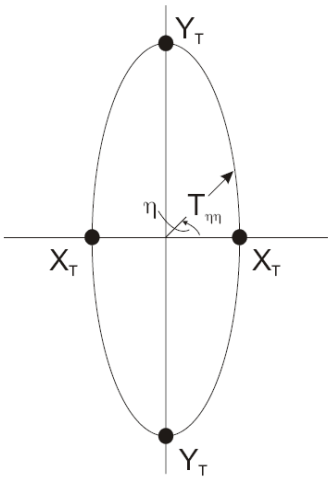

Figure 4-2. Elliptical relationship for $T_{\eta\eta}$

The crack will turn, according to Buzek and Herakovich, in the direction where the ratio of the hoop stress to T is a maximum. The hoop stress, sometimes called the tangential stress (or σ_ω), is defined in Figure 4-3. Consider a point P and a vector

connecting that point to the crack tip. The hoop stress is normal to this vector that connects P to the crack tip.

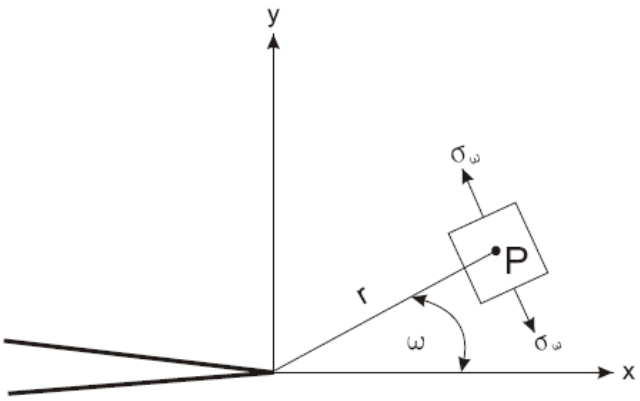

Figure 4-3. Definition of hoop stress

Mixed mode crack propagation in anisotropic materials is also investigated by Saouma *et al.* (1987). The near-tip stresses are obtained via Sih *et al.* (1965) and in their analysis the maximum tangential stress theory is used to predict the angle of propagation. Saouma *et al.* use a slightly different criterion for crack turning, but it is of similar flavor to what Buzek and Herakovich propose. Instead of using strength as a fracture resistance parameter, the plane strain fracture toughness is utilized.

Boone *et al.*1987) use FE models to study crack propagation in orthotropic materials. The idea of maximizing the ratio of the hoop stress to some strength parameter is once again utilized to predict the crack turning angle. Chen (1999) analyzes crack propagation in aircraft fuselages. He, too, makes use of a ratio of the hoop stress to the plane strain fracture toughness. In this case, the material in question has isotropic elastic moduli, but the fracture properties are direction dependent. A similar analysis is conducted by Pettit (2000). He examines crack turning in rolled aluminum, which again, has isotropic stiffness properties but anisotropic fracture characteristics.

Carloni *et al.* (2003) and Nobile and Carloni (2005) consider incipient crack turning for an orthotropic plate under biaxial loading. The former researchers utilize essentially the same fracture resistance parameter as Buzek and Herakovich, whereas the latter study uses a slightly modified version of the Saouma *et al.* turning criterion. Carloni *et al.* and Nobile and Carloni also call on complex variables and stress functions in their formulations for near-tip stresses. Both studies, however, make assumptions that reduce the order of the characteristic equation that arises in such derivations (see chapter three), down to order four.

While Pettit's analysis is for a material with isotropic stiffness properties, he generalizes the fracture resistance parameter to three dimensions. His analysis accounts for an arbitrary location of the crack with respect to the material. Thus, we would like to use the method to obtain stress intensity factors given by Banks-Sills *et al.* (2005) in conjunction with Pettit's formulation for a fracture resistance parameter. This approach is a bit more generalized than the aforementioned studies because their work seems to be confined to specific configurations that usually decouple the in-plane and anti-plane displacements.

Pettit's method for determining the fracture resistance is formulated for orthotropic materials which possess cubic symmetry, i.e. three orthogonal planes of symmetry and within each plane lay two principal toughness values resulting in six principal toughness values: K_{12}, K_{21}, K_{23}, K_{32}, K_{13}, and K_{31}. The first number in that nomenclature is the vector normal to the crack plane and the second number corresponds to the direction of propagation. It is difficult to obtain a toughness for all possible orientations for materials that exhibit some form direction dependence. Essentially we are interpolating between

the six principal toughness values for the orthotropic material. This gives us an estimate of the toughness in any direction we desire. Consider Figure 4-4 and the material orientation as shown. What we see in that figure is block of foam with various M(T) specimens oriented within it. If the M(T) specimens are aligned with the principal axes of the large block of foam, there are six possible orientations and with each orientation there is a corresponding toughness.

Pettit's interpolation equation, then, requires six unique toughness values for the orientations shown in Figure 4-4. In our case, only three toughness values are needed, however. In Figure 4-4, consider the M(T) specimens that have the K_{31} and K_{32} labels. Here the load is applied in the 3-direction and the crack is propagating in the 1 and 2-directions, respectively. Since the 3-direction is the rise direction and the 1-2 plane is a plane of isotropy, it is reasonable to assume that $K_{31} = K_{32}$. That is to say, the crack is resting in the plane of the knit line for those two cases. For the other four cases, the fracture plane is normal to the knit line plane. Thus, $K_{21} = K_{12}$ and $K_{13} = K_{23}$. So the total number of required toughness values has been reduced to three and NASA did conduct tests, at room temperature, to obtain them: $K_{32} = 22.4$ psi$\sqrt{\text{in}}$, $K_{12} = 17.4$ psi$\sqrt{\text{in}}$, and $K_{23} = 19.5$ psi$\sqrt{\text{in}}$.

Pettit's equation that will determine the effective K needs several variables besides the six principal toughness values. Remember, the goal here is to try and predict the direction of propagation. We can conveniently describe this direction with a vector, denoted as **a**. That vector lies in a plane tangent to the fracture surface, whose normal vector will be defined as **n**. These two vectors are shown in Figure 4-5.

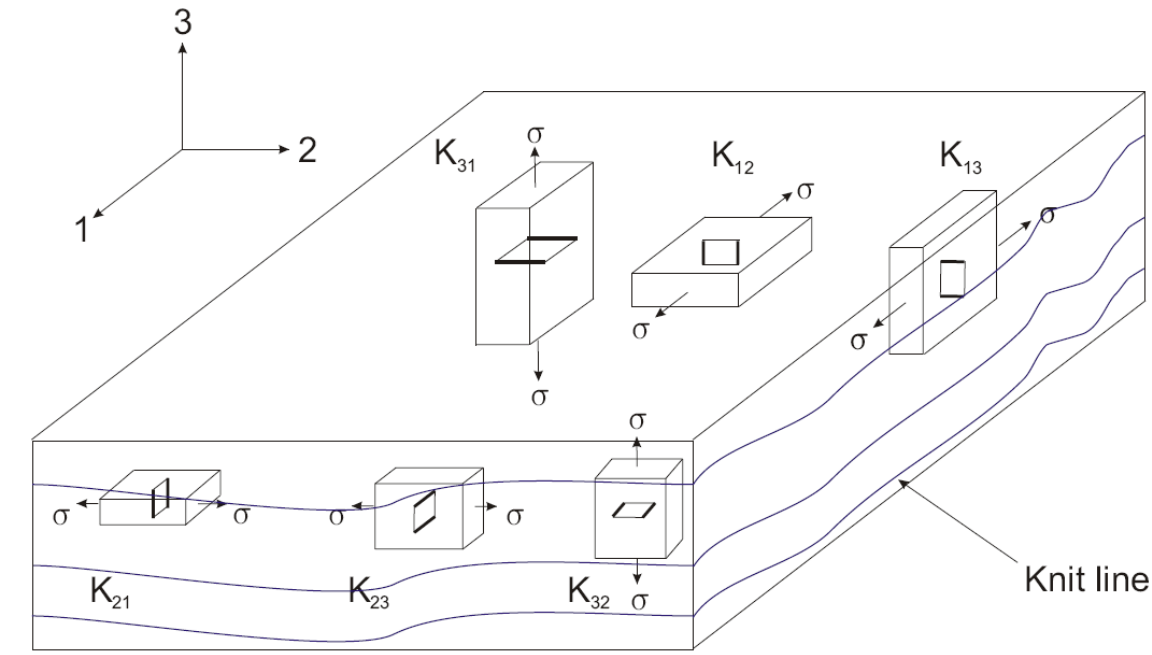

Figure 4-4. Orthotropic toughness values

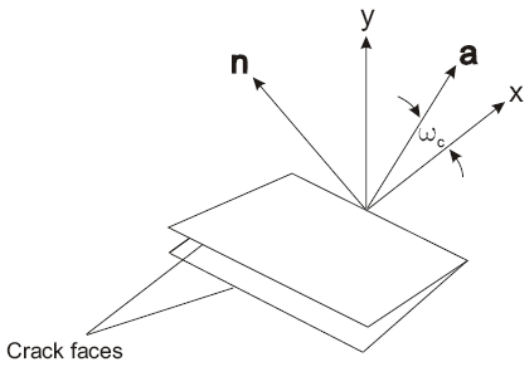

Figure 4-5. Definition of the **a** and **n** vectors

To develop the equation for the effective K, we first define the trace angles of the vector **a** makes with the principal planes. These are

$$\tan(\omega_1) = \frac{a_3}{a_2} \qquad \tan(\omega_2) = \frac{a_1}{a_3} \qquad \tan(\omega_3) = \frac{a_2}{a_1} \tag{4-6}$$

The subscript in the theta term denotes the axis normal to the principal plane. Using equation (4-5) we can write a 2D interpolation function of the form

$$K_k\left(\omega_k\right) = K_{ki}\cos^2\left(\omega_k\right) + K_{kj}\sin^2\left(\omega_k\right) \tag{4-7}$$

We also observe the following trigonometric identities

$$\begin{aligned}\cos^2\left(\tan^{-1}\frac{b}{c}\right) &= \frac{c^2}{b^2+c^2}\\ \sin^2\left(\tan^{-1}\frac{b}{c}\right) &= \frac{b^2}{b^2+c^2}\end{aligned} \tag{4-8}$$

and the components of unit vector **a** must satisfy the relation

$$a_1^{\,2} + a_2^{\,2} + a_3^{\,2} = 1 \tag{4-9}$$

Pettit goes on to define equations that can be interpreted as the fracture resistance components of **a** in the principal planes. Consider Figure 4-4 once more where the 1-axis is the loading direction. To estimate an effective K on this plane, we will interpolate between two toughness values, K_{12} and K_{13}. Using (4-7) through (4-9) we can write K_1 as

$$K_1(a) = \frac{1}{1-a_1^{\,2}}\left(K_{12}a_2^{\,2} + K_{13}a_3^{\,2}\right) \tag{4-10}$$

In a similar fashion we can determine K_2 and K_3

$$\begin{aligned}K_2(a) &= \frac{1}{1-a_2^{\,2}}\left(K_{23}a_3^{\,2} + K_{21}a_1^{\,2}\right)\\ K_3(a) &= \frac{1}{1-a_3^{\,2}}\left(K_{31}a_1^{\,2} + K_{32}a_2^{\,2}\right)\end{aligned} \tag{4-11}$$

Finally, Pettit sums the relations in (4-10) through (4-11). The effective K, denoted as K_p, can now be written as

$$\begin{aligned}K_p(\mathrm{a},\mathrm{n}) = K_1n_1^{\,2} + K_2n_2^{\,2} + K_3n_3^{\,2} &= \frac{n_1^{\,2}}{1-a_1^{\,2}}\left(K_{12}a_2^{\,2} + K_{13}a_3^{\,2}\right)\\ &+ \frac{n_2^{\,2}}{1-a_2^{\,2}}\left(K_{23}a_3^{\,2} + K_{21}a_1^{\,2}\right) + \frac{n_3^{\,2}}{1-a_3^{\,2}}\left(K_{31}a_1^{\,2} + K_{32}a_2^{\,2}\right)\end{aligned} \tag{4-12}$$

FE Modeling of the M(T) Specimen

While the importance of crack turning was made evident by the divot test, this experiment is highly specialized and is not recognized as a standard fracture test specimen. A more conventional way of analyzing crack turning can be performed with the middle tension, M(T), test specimen. Material orientation, mode mixity, and boundary conditions can all be carefully controlled with the M(T) specimen.

The idea behind creating FE models of M(T) specimens is two-fold. One of the objectives of this study is to examine the effect of mode mixity on the K-solution, or stated differently, as the material orientation is changed how does this impact KI-KIII along the crack front? Also, several foam M(T) specimens were fabricated and the resulting crack turning angles measured. Numerical predictions, based on Ks extracted from the FE models are used to make predictions via the maximum hoop stress theory discussed earlier.

M(T) FE models are built using ANSYS FE software. Crack meshing is handled by FRANC3D, a FE software package developed by the Cornell Fracture Group. Figure 4-6 shows a schematic of the M(T) specimen and Figure 4-7 displays one of the FE models used in this analysis. The FE model has a unit applied pressure at the top and bottom faces and is simply supported. The model is comprised of entirely of SOLID92 and SOLID95 elements (ANSYS™, 1999) which are used to make 3D models and have the capability to handle anisotropic material properties. The model is twelve inches high, five-and-a-half inches wide, and an inch-and-half thick. The boxed in area in Figure 4-7 highlights the densely meshed region containing the crack.

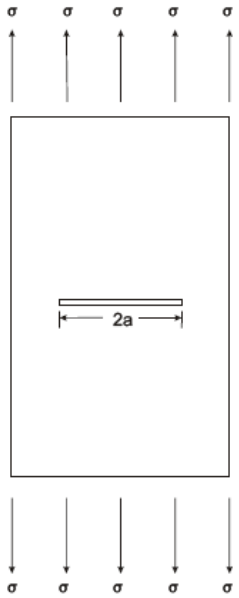

Figure 4-6. Schematic of M(T) specimen

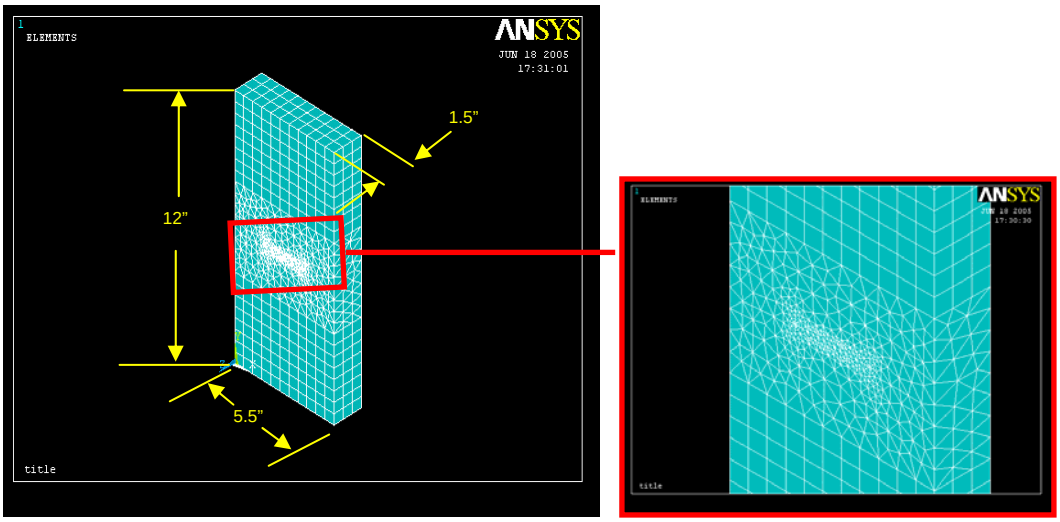

Figure 4-7. M(T) model created in ANSYS

Since the foam has direction dependent properties, this needs to be accounted for in the FE models. This is best done by using direction cosines. Using Figure 4-8, let us look at simple transformation of axes to define a new material orientation. Consider two sets of axes: x, y, z and x', y', z'. Initially, the both sets of axes are aligned and then a rotation, anti-clockwise (of angle zeta) about the x axis, takes place. Table 4-1 lists the

direction cosines, i.e. the cosines of the angles between the primed and unprimed axes. Here α_1 is the cosine of the angle between the x' and x axis, α_2 is the cosine of the angle between the y' and x axis, and so on. We will examine several material orientations with different initial crack inclinations. In this way, mode mixity is introduced into the problem and we also examine the effect of material orientation on the predicted propagation path.

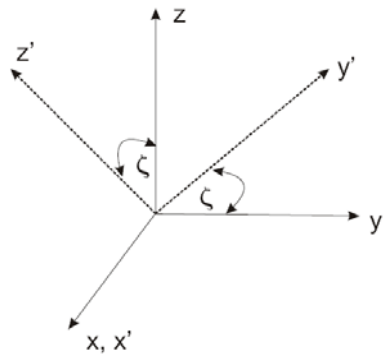

Figure 4-8. Sample transformation

Table 4-1. Direction cosines

	x	y	z
x'	α_1	β_1	γ_1
y'	α_2	β_2	γ_2
z'	α_3	β_3	γ_3

As mentioned in an earlier section, for typical acreage sprays there is little offset between the material and substrate coordinate systems except when the foam is applied near fittings and/or bolts where the foam can to rise at angles as high as 30 degrees relative to the ET. Twelve M(T) fracture test samples with varying material orientation and crack inclination were fabricated and tested. A broken M(T) specimen is shown in Figure 4-9 and a comparison between the numerical prediction and the measured turning

angle, as well as how the foam M(T) specimens are fabricated, will be made in chapter five.

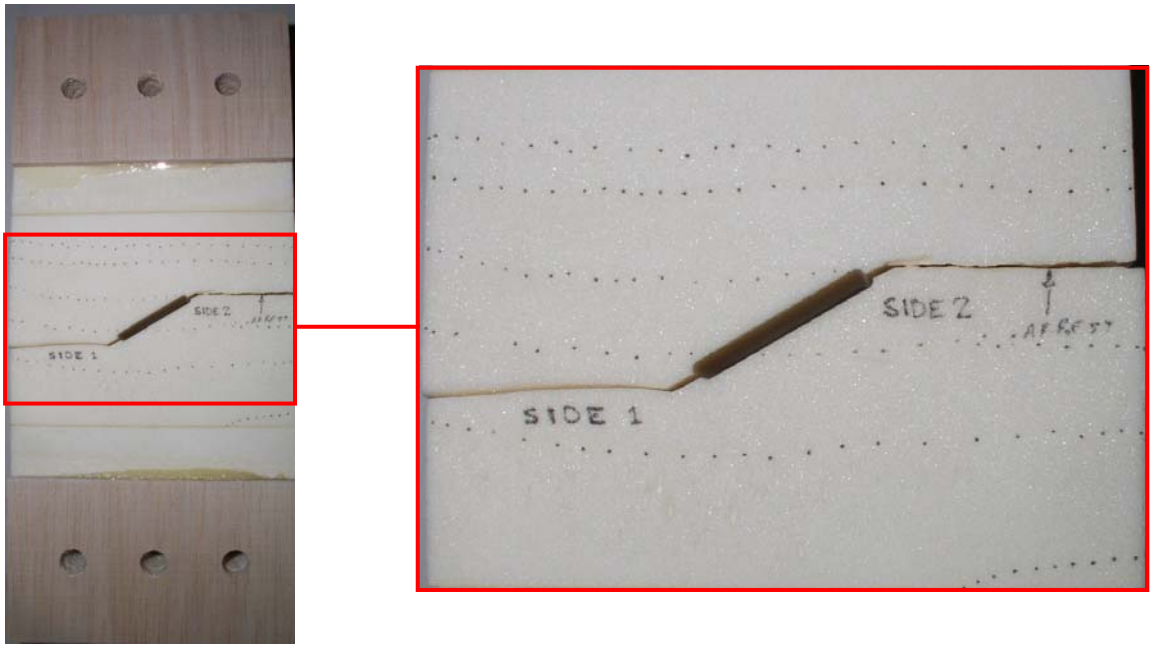

Figure 4-9. Fractured M(T) specimen: the dotted line is added to show the location of the knit line

CHAPTER 5
RESULTS AND DISCUSSION

Effect of Material Orientation on the SIF Solution

On most sections of the ET, the foam is sprayed on in such a fashion that it rises normal to the surface. In that sense, there is very little offset between the tank (substrate) coordinate system and the foam (material) coordinate system. Also, when modeling these specimens, we should note that the curvature of the ET is rather large; some 28 ft in diameter and our specimens tend to include small defects (usually two inches). Thus, it seems reasonable to assume that curvature effects are minimal. But when the spraying process takes place near a bolt or fitting point, the foam must be applied around, and over top of, these parts. In this situation it is possible to have the foam rising at different angles relative to the surface.

The anisotropic nature of the foam requires 3-D FE models to be employed so the SIFs can be evaluated along the crack front. To that end, the effect of material orientation on the K-solution will be examined within models that have both straight and diagonal cracks. Before moving on with this discussion, let us define a few important terms that we will use extensively throughout this chapter. The crack inclination angle, φ, is the angle the crack makes with the horizontal as shown in Figure 5-1. M(T) models use though-cracks, or flaws that are placed through the thickness of the specimen, or model, in question. The crack front distance defined as the length of the crack in the thickness direction, shown in Figure 5-2.

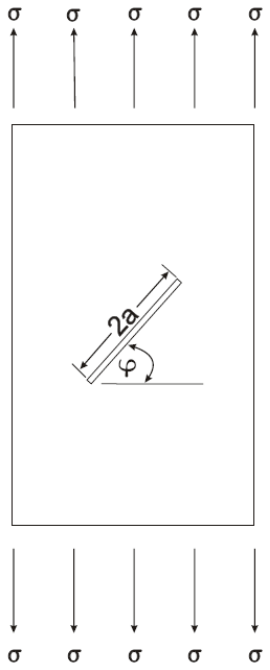

Figure 5-1. Definition of crack inclination angle

To analyze the effect of material orientation of the SIF solution, 17 material orientation cases are defined; see Figures 5-4 and 5-5. M(T) models are constructed using ANSYS™ FE software and the flaw is inserted using FRANC3D Next Generation.

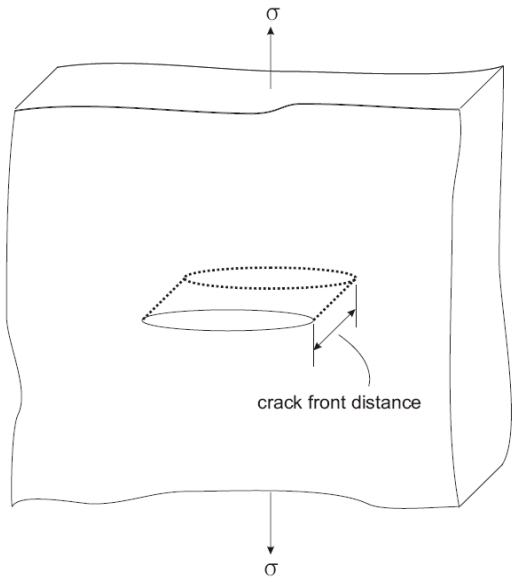

Figure 5-2. Definition of crack front distance

A unit pressure is applied to the simply supported M(T) models and in all cases, the crack length is two inches. A picture of the ANSYS model (with dimensions) is shown below. The material orientations are also input into the FE models along with the loads

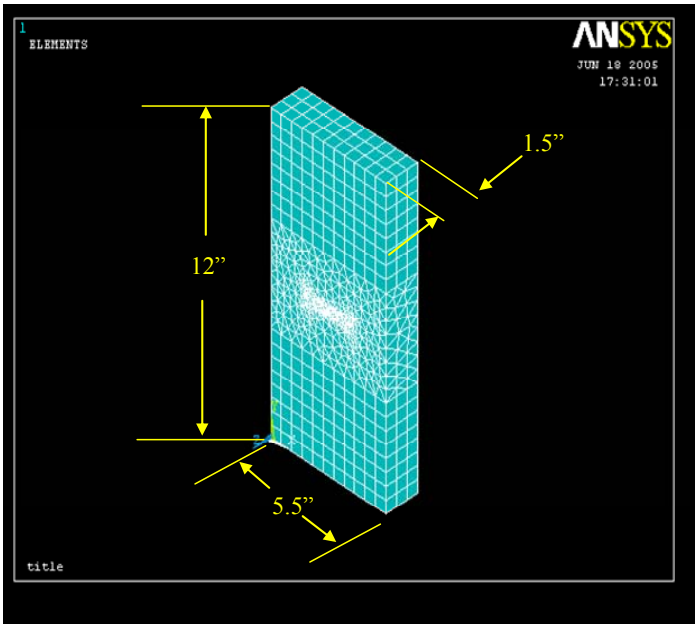

Figure 5-3. M(T) model built in ANSYS

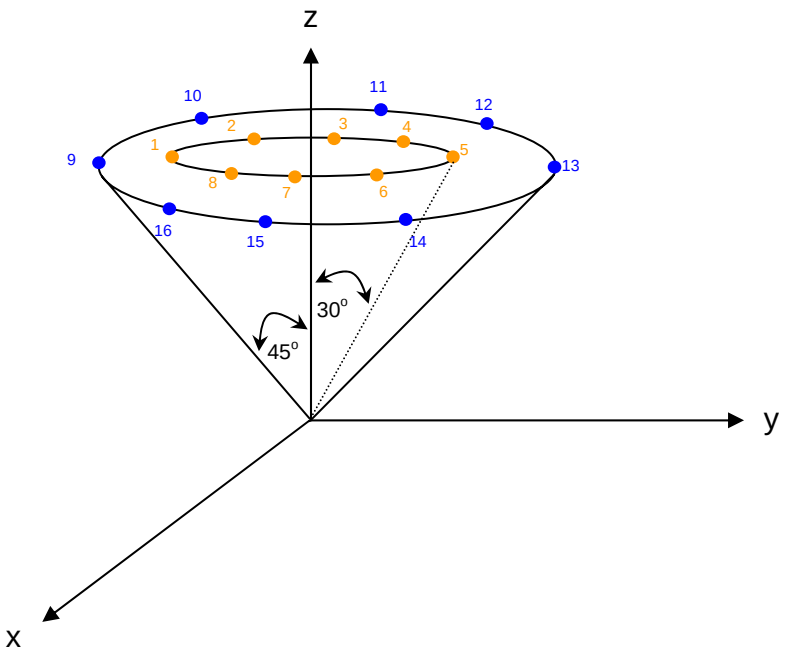

Figure 5-4. Definition of material orientation

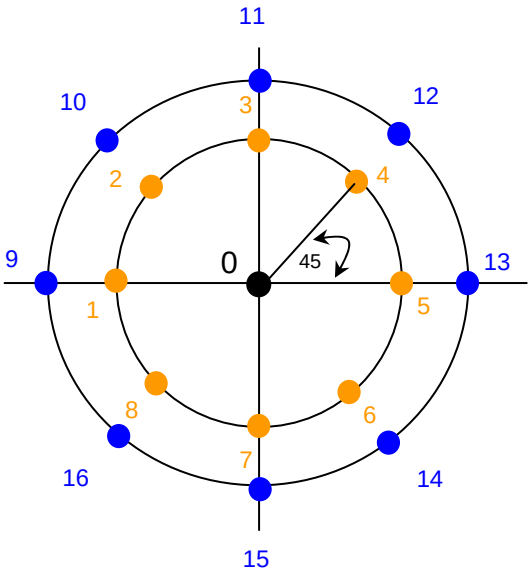

Figure 5-5. Top view of the cones shown in Figure 5-4

and boundary conditions. There are many different orientations at which the foam can rise relative to the tank. But when the foam is sprayed down, at some locations, the rise direction relative to the tank can be as high as thirty degrees. An example of this happening is shown in Figure 5-5.

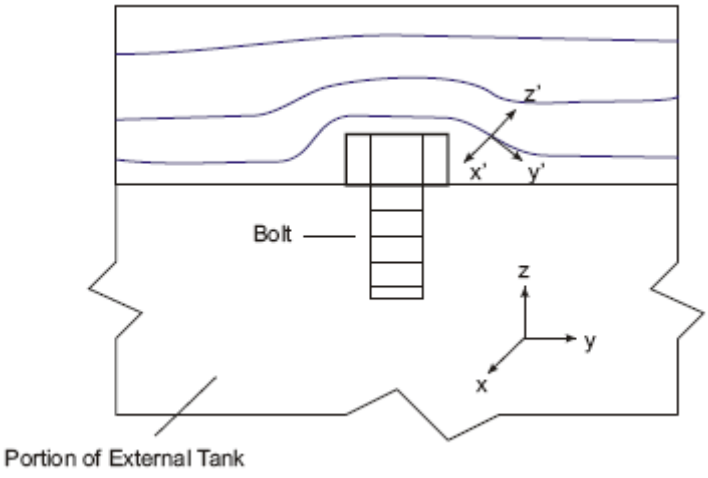

Figure 5-6. Hypothetical material orientation relative to the ET

One can see how the foam can rise at angle when it sprayed out the bolt shown in the above in Figure 5-6. As such we would like to have a reasonable 'tolerance' that the rise

direction can fall into. This would give rise to a range, or set, of possible orientations that could occur when the foam is being applied. Since the foam can rise at thirty degrees, it might be interesting to examine the possibility of the foam rising at another, larger, angle; 45 degrees, for example. Thus we now have two possible cases to examine; a rise angle that is typical near fitting points and bolts, and one that is slightly larger.

The material orientations used in this study can be visualized by setting up two concentric cones. The points on the 'rims' of the cones denote where the z'-axis (local rise direction) will be for each material case. Let us consider an example. Point one in Figure 5-4 lies on the inner, 30 degree, cone. To define the material axes for this case, a single transformation of 30 degrees, denoted by zeta, in Figure 5-7 is performed. This can be likened to the knit lines being oriented within the M(T) specimen shown in Figure 5-7. Table 5-1 lists the direction cosines, i.e. the cosines of the angles, between the primed and unprimed axes. Here α_1 is the cosine of the angle between the x' and x axis, $\alpha 2$ is the cosine of the angle between the y' and x axis, and so on.

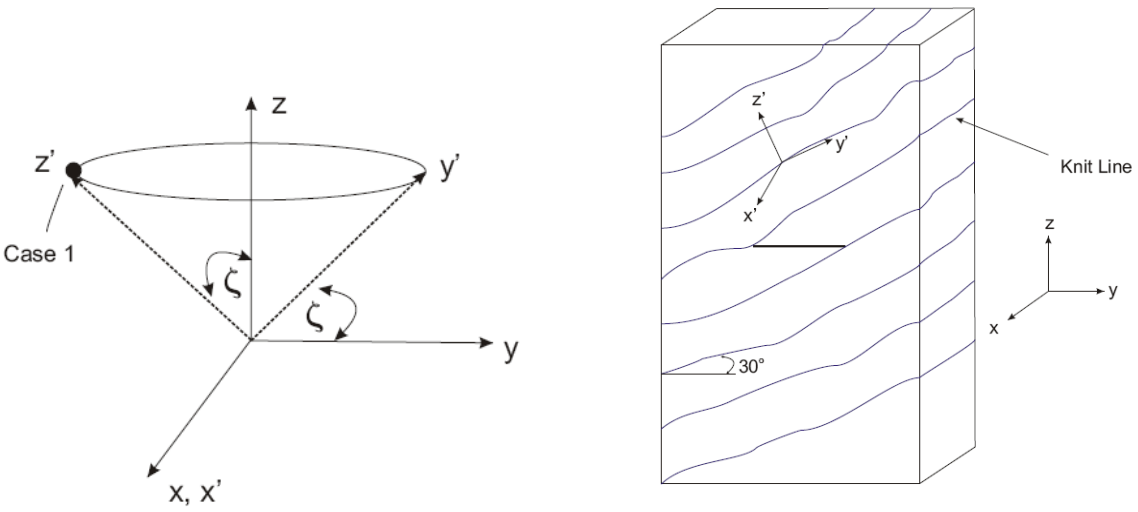

Figure 5-7. Definition of case one material orientation for the M(T) FE model

Table 5-1. Direction cosines for the case one material orientation

	x	y	z
x'	$\alpha_1 = 1$	$\beta_1 = 0$	$\gamma_1 = 0$
y'	$\alpha_2 = 0$	$\beta_2 = 0.866$	$\gamma_2 = 0.5$
z'	$\alpha_3 = 0$	$\beta_3 = -0.5$	$\gamma_3 = 0.866$

Figure 5-8 is a plot of the mode I SIF against normalized crack front distance for cases 1- 4. The mode I SIF for the case zero orientation, the case where the material and substrate axes are coincident, is also plotted to make a comparison. Figure 5-8 pertains to a straight crack that is parallel to the horizontal (no inclination). Even though this material is anisotropic, for this geometry, KII and KIII remain small compared to KI. This is not always the case, however, particularly when the crack is inclined. To examine the effect of mode mixity, the crack in the M(T) model is inclined by 30 degrees. All cases are rerun and in Figures 5-9 through 5-11, the mode I-III SIF is plotted versus the normalized crack front distance for cases one through four. As expected, when the crack is inclined KI decreases, and KII-KIII increase. This is consistent with isotropic assumptions. For the configuration shown in Figure 6-1, the KI and KII are related to φ, or the crack inclination angle (Anderson, 1991)

$$KI = \sigma \cos^2(\varphi)\sqrt{\pi a}$$
$$KII = \sigma \sin(\varphi)\cos(\varphi)\sqrt{\pi a} \qquad (5\text{-}1)$$

We can see that KII is zero when φ = 0 and that KI will decrease for increasing values of φ.

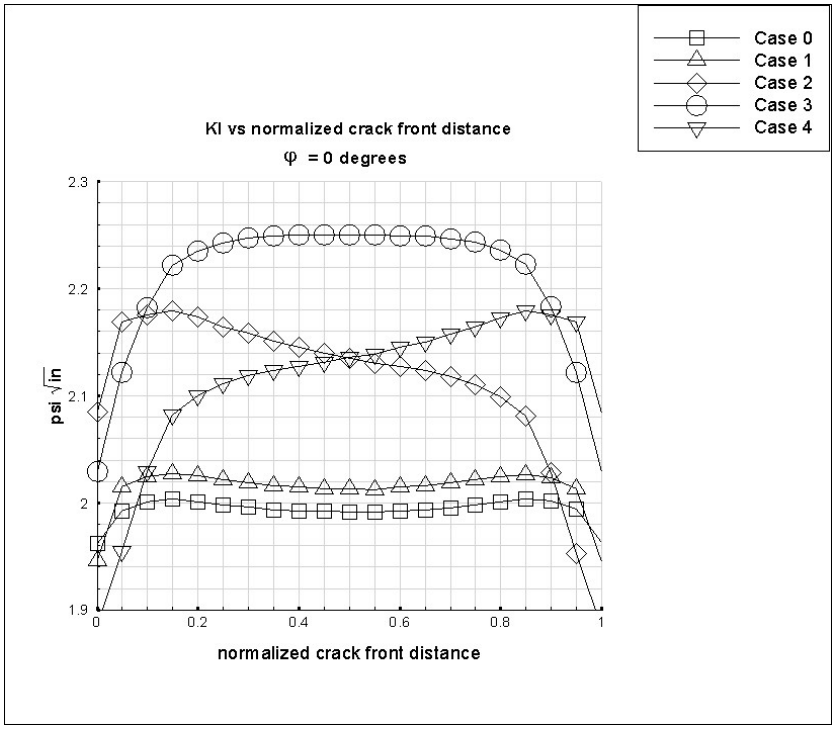

Figure 5-8. Mode I SIF for cases 1-4; 0 degree crack inclination

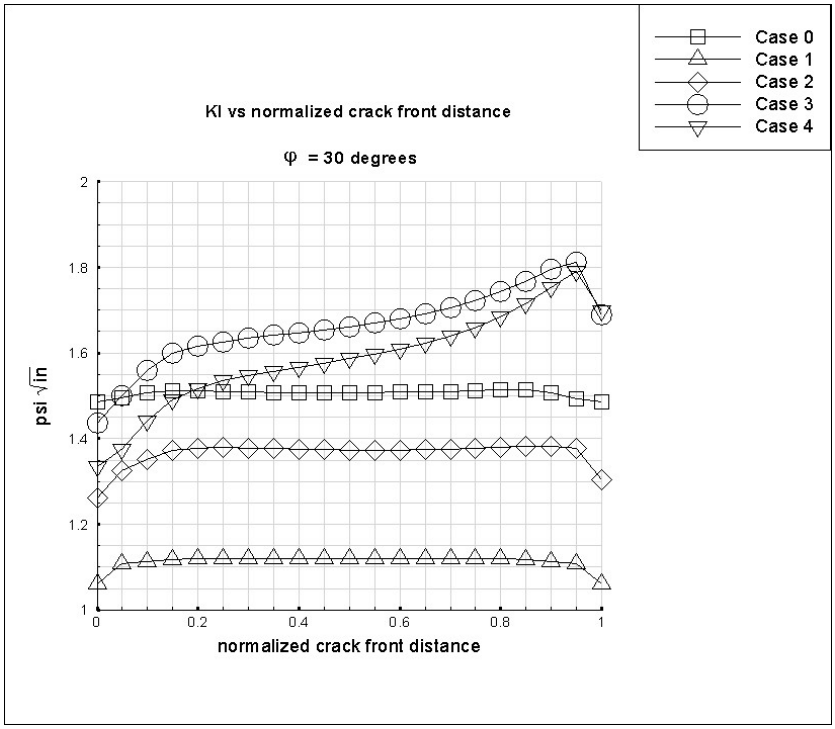

Figure 5-9. Mode I SIF for cases 1-4; 30 degree crack inclination

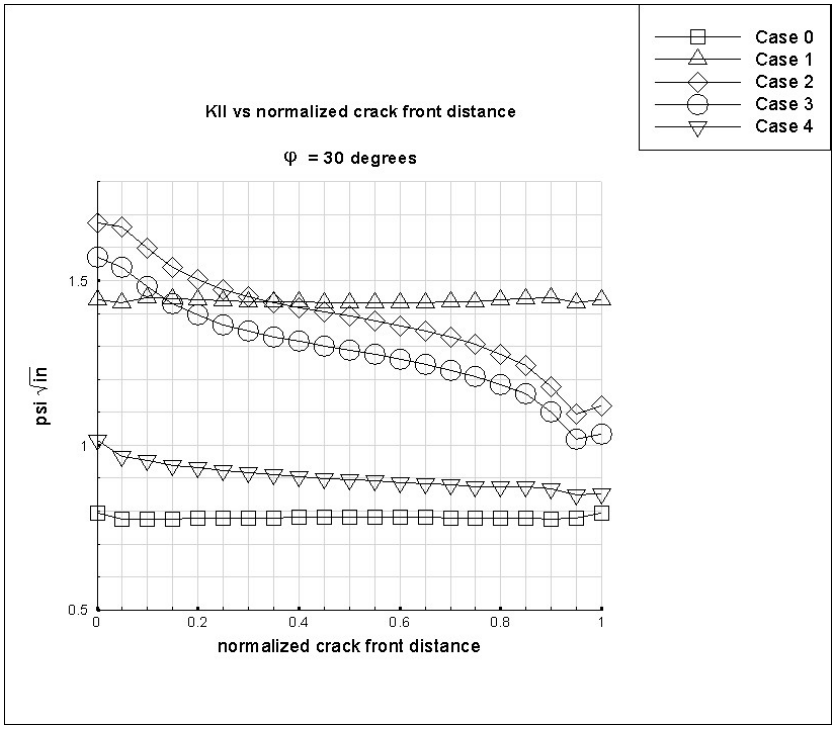

Figure 5-10. Mode II SIF for cases 1-4; 30 degree crack inclination

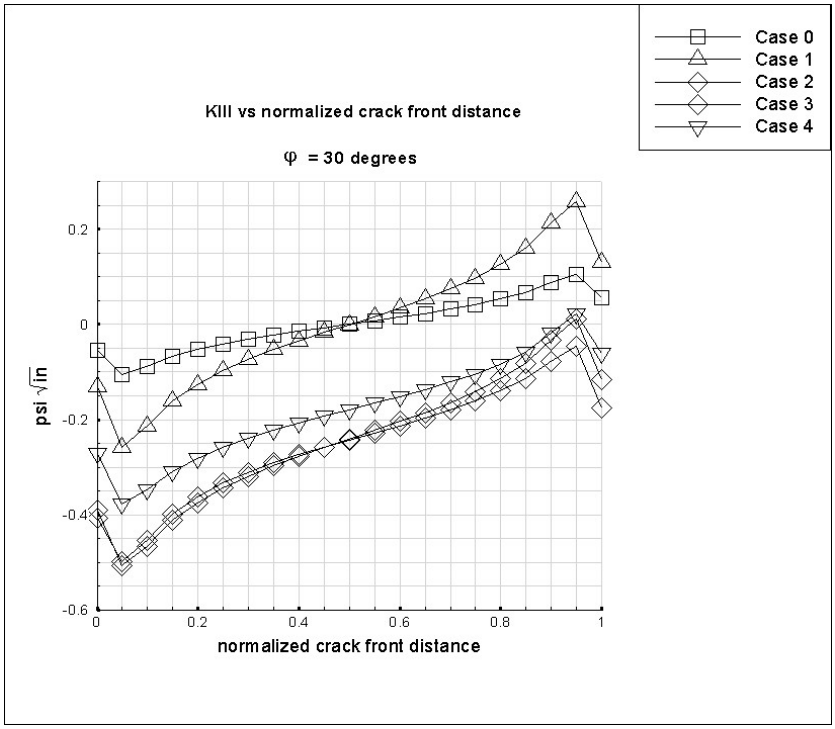

Figure 5-11. Mode III SIF for cases 1-4; 30 degree crack inclination

The mode I SIF for φ = 0 is listed in tables 5-2 and 5-3. Here we can see the variation of the mode I SIF as the material orientation is changed. For these cases, the ones that resulted in the largest KI are: 11 and 15 (2.27 psi √in). When you compare that number to the KI for case zero, the orientation for typical acreage sprays, the largest KI is just 14% higher. This is an interesting result in that even if we 'lean' the z-axis by quite a bit, the resulting mode I SIF is not much greater than the mode I SIF for the case 0 orientation. However, it is possible to orient this material in an infinite number of ways and it could be possible to obtain a KI value for an arbitrary orientation that is greater than the largest value determined in this section (2.27 psi √in).

Table 5-2. KI for cases 0-8, 0 degree inclination

	Case 0	1	2	3	4	5	6	7	8
KI (psi √in)	1.99	2.01	2.14	2.25	2.14	2.01	2.14	2.25	2.14

Table 5-3. KI for cases 9-16, 0 degree crack inclination

	Case 9	10	11	12	13	14	15	16
KI (psi √in)	2.07	2.19	2.27	2.19	2.07	2.19	2.27	2.19

Crack Turning Predictions

We can numerically predict the crack turning angles using the maximum tangential stress criteria since we have SIFs from FE models and the near-tip stress solutions from Hoenig (1982). As discussed in chapter four, we will use a ratio of the tangential stress, $\sigma_{\omega\omega}$, to K_p for turning angle estimations. Let us denote the ratio of $\sigma_{\omega\omega}/K_p$ as *R* and where R is a maximum, that is the direction of predicted propagation. To make a comparison, NASA has donated several broken M(T) specimens with various material orientations. The turning angles within these specimens will be measured and compared to their numerical counterparts.

M(T) Specimen Fabrication and Determination of Local Knit Line Axes

Fabrication of the M(T) specimens involves spraying the foam on a metal plate, it rises and eventually a rind forms. When the foam has settled, the next layer is applied until the desired thickness is achieved. From here, the foam is cut, or machined, from this parent block so the knit lines are running in the desired directions. One of the foam samples is shown in Figures 5-12.

Three M(T) foam test specimens are analyzed in this section. These samples have various orientations and crack inclinations (φ values). The first step in this analysis is to determine what the material orientation is for each specimen and we do this by measuring

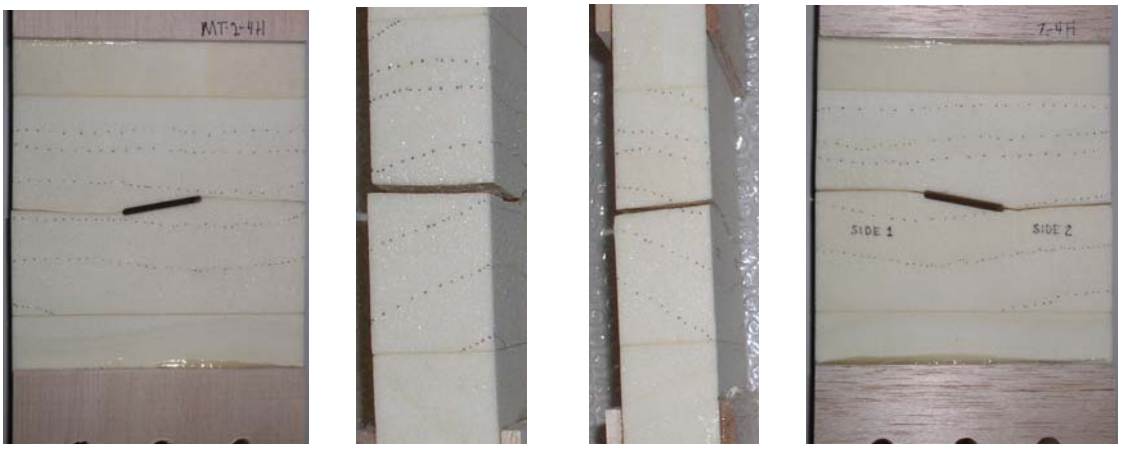

Figure 5-12. From left to right: front, left, right, and rear sides of the M(T) specimen

the angles of the knit lines on the specimen's surface. Consider Figure 5-13. We need to determine the orientation of the x', y' and z' vectors in order to define the material orientation. This information is used to define the element coordinate system in ANSYS.

The intersection of two planes is determined by taking the cross-product of their normal vectors. If one wants the 'trace' angle on a particular face of the M(T) specimen, the dot product can be used. In our case, the normal to the knit line plane is not known beforehand. Instead we will measure two angles, θ and Γ, and use them to define the knit

line plane shown in Figure 5-13. What we are interested in, is the trace, or intersection, the knit line plane makes on the x and y = 0 faces. Along the x = 0 face, we need the angle of the knit line measured from the horizontal, or y-axis. In this case the knit lines on the x = 0 face are relatively straight; θ is approximately zero. On the y = 0 face the angle, Γ, is also measured relative to the horizontal, or the x-axis. Thus, the traces on the y and x = 0 faces define the x' and y' material axes respectively. Using the cross product, the axis normal to knit line plane is determined, i.e. z' = x' × y'.

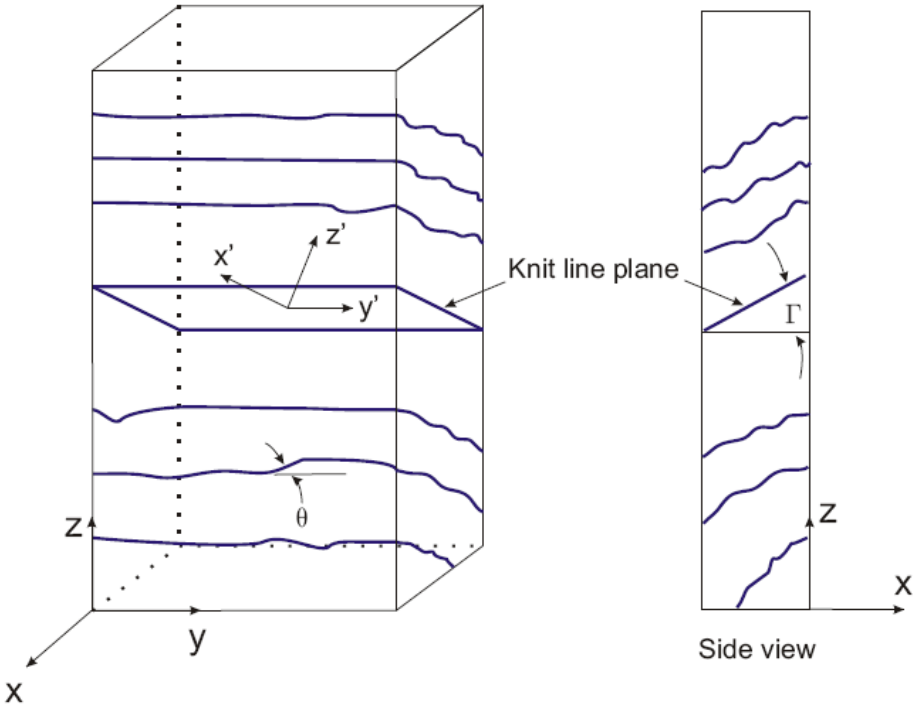

Figure 5-13. Determination of knit line plane

Local Crack Tip Computations

For crack tip computations involving stresses, there are a few subtleties that should be addressed in this section because the material classifications discussed in chapter three are in a 'global' sense. When looking at a foam M(T) specimen, one would say it is indeed a transversely isotropic material. However, the post-processing of near-tip

stresses requires material properties rotated into a local crack front coordinate system. Let us consider an example. First, assume we have the case one orientation; a material rotation ($\theta = 30^{o}$) takes place about the global x axis shown in Figure 5-13. If the inclined crack is oriented in such a fashion so that it rests in the plane of symmetry, the out-of-plane and in-plane displacements become decoupled and this is a so-called degenerate case described by Hoenig. His formulation cannot be applied for this special case. As described in chapter three, when this situation arises (crack lying in a symmetry plane) the usual isotropic near-tip formulas are utilized.

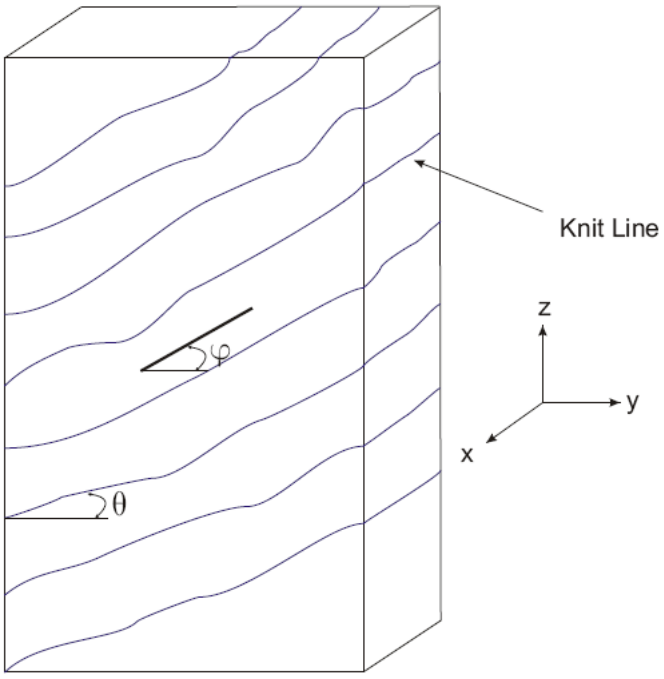

Figure 5-14. M(T) model with inclined crack

Now set $\varphi = 15$ degrees. The crack is no longer resting in the symmetry plane. Let us denote this as a 'general' case and a rotation is needed to set the properties in the local crack front system. The way the constitutive matrices are transformed depends on how they are defined. If they are in *compliance* form

$$\{\varepsilon\} = [S]\{\sigma\} \tag{5-2}$$

then the transformation formulas (Ting, 1996) for the elastic constants are

$$[S'] = [Q_S][S][Q_S]^T \tag{5-2}$$

where $[S']$ is the matrix of elastic constants in the rotated system and

$$[Q_S] = \begin{bmatrix} \alpha_1^2 & \beta_1^2 & \gamma_1^2 & \beta_1\gamma_1 & \alpha_1\gamma_1 & \alpha_1\beta_1 \\ \alpha_2^2 & \beta_2^2 & \gamma_2^2 & \beta_2\gamma_2 & \alpha_2\gamma_2 & \alpha_2\beta_2 \\ \alpha_3^2 & \beta_3^2 & \gamma_3^2 & \beta_3\gamma_3 & \alpha_3\gamma_3 & \alpha_3\beta_3 \\ 2\alpha_2\alpha_3 & 2\beta_2\beta_3 & 2\gamma_2\gamma_3 & \beta_2\gamma_3+\gamma_2\beta_3 & \gamma_2\alpha_3+\alpha_2\gamma_3 & \alpha_2\beta_2+\beta_2\alpha_3 \\ 2\alpha_3\alpha_1 & 2\beta_3\beta_1 & 2\gamma_3\gamma_1 & \beta_3\gamma_1+\gamma_3\beta_1 & \alpha_3\gamma_1+\gamma_3\alpha_1 & \alpha_3\beta_1+\beta_3\alpha_1 \\ 2\alpha_1\alpha_2 & 2\beta_1\beta_2 & 2\gamma_1\gamma_2 & \beta_1\gamma_2+\gamma_1\beta_2 & \alpha_1\gamma_2+\gamma_1\alpha_2 & \alpha_1\beta_2+\beta_1\alpha_2 \end{bmatrix} \tag{5-3}$$

The order of the terms in and (5-2) and (5-3) is based on the convention commonly used by the composites and elasticity community where the stresses and strains are ordered as $\{\sigma_x, \sigma_y, \sigma_z, \tau_{yz}, \tau_{xz}, \tau_{xy}\}^T$. If the constitutive matrix is in *stiffness* form

$$\{\sigma\} = [C]\{\varepsilon\} \tag{5-4}$$

there is an alternate definition of the $[Q_S]$ matrix

$$[Q_C] = \begin{bmatrix} \alpha_1^2 & \beta_1^2 & \gamma_1^2 & 2\beta_1\gamma_1 & 2\alpha_1\gamma_1 & 2\alpha_1\beta_1 \\ \alpha_2^2 & \beta_2^2 & \gamma_2^2 & 2\beta_2\gamma_2 & 2\alpha_2\gamma_2 & 2\alpha_2\beta_2 \\ \alpha_3^2 & \beta_3^2 & \gamma_3^2 & 2\beta_3\gamma_3 & 2\alpha_3\gamma_3 & 2\alpha_3\beta_3 \\ \alpha_2\alpha_3 & \beta_2\beta_3 & \gamma_2\gamma_3 & \beta_2\gamma_3+\gamma_2\beta_3 & \gamma_2\alpha_3+\alpha_2\gamma_3 & \alpha_2\beta_2+\beta_2\alpha_3 \\ \alpha_3\alpha_1 & \beta_3\beta_1 & \gamma_3\gamma_1 & \beta_3\gamma_1+\gamma_3\beta_1 & \alpha_3\gamma_1+\gamma_3\alpha_1 & \alpha_3\beta_1+\beta_3\alpha_1 \\ \alpha_1\alpha_2 & \beta_1\beta_2 & \gamma_1\gamma_2 & \beta_1\gamma_2+\gamma_1\beta_2 & \alpha_1\gamma_2+\gamma_1\alpha_2 & \alpha_1\beta_2+\beta_1\alpha_2 \end{bmatrix} \tag{5-5}$$

The transformed elastic constants in stiffness form are therefore determined by

$$C' = [Q_C][C][Q_C]^T \tag{5-6}$$

The two [Q] matrices are related

$$[Q_S] = \left[Q_C^{-1}\right]^T \tag{5-7}$$

Equations (5-2) or (5-6) allow us to transform the material properties from one Cartesian coordinate system to another. The only information we need for such a transformation is the direction cosines of the angles between the coordinate axes where we start, or the system where the material properties are initially defined, and the system where we want to set the properties.

The incipient turning angles analyzed in this program use the maximum tangential stress theory. In order to apply it, the first thing we need is the hoop, or $\sigma_{\omega\omega}$, component shown in Figure 5-15. The near-tip stresses derived by Hoenig are in a (x, y, z) Cartesian coordinate system. To obtain the hoop stress, we transform axes, in this case a rotation anti-clockwise about the z-axis by ω degrees. This is done using standard transformation equations (Boresi et al 1993).

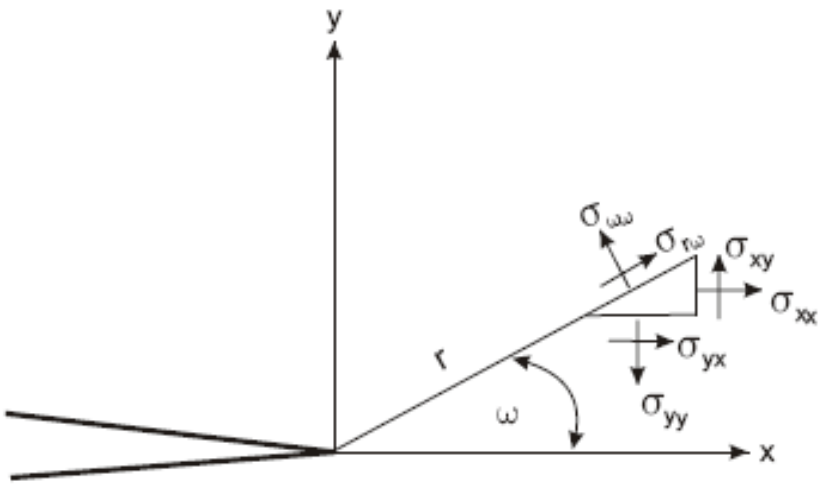

Figure 5-15. Cartesian and cylindrical stresses

Calculating $\sigma_{\omega\omega}$ is done via

$$\sigma_{\omega\omega} = \alpha_2^2\sigma_{xx} + \beta_2^2\sigma_{yy} + \gamma_2^2\sigma_{zz} + 2\beta_2\gamma_2\sigma_{yz} + 2\gamma_2\alpha_2\sigma_{zx} + 2\alpha_2\beta_2\sigma_{xy} \qquad (5\text{-}4)$$

Here the α_2, β_2, γ_2 terms are the direction cosines of the angles between the old and new axes

Now we can calculate the hoop stress at any r and ω of our choosing. The next step is to divide the hoop stress by the effective K, K_p. We do this because not only are the elastic constants direction dependent, but the fracture properties are as well. The crack is predicted to turn in the direction where R is a maximum. The crack turning angle, defined as ω_c is shown in Figure 5-16. Here we have a close-up view of a M(T) specimen containing an inclined crack. The inclined crack offset by angle, φ, and the direction of incipient turning is denoted by the dashed line.

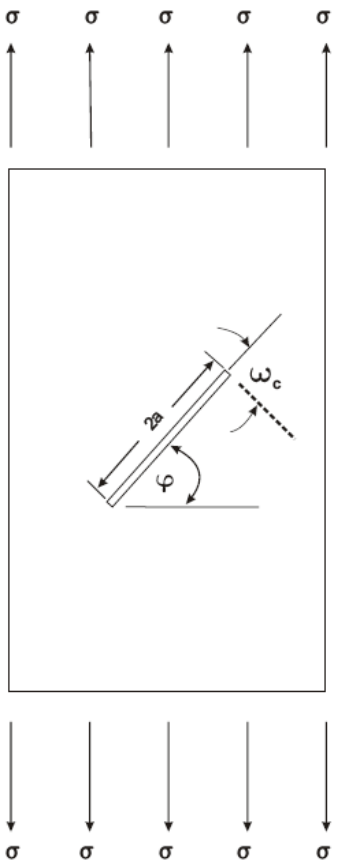

Figure 5-16. Crack turning angle

Let us pause briefly and quickly summarize the procedure needed to compute near-tip hoop stresses and the predicted turning angle

- Enter material orientation (denoted by case number in Figure 5-2) into a FE model coordinate system

- Run the model and extract the mode I-III SIFs via FRANC3D
- Rotate material properties into a local crack front coordinate system
- Compute near-tip stresses using Hoenig's formulas
- Transform σ_{yy} to $\sigma_{\omega\omega}$ via the transformation equations found in Boresi et al
- Divide σ_{yy} by K_p and determine where this ratio is a maximum to predict the turning angle, ω_c

Table 5-4. Measured and predicted turning angles (in degrees)

	ω_c (measured)	ω_c (predicted)	ω_c (isotropic prediction)
specimen A	27	32	43
specimen B	9.7	21	27
specimen C	12	19	27

For the three test specimens, one of them had a crack inclination of 30 degrees (specimen A). The other two specimens (B and C) had crack inclinations of 10 degrees. All three specimens have different material orientations. Table 5-4 lists the measured and predicted incipient turning angles. The SIFs can vary along the crack front and since the free surface can influence the numerical K-solution, the measured and predicted angles are computed at the mid-plane. For comparison's sake, isotropic predictions for the same M(T) geometries are also tabulated. The isotropic angle is the critical angle, ω_c, from equation (4-4). The experimental tests were carried out at 75^{o}F and as such, the elastic properties at that temperature are used to predict the turning angle.

The turning angle was measured using a Brown and Sharpe coordinate measuring machine. These devices are used to inspect various geometries such as cylinder heads or gear boxes. This instrument uses a probe that physically touches the work piece and the points are recorded digitally. In this case, we wish to use the points to define the fracture planes. The angle between these planes is the crack turning angle. Within each specimen

are four fracture surfaces. The fracture angle was measured at a location near the middle and an average of the four values is taken and listed in Table 5-4.

Specimen A had the best agreement with experiment whereas the other two predictions fall somewhere between the isotropic prediction and actual values. Even though both the direction dependence of both the fracture toughness and near-tip stresses are accounted for in these predictions, the results presented here still vary by large amount. One possible source for the difference is how the material orientation is defined and modeled. When tasked to predict the turning angle, NASA furnished us with the three test specimens but the orientations were not specified beforehand. These particular specimens were initially fabricated to analyze mode mixity, not the effects of material orientation. As such, the orientations of the knit lines vary throughout the specimens. When defining the knit line plane, the knit lines (denoted with black dots in Figure 5-12) closest to the crack were used to define the orientation, even though the material orientation can vary over the specimen.

Based on the results seen here, it seems that perhaps the crack is seeking a pure mode I condition, or that the crack is seeking a direction that is normal to the highest principal stress. In such cases, if a crack, for example, is orientated at 30 degrees relative to the horizontal, the crack will turn -30 degrees to it is running straight across or in a direction normal to the maximum principal stress. However, only three specimens are analyzed in this section and to some extent, the material orientation can be more carefully controlled. Obviously more samples would have to be analyzed to determine if the cracks favor a direction that is normal to the highest principal stress.

Influence of Thermal Loads on the SIF Solution

FRANC3D is very versatile in that it can generate different types of crack meshes and also compute a K-solution for both isotropic and fully anisotropic materials but at the time of this writing, it is unable to handle problems with a thermal gradient. This is main reason why the DC technique outlined in chapter three is utilized. To examine the effect of a thermal gradient throughout the M(T) specimen we will examine the case two orientation with a straight and inclined crack. This varies the amount of mode mixity and two different sets of temperatures are applied to the top and bottom faces of the M(T) specimen shown in Figure 5-17.

In the figures that follow the primary aim is to see how the SIFs change when temperatures are applied to the M(T) specimen. Since the Ks are evaluated using a different method, it is useful to compare the results of these two approaches when the same set of boundary conditions is applied. We have results tabulated for several cases at room temperature. Selecting one of them, case 1 for example, we can compare the SIF results for a straight crack. The mid-plane KI at room temperature is 2.01 psi √in. Using the DC method we obtain a value of 1.8 psi √in, a difference of approximately 10%. The quality and density of the mesh does impact the alternate solution presented here. In Banks-Sills *et al.* (2005) study a similar routine is used to check the M-integral computations. Recall that the interaction, or M, integral is used to compute the anisotropic K-solution in FRANC3D. Excellent agreement is shown between their various schemes, but much denser meshes are utilized within their FE models.

In this study it is possible to refine the mesh, perhaps by changing the location of the quarter point elements by some degree, but this may not be feasible because there is a

node and element limitation within this FE software. Banks-Sills *et al.* use 2-D models and that allows one to change the mesh density extensively without adding a lot of computational cost in terms of physical model size or run time.

Consider Figure 5-17 with $\varphi = 0$ degrees (straight crack). Here $T_1 = 0^{o}F$ and $T_2 = 100^{o}F$. The same unit pressure is also applied. All SIF data from FRANC3D is at room temperature ($75^{o}F$). The DC method used to compute the SIFs is able to determine these parameters at any temperature. To examine the influence of thermal loads on the K-solution, the mode I-III SIF for case two at both room temperature and with a thermal gradient is plotted in Figure 5-18. From Table 5-2, the room temperature mid-plane value for KI is approximately 2.14 psi √in. With the prescribed thermal boundary conditions, the mid-plane KI drops to 1.44 psi √in; a 33% reduction.

Also, in a few of the figures, some odd activity takes place near the free surface. When looking at Figure 5-18, and the line that pertains the to KI, for the DC solution, the third point drops down to approximately 0.946 psi √in. This happens again in the rest of the figures that pertain to the DC solution. One possible explanation is that the free surface along with the boundary conditions is influencing the displacement results at that point.

Sometimes quadratic elements are prone to spurious oscillations. Within Dhondt's (2002) paper on computing mixed-mode anisotropic SIFs, he performs a smoothing operation via an averaging technique to remove the unwanted oscillations. Likewise Man et al (1993) encounter a similar problem when using boundary elements to model a contact problem. Their solution involves removing the higher order elements in the

problem area, and replacing them with linear elements instead. No such averaging technique or element modification is employed here.

There is a marked change in KI, and the other SIFs (KII and KIII) also had fairly substantial changes for this particular orientation and geometry. In this case KIII remains small across the crack front. But KII increases by quite a bit, just like KI does. KII at the mid-plane is roughly -0.04 psi √in at room temperature. With the addition of temperature to this model, KII rises to 0.315 psi √in. Granted for this geometry and set of loads, KII and KIII still remain small when compared to KI. Let us now consider a case where we have a larger gradient applied to the M(T) model in Figure 5-17. The next set of results for this material orientation are for $T_1 = -200^oF$ and $T_2 = 100^oF$.

In Figure 5-19 we see how the larger thermal gradient impacts the mode I SIF. With these boundary conditions, KI, at the mid-plane, is 1.78 psi √in. But this time, KII and KIII both show a fairly large increase after this gradient is applied. Here KII at the mid-plane reaches -0.122 psi √in and KIII = 0.355 psi √in.

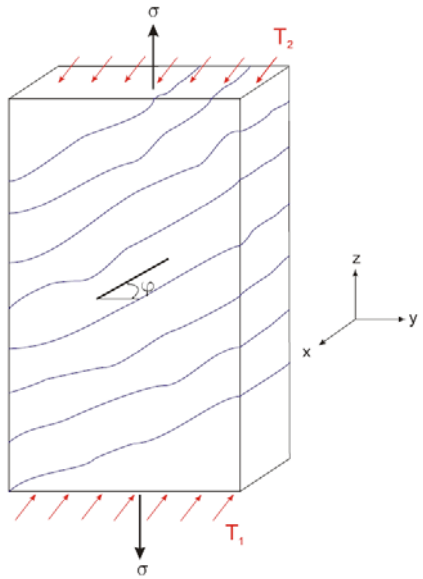

Figure 5-17. Application of thermal loads

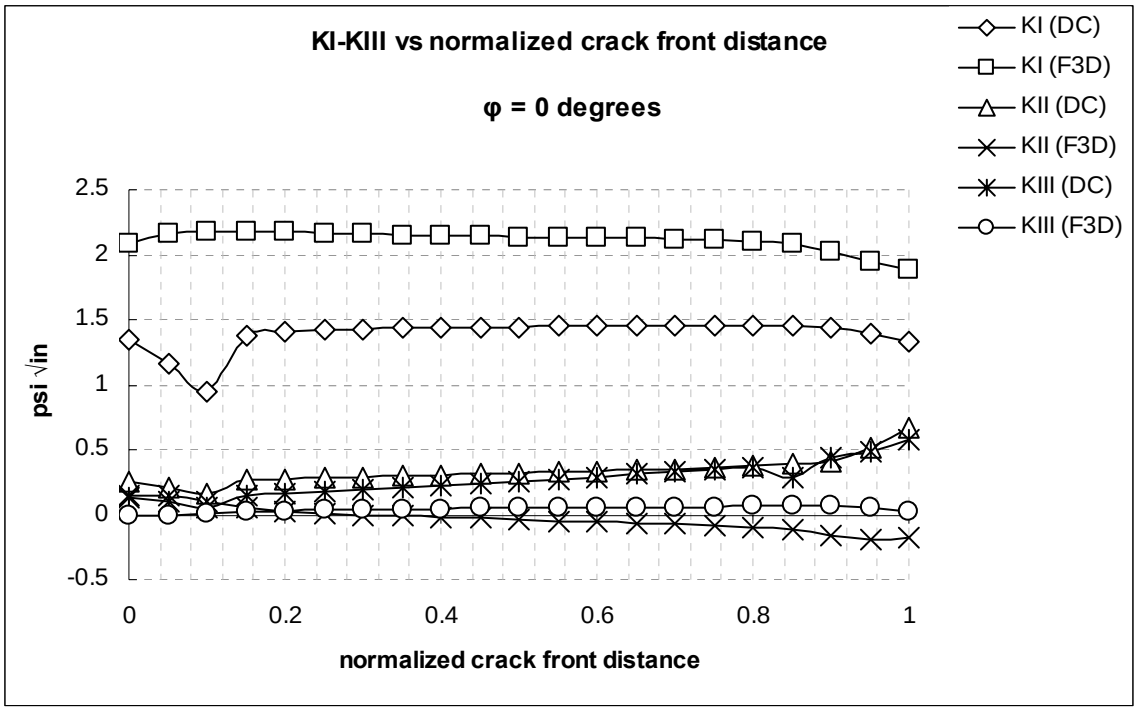

Figure 5-18. Room temperature KI-KIII (F3D) vs. KI-KIII (DC) with $T_1 = 0^oF$ and $T_2 = 100^oF$

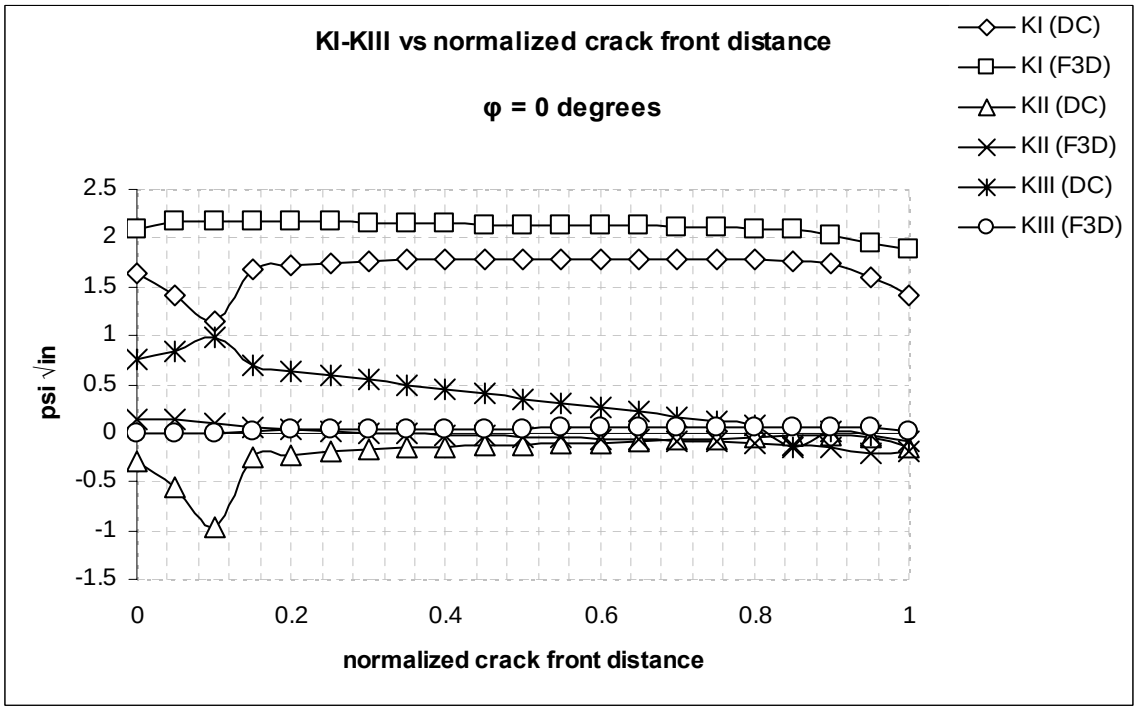

Figure 5-19. Room temperature KI (F3D) vs. KI (DC) with $T_1 = -200^oF$ and $T_2 = 100^oF$

We see in the above simulations that adding a thermal gradient can impact the mode I-III SIFs. In the first section of this chapter, we looked at SIFs for various orientations for straight and diagonal cracks alike. When the crack is straight ($\varphi = 0$), at room temperature, the KII and KIII are small compared to KI. Again using the same geometry, when thermal loads are applied to the top and bottom faces of the M(T) model, KII and KIII are still small compared to KI, but they do exhibit a change from the room temperature reference state. As we have seen with the room temperature results, KII and KIII become more significant when the crack is inclined. This introduces a degree of load asymmetry, or mode mixity. To further explore the influence of mode mixity along with the thermal gradient, let us consider the case two orientation but with a 30 degree inclined crack.

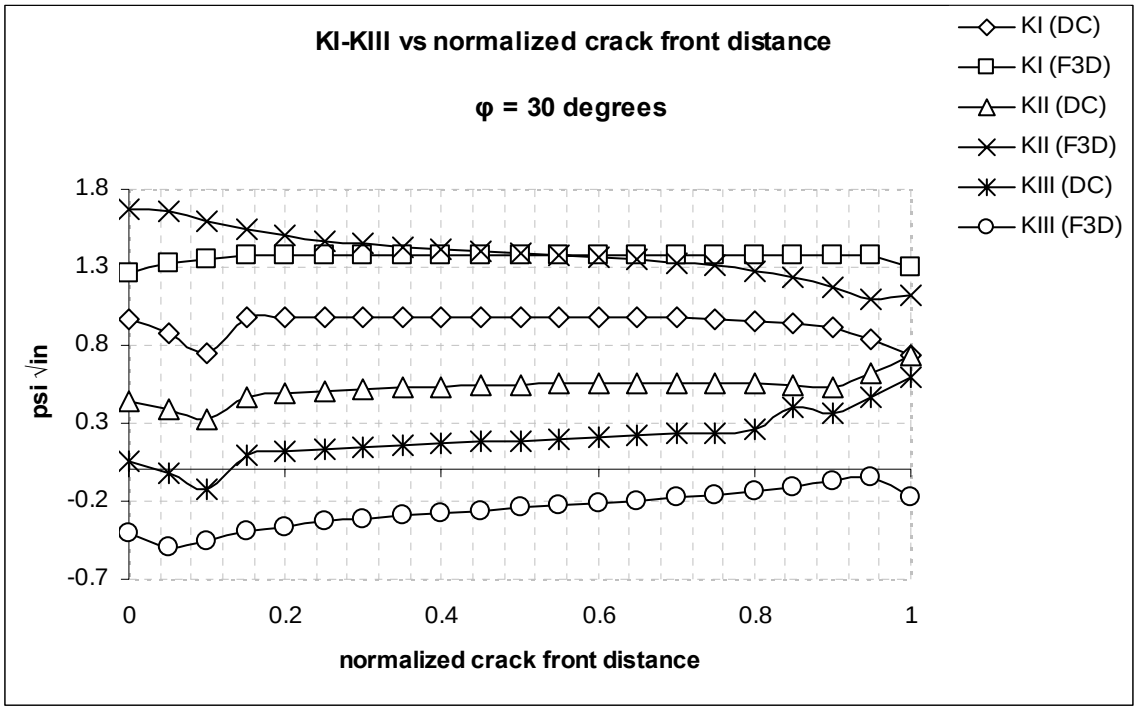

Figure 5-20. $\varphi = 30$ degrees: room temperature KI (F3D) vs. KI (DC) with $T_1 = 0^oF$ and $T_2 = 100^oF$

Taking a look at KI at the mid-plane in Figure 5-20, KI goes from 1.37 psi √in at room temperature to 0.978 psi √in when the thermal gradient is present. KII and KIII are 0.545 and 0.188 psi √in at the mid-plane, respectively. Our final set of plots is again for case two with a thirty degree inclined crack, but now $T_1 = -200^oF$ and $T_2 = 100^oF$. KI at the mid-plane is approximately 1.74 psi √in, and KII and KIII are -0.455 psi √in 0.0394 psi √in, respectively.

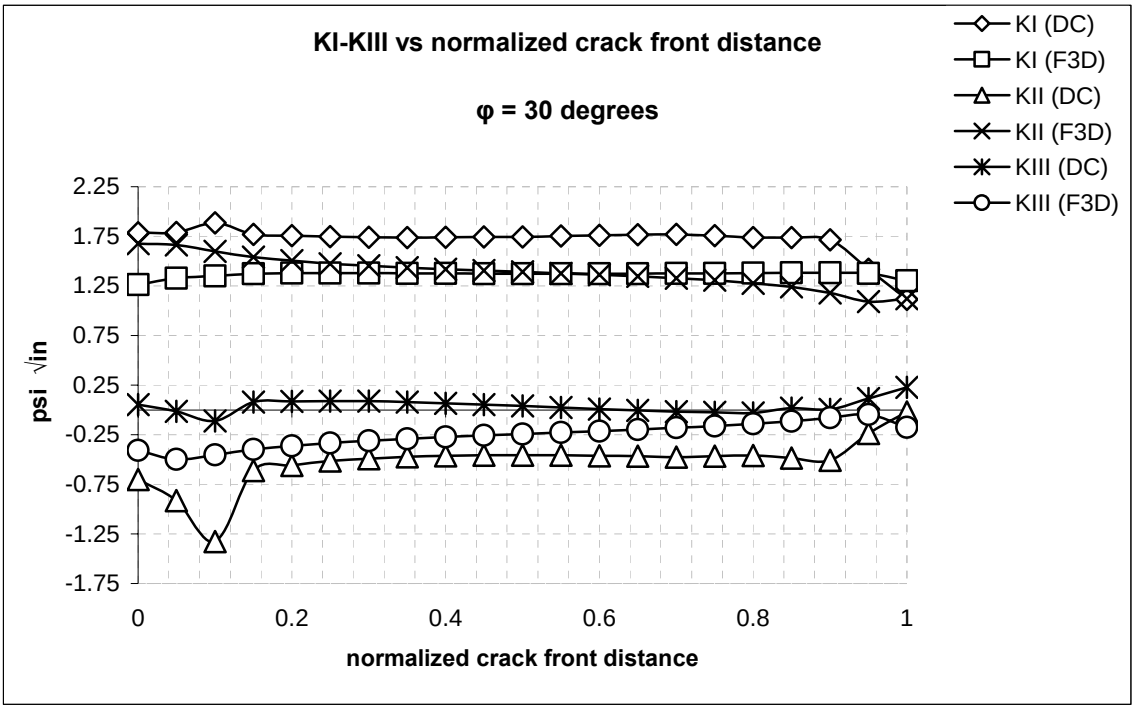

Figure 5-21. φ = 30 degrees: room temperature KI (F3D) vs. KI (DC) with $T_1 = -200^oF$ and $T_2 = 100^oF$

A final summary of the mid-plane values shown in the tables below. The abbreviations are as follows RT = room temperature, TG1 ($T_1 = 0^oF$ and $T_2 = 100^oF$), TG2 ($T_1 = -200^oF$ and $T_2 = 100^oF$). The values are taken at the mid-plane. The units for KI-KIII are psi √in.

Table 5-5. Summary of mid-plane KI-KII

	KI (RT)	KI (TG1)	KI (TG2)	KII (RT)	KII (TG1)	KII (TG2)
Case 2 (φ = 0)	2.13	1.44	1.78	-0.038	-0.315	-0.122
Case 2 (φ = 30)	1.37	0.978	1.74	1.39	0.545	-0.455

There are many more ways to apply boundary conditions to this problem. In the above analysis, since the specimen is 12 inches long, the temperature is different than room temperature, but still fairly uniform across the crack front.

Table 5-6. Summary of mid-plane KIII

	KIII (RT)	KIII (TG1)	KIII (TG2)
Case 2 (φ = 0)	0.049	0.258	0.289
Case 2 (φ = 30)	-0.242	0.206	0.0394

The information presented in chapter two allows an estimation of the elastic constants over wide range of temperatures. Perhaps in some instances, the flaw can be six inches, or more, away from the surface of the ET. In that case, given the foam's very low thermal conductivity, it is possible to have a temperature over the crack front that does not vary substantially. But over typical acreage sprays the thickness of the insulation is roughly three inches. That is to say, there certainly are conditions where the temperature across the crack front will not be uniform.

To investigate this scenario let us re-use the same M(T) model as before but now the gradient will applied to through the thickness, or 1.5 inch dimension. Once again, the case two orientation along with a 30 degree inclined crack. The TG2 boundary conditions are applied and the resulting temperature distribution along the crack front is plotted in Figure 5-22. Here the temperature varies appreciably. To analyze this problem, the elastic constants are evaluated using Figures 2-5 and 2-6. With those values the sixth order characteristic equation is solved at each point, and those roots are used in equation in (3-58) to obtain the corresponding Ks along the front.

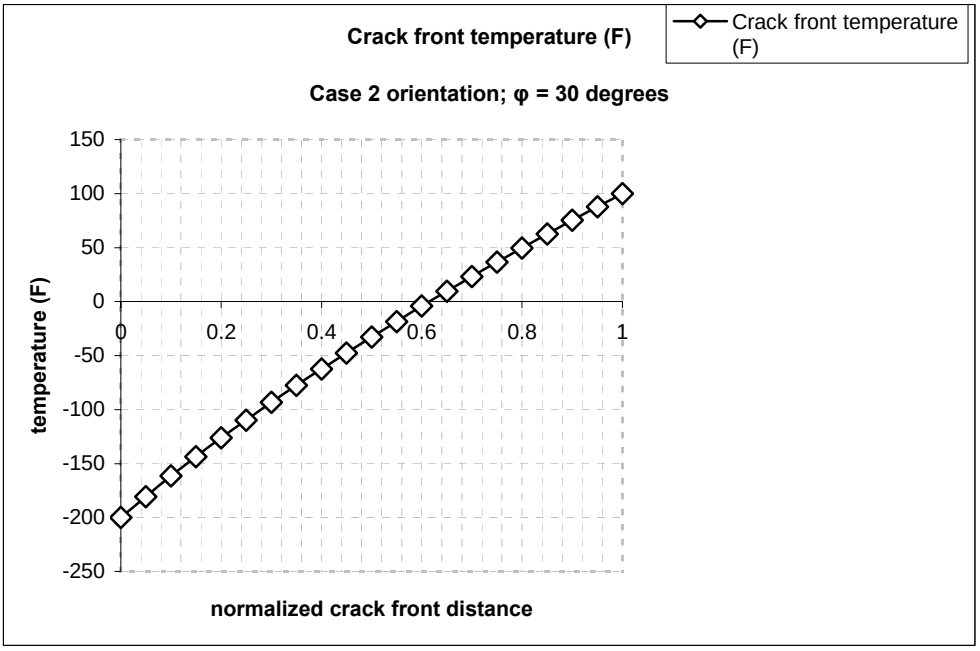

Figure 5-22. Temperature distribution along the crack front

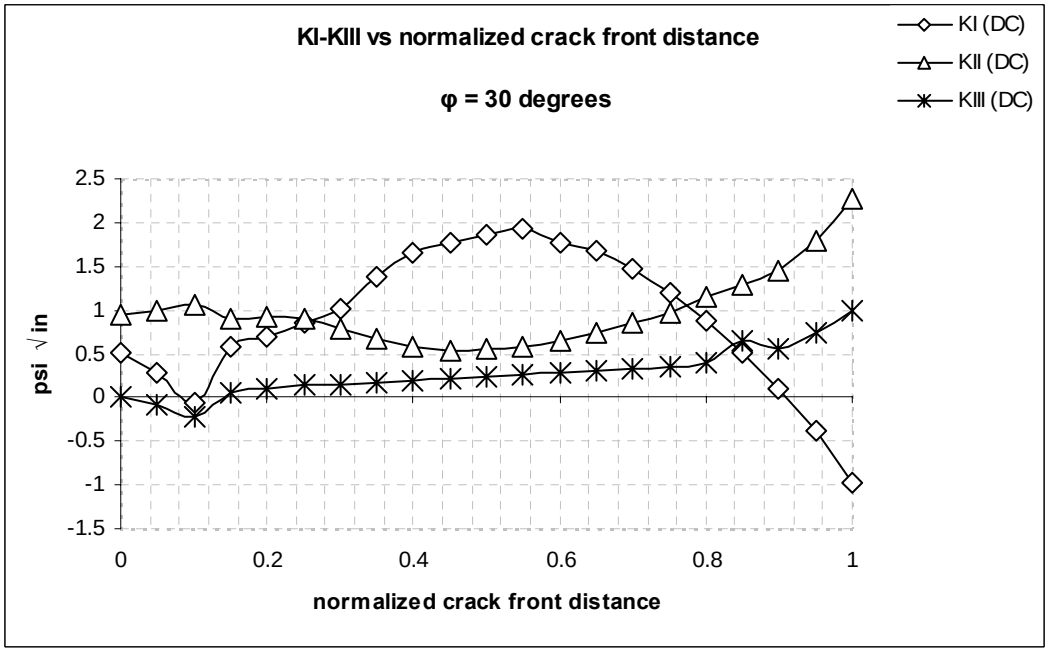

Figure 5-23. KI-KIII vs. normalized crack front distance; TG2 applied in thickness direction

The results of this model are shown in Figure 5-23. Since the temperatures changes with respect to crack front distance, the elastic constants also vary which impact the K-solution. In some parts of the plot, KII is larger than KI, but the mode I SIF dominates in the middle portion of the crack front. At the mid-plane, KI = 1.92 psi √in. Comparing this to the mid-plane value in Figure 5-21, KI = 1.74 psi √in; the value increased by approximately 10%.

Summary

The effect of material orientation on the anisotropic K-solution is examined. Seventeen material cases are examined and when the crack is straight we do not see a large difference in the mode I SIF even for orientations that depart quite a bit from the norm. The SIFs are also computed for an inclined crack. From the isotropic relations in (5-1) we see that KI should decrease while the remaining modes will increase as the φ gets larger. This trend is evident in Figures 5-9 through 5-11.

Crack turning, at room temperature, was also estimated using both anisotropic and isotropic turning assumptions. In all cases the isotropic calculations predicted a higher turning angle than seen within the three samples presented here. Along with isotropic predictions, crack turning estimations that account for the direction dependence of the elastic constants and fracture toughness. Here the predictions are somewhat closer to the experimental results, but there is still a sizable difference. Perhaps one reason why this is so, is because when these specimens were fabricated the material orientation was not carefully controlled. This makes the determination of the knit line orientation somewhat difficult and this can certainly influence the results because nearly all of the terms in Hoenig's equations depend on the elastic constants.

Finally, the effect of temperature is analyzed for the case two orientation. Several different sets of temperature boundary conditions are applied along with the unit pressure. This analysis is conducted for both a straight and inclined crack. It is here that an important distinction can be made between the SIFs evaluated at room temperature and those done so with the DC method with the applied temperatures. This method, while simple to use, is not without its deficiencies. Mid-plane results were compared for the case 1 orientation and a difference of 10% between the mode I SIF is encountered. Thus, the numbers presented here should not be taken as absolutes and better agreement might be obtained by using more refined models. Within the realm of the material orientations examined in this chapter, the mode I SIF did not vary a great deal, but when there is a thermal gradient present, significant changes in KI are encountered. The mode II and III SIFs also saw marked changes when the crack is no longer horizontal. In particular KIII, which is relatively small compared to KI and KII, for all of the room temperature tests showed large increases particularly when the second set of thermal boundary conditions are applied.

In our last example, the thermal gradient is applied through the thickness where this dimension is much smaller than the height. Such a large gradient over a small thickness (1.5 inches) should translate into a thermal gradient that varies over the crack front. In this case the gradient does indeed change substantially and, unlike the prior thermal analysis, one can no longer assume a uniform temperature and properties along the crack tip. Thus, at each point the constants are re-evaluated and the resulting Ks are plotted against the normalized crack front distance. In this scenario, KI is the largest at the mid-plane.

CHAPTER 6
CONCLUSIONS AND RECOMMENDATIONS FOR FUTURE WORK

Conclusions

Initial investigations of analytical solutions for cracked anisotropic elastic solids have existed since the 1960s and the overwhelming majority of literature on this subject assumes the crack lies in a symmetry plane where anti-plane decoupling of displacements takes place. Relatively few studies take on the issue of general anisotropy where no assumptions are made to simplify the mathematical treatment of such a complex problem. In this study, two such methods are presented to provide a solution to obtain near-tip stresses for a cracked anisotropic elastic body. The first of which uses Hoenig's (1982) derivation of an energy release rate for general anisotropy. This is the preferred choice for the computation of SIFs because of the inherent accuracy in this method. As such, the Cornell Fracture Group developed a software package, FRANC3D, which is able to not only create crack meshes but also compute an anisotropic K-solution for a variety of material orientations: isotropy, monoclinic, and general anisotropy.

Alternatively, using the DC method, another approach to determining the anisotropic K-solution is developed to not only provide another general approach as far as material orientation goes, but also one that can provide a solution for problems containing both mechanical and thermal loads. FRANC3D does provide a very versatile solution. But only structures subjected to isothermal conditions can be analyzed with this software. However, the problem that NASA is encountering likely involves the effects of a thermal gradient within the foam insulation. It was intended that these methods would

provide NASA with a more complete and fundamental understanding with regard to the fracture response of this material. The various conclusions are summarized below:

1. Numerical studies conducted at room temperature over a range of material orientations showed us that the mode I SIF did not depart substantially from the solution that arises from the orientation (case 0) which is present over the vast majority of the tank. The maximum difference in the mode I SIFs between the prescribed orientations and the case 0 scenario was shown to be 14%.

2. The specialized divot testing conducted by NASA gave some insight as to how subsurface crack, perhaps emanating from sharp void, could propagate toward the surface. It is here that crack turning analysis could be useful. While the physics, loading, and geometry are quite complicated, there are several theories available in the literature that are applicable to this problem since it is one involving brittle fracture. The fracture toughness and elastic constants are direction dependent in this type of foam material. As such, crack turning predictions that account for both of these characteristics were performed on three M(T) specimens provided by NASA. One of the three analytical predictions had reasonable agreement and while the remaining two had a large difference relative to the experimental value, they are closer than what isotropic assumptions would predict.

3. Temperature effects play an important role in this study. This is among the main reasons why NASA chose to initiate an exhaustive series of tests over range of temperatures. A large body of literature is available on foams, covering their applications and ways to estimate elastic and fracture response, but few studies deal with the harsh environment that this foam is subjected to. Since the range of temperatures involved in this problem is quite large, the effects of thermal gradients on the anisotropic K-solution were studied. Several variables come into play with this type of analysis, namely the amount of mode mixity, specimen geometry, material orientation, and boundary conditions (be it thermal, mechanical, or a combination of both). Many of the above variables were manipulated and the DC method developed was able to produce an anisotropic SIF solution that showed how the individual Ks varied over the crack front. It was shown that the SIFs could change dramatically depending on the level of mode mixity and the manner in which the thermal boundary conditions are applied. The results obtained in this study represent a quantitative basis for determining the response of this material for a given set of boundary conditions using the computational methods outlined in earlier chapters.

Recommendations for Future Work

One of the primary aims of this study was to help NASA acquire a more fundamental understanding of the fracture response of the BX-265 foam insulation. To some extent that was achieved as made evident by the conclusions made in the previous

section. Nevertheless, much remains to further our understanding of such a complex material. What follows is a list of recommended work for future study:

1. Various models exist in the literature to evaluate the material properties and fracture response for foam materials. Such estimations come from considering the geometry of the cells that comprise the cellular material. While the density does vary over any given test specimen, or volume of foam, perhaps a wide range of measurements could be taken so an average can be made. This enables us to compute the relative density and this dimensionless parameter is quite useful in estimating the elastic properties, even for anisotropic materials.

2. The crack turning investigation presented here is far from comprehensive. A more complete testing program involving many different orientations and crack inclinations should be developed so better criteria can be developed for more accurate predictions. Within the three test samples studied, it appears that the crack is seeking a path normal to the maximum principal stress. But with only three specimens on hand, it is difficult to generalize results.

3. While this study made use of simple and standardized geometries, the problem NASA is faced with is one that involves a rather complicated geometry. Divot models can be built using FE software and crack turning analysis similar to what was done in this program can be performed. This should provide NASA with a very comprehensive representation of the actual problem since anisotropy and temperature effects can be accounted for. Many different geometries and loads could be applied and the resulting turning angles could be compared to experiment. This could lead to additional refinements being made to the crack turning theories for anisotropic materials.

4. While the analysis in this study is confined to foam, there is no reason why it cannot be extended to other engineering materials that exhibit direction dependent properties. For example, perhaps crack turning calculations can be performed on various types of aluminum, or other metals where the crystal orientation influences the behavior. Additional work can be done to modify the various theories, crack turning for example, to account for a plastic zone in front of the crack tip. Plasticity is neglected in this study because the foam is so brittle, but many engineering materials are quite a bit more ductile which means that a process, or plastic zone, needs to be accounted for.

APPENDIX
GENERAL SOLUTION FOR THE PLANE PROBLEM OF A LINEAR ELASTIC ANISOTROPIC BODY

Following Lehkhnitskii (1963), Sih et al (1965), Ting (1996), and Cherepanov (1979) the characteristic equation described in chapter three will be derived here. The ensuing discussion is for a 'plane' problem, meaning the stresses, strains, and displacements have no dependence on the z coordinate. We start by listing the equations of equilibrium

$$\frac{\partial \sigma_x}{\partial x}+\frac{\partial \tau_{xy}}{\partial y}=0 \qquad \frac{\partial \sigma_y}{\partial y}+\frac{\partial \tau_{xy}}{\partial x}=0 \qquad \frac{\partial \tau_{xz}}{\partial x}+\frac{\partial \tau_{yz}}{\partial y}=0 \tag{A-1}$$

Since this a plane problem, the reduced compliance matrix becomes

$$S'_{ij}=S_{ij}-\frac{S_{i3}S_{3j}}{S_{33}}$$

The strains and displacements are related to each other

$$\begin{aligned} &\varepsilon_x=\frac{\partial u}{\partial x} \qquad \varepsilon_y=\frac{\partial v}{\partial y} \qquad \varepsilon_z=\frac{\partial w}{\partial z}=0 \\ &\gamma_{xy}=\frac{\partial u}{\partial y}+\frac{\partial v}{\partial x} \quad \gamma_{xz}=\frac{\partial w}{\partial x} \quad \gamma_{yz}=\frac{\partial w}{\partial y} \end{aligned} \tag{A-2}$$

Finally we have the compatibility equations

$$\frac{\partial^2 \varepsilon_x}{\partial y^2}+\frac{\partial^2 \varepsilon_y}{\partial x^2}=\frac{\partial^2 \gamma_{xy}}{\partial x \partial y} \qquad \frac{\partial \gamma_{xz}}{\partial y}=\frac{\partial \gamma_{yz}}{\partial x} \tag{A-3}$$

Two arbitrary stress functions (U and F) are introduced as a means to solve the equilibrium equations

$$\sigma_x = \frac{\partial^2 U}{\partial y^2} \qquad \sigma_y = \frac{\partial^2 U}{\partial x^2}$$
$$\tau_{xy} = -\frac{\partial^2 U}{\partial x \partial y} \quad \tau_{xz} = \frac{\partial F}{\partial y} \tag{A-4}$$
$$\tau_{yz} = -\frac{\partial F}{\partial x}$$

If we substitute (A-4) into the compatibility relations we have a system of equations in terms of U and F

$$L_4 U + L_3 F = 0$$
$$L_3 U + L_2 F = 0 \tag{A-5}$$

Where

$$L_4 = S'_{22}\frac{\partial^4}{\partial x^4} - 2S'_{26}\frac{\partial^4}{\partial x^3 \partial y} + \left(2S'_{12} + S'_{66}\right)\frac{\partial^4}{\partial x^2 \partial y^2} - 2S'_{16}\frac{\partial^4}{\partial x \partial y^3} + S'_{11}\frac{\partial^4}{\partial y^4}$$
$$L_3 = -S'_{24}\frac{\partial^3}{\partial x^3} + \left(S'_{25} + S'_{46}\right)\frac{\partial^3}{\partial x^2 \partial y} - \left(S'_{14} + S'_{56}\right)\frac{\partial^3}{\partial x \partial y^2} + S'_{15}\frac{\partial^3}{\partial y^3} \tag{A-6}$$
$$L_2 = S'_{55}\frac{\partial^2}{\partial x^2} - 2S'_{45}\frac{\partial^2}{\partial x \partial y} + S'_{44}\frac{\partial^2}{\partial y^2}$$

Through equation (A-5) we can eliminate one of the stress functions, F for example, and it can be shown that

$$\left(L_4 L_2 - L_3^{\,2}\right)U = 0 \tag{A-7}$$

We note that the stress functions are in terms of the x and y coordinates and the $\left(L_4 L_2 - L_3^{\,2}\right)U$ operator is of order of order six. The solution to this problem will use a composite variable, z such that

$$U(x, y) = F(z) \tag{A-8}$$

$$z = x + \mu y \tag{A-9}$$

Before moving on with this discussion, let us define the term ‘characteristic equation’ with a simple example. Consider, for a moment, a linear second order homogeneous equation such as

$$y''+ay'+by=0 \tag{A-10}$$

where a and b are constants, one method (Kreyszig, 1962) used to solve this type of differential equation is to assume the solution takes the form

$$y=e^{\lambda x} \tag{A-11}$$

with first and second derivatives

$$y'=\lambda e^{\lambda x} \qquad y''=\lambda^2 e^{\lambda x} \tag{A-12}$$

If we substitute the derivates into equations (A-12) we get

$$\lambda^2+a\lambda+b=0 \tag{A-13}$$

This equation is called the characteristic, or auxiliary, equation whose solution is readily determined by the quadratic formula. Here well will obtain two roots that can be real and distinct, complex conjugates, or double real. The above procedure is not just valid for second order linear differential equations, but can be applied to another equation of order n.

Continuing on, we now substitute (A-8) into (A-7) which results in

$$l_2(\mu)l_4(\mu)-l_3^{\,2}(\mu) \tag{A-14}$$

where

$$\begin{aligned} l_2(\mu) &= S'_{55}\,\mu^2 = 2S'_{45}\,\mu + S'_{45} \\ l_3(\mu) &= S'_{15}\,\mu^3 - \left(S'_{14}+S'_{56}\right)\mu^2 \left(S'_{25}+S'_{46}\right)\mu - S'_{24} \\ l_4(\mu) &= S'_{11}\,\mu^4 - 2S'_{16}\,\mu^3 + \left(2S'_{12}+S'_{66}\right)\mu^2 - 2S'_{26}\,\mu + S'_{22} \end{aligned} \tag{A-15}$$

The coefficients in (A-14) are real and the corresponding roots are going to be complex and occur in conjugate pairs. The general case of the plane problem makes no assumptions that decouple the out-of-plane and in-plane displacements. This decoupling can take place, depending on the type of material one is analyzing. Sih et al consider monoclinic materials. In this special case, Cherepanov derives an alternate solution where a fourth order characteristic equation is developed

$$S'_{11}\,\mu^4 + 2S'_{13}\,\mu^3 + \left(2S'_{12} + S'_{33}\right)\mu^2 - 2S'_{23}\,\mu + S'_{22} = 0 \tag{A-16}$$

$$S'_{55}\,\mu^2 + 2S'_{45}\,\mu + S'_{44} = 0 \tag{A-17}$$

The roots μ_1, μ_2 and their conjugates are determined from the first equation and μ_3 and it's conjugate is obtained by the latter. Finally, the near-tip solution for such a material is

$$\begin{Bmatrix} \sigma_{xx} \\ \sigma_{yy} \\ \sigma_{xy} \\ \sigma_{zx} \\ \sigma_{yz} \end{Bmatrix} = \frac{1}{\sqrt{2\pi r}} \begin{Bmatrix} KI\,\mathrm{Re}\left[\left(\frac{\mu_1\mu_2}{\mu_1-\mu_2}\right)\left(\frac{\mu_2}{Q_2}-\frac{\mu_1}{Q_1}\right)\right] + KII\,\mathrm{Re}\left[\left(\frac{1}{\mu_1-\mu_2}\right)\left(\frac{\mu_2^2}{Q_2}-\frac{\mu_1^2}{Q_1}\right)\right] \\ KI\,\mathrm{Re}\left[\left(\frac{1}{\mu_1-\mu_2}\right)\left(\frac{\mu_1}{Q_2}-\frac{\mu_2}{Q_1}\right)\right] + KII\,\mathrm{Re}\left[\left(\frac{1}{\mu_1-\mu_2}\right)\left(\frac{1}{Q_2}-\frac{1}{Q_1}\right)\right] \\ KI\,\mathrm{Re}\left[\left(\frac{\mu_1\mu_2}{\mu_1-\mu_2}\right)\left(\frac{1}{Q_1}-\frac{1}{Q_2}\right)\right] + KII\,\mathrm{Re}\left[\left(\frac{1}{\mu_1-\mu_2}\right)\left(\frac{\mu_1}{Q_1}-\frac{\mu_2}{Q_2}\right)\right] \\ -KIII\,\mathrm{Re}\left[\frac{\mu_3}{Q_3}\right] \\ KIII\,\mathrm{Re}\left[\frac{1}{Q_3}\right] \end{Bmatrix} \tag{A-18}$$

$$\sigma_{zz} = -\left(S_{31}\sigma_{xx} + S_{32}\sigma_{yy} + S_{36}\sigma_{xy}\right)\Big/ A_{33} \tag{A-19}$$

$$p_j = S'_{11}\,\mu_j^2 - S'_{16}\,\mu_j + S'_{12} \tag{A-20}$$

$$q_j = S'_{12}\,\mu_j - S'_{26} + S'_{22}\big/\mu_j \tag{A-21}$$

$$Q_i = \sqrt{\cos\omega + \mu_i \sin\omega} \tag{A-22}$$

$$\begin{Bmatrix} u_1 \\ u_2 \\ u_3 \end{Bmatrix} = \sqrt{\frac{2r}{\pi}} \begin{Bmatrix} KI\,\mathrm{Re}\left[\left(\frac{1}{\mu_1-\mu_2}\right)\left(\mu_1 p_2 Q_2 - \mu_2 p_1 Q_1\right)\right] + KII\,\mathrm{Re}\left[\left(\frac{1}{\mu_1-\mu_2}\right)\left(p_2 Q_2 - p_1 Q_1\right)\right] \\ KI\,\mathrm{Re}\left[\left(\frac{1}{\mu_1-\mu_2}\right)\left(\mu_1 q_2 Q_2 - \mu_2 q_1 Q_1\right)\right] + KII\,\mathrm{Re}\left[\left(\frac{1}{\mu_1-\mu_2}\right)\left(q_2 Q_2 - q_1 Q_1\right)\right] \\ KIII\,\mathrm{Re}\left[\frac{Q_3}{C_{45}+\mu_3 C_{44}}\right] \end{Bmatrix} \tag{A-23}$$

where C_{45} and C_{44} are the elastic constants in stiffness form

$$\sigma = C\varepsilon \tag{A-24}$$

where

$$C_{ij} = S_{ij}^{-1} \tag{A-25}$$

LIST OF REFERENCES

Aliabadi and Rooke D.P. *Numerical Fracture Mechanics*, Boston: Computational Mechanics Publications, 1991, pp. 45.

Anderson T.L. *Fracture Mechanics*, Boca Raton, FL: CRC Press, 1991, pp. 70, 120-121, 430-431.

ANSYS Elements Reference, ANSYS Release 5.6; ANSYS, Inc. November 1999.

Banks-Sills L., Hershkovitz I., Wawrzynek P., Eliasi R., and Ingraffea T., "Methods for Calculating Stress Intensity Factors in Anisotropic Materials: Part 1-Z = 0 is a Symmetric Plane," Engineering Fracture Mechanics, 2005, Vol. 72, pp. 2328-2358.

Barnett D.M., and Asaro R.J., "The Fracture Mechanics of Slit-Like Cracks in Anisotropic Elastic Media," Journal of the Mechanics and Physics of Solids, 1972, Vol. 20, pp. 353-366.

Barsom, and Rolfe S. *Fracture and Fatigue Control in Structures: Applications of Fracture Mechanics*, Woburn, MA: Butterworth-Heinemann, 1999, pp. 55, 77, 80-81.

Barsoum R.S., "On the Use of Isoparametric Finite Elements in Linear Fracture Mechanics," International Journal for Numerical Methods in Engineering, 1976, Vol. 10, pp. 25-37.

Bowie O.L., and Freese C.E., "Central Crack in Plane Orthotropic Rectangular Sheet," Engineering Fracture Mechanics, 1972, Vol. 8, pp. 49-58.

Bogy D.B., "The Plane Solution for Anisotropic Elastic Wedges Under Normal and Shear Traction," Journal of Applied Mechanics, 1972,Vol. 39, pp. 1103-1109.

Boone T.J., Wawrzynek P.A., and Ingraffea A.R., "Finite Element Modeling of Fracture Propagation in Orthotropic Materials," Engineering Fracture Mechanics, 1987, Vol. 26, pp. 185-201.

Boresi A.P., Schmidt R.J., Sidebottom O.M. *Advanced Mechanics of Materials*, New York: John Wiley and Sons, Inc., 1993, pp. 36.

Brezny R., and Green D.J., "Factors Controlling Fracture Resistance of Brittle Cellular Materials," Journal of the American Ceramics Society, 1991, Vol. 78, 1061-1065.

Buczek M.B., and Herakovich C.T., "A Normal Stress Criterion for Crack Extension Direction in Orthotropic Composite Materials," Journal of Composite Materials, 1985, Vol. 19, pp. 544-553.

Carloni C., Piva A., and Viola E., "An Alternative Complex Variable Formulation for an Inclined Crack in an Orthotropic Medium," Engineering Fracture Mechanics, 2003, Vol. 70, pp. 2033-2058.

Chan S.K., Tuba I.S., and Wilson W.K., "On the Finite Element Method in Linear Fracture Mechanics," Engineering Fracture Mechanics, 1970, Vol. 2, pp. 1-17.

Cherepanov G.P. *Mechanics of Brittle Fracture*, New York: McGraw-Hill, 1979, pp. 71-78.

Chen C.S., "Crack Growth Simulation and Residual Strength Prediction in Thin Shell Structures," Ph. D Thesis, Cornell University, 1999.

Dhondt G., "Mixed-Mode K-Calculations for Anisotropic Materials," Engineering Fracture Mechanics, 2002, Vol. 69, pp. 909-922.

Dieter G.E. *Mechanical Metallurgy*, New York: McGraw-Hill Inc., 1976, pp. 55-64.

Erdogan F., and Sih G.C., "On the Extension of Plates Under Plane Loading and Transverse shear," Journal of Basic Engineering, 1963, Vol. 85, pp. 519-527.

Fowlkes C.W., "Fracture Toughness Tests of a Rigid Polyurethane Foam," International Journal of Fracture, 1974, Vol. 10, pp. 99-108.

Freund L.B., "Stress Intensity Factor Calculations Based on a Conservation Integral," International Journal of Solids and Structures 1978, Vol. 14, pp. 241-250.

Gent A.N., and Thomas A.G., "The Deformation of Foamed Elastic Materials," Journal of Applied Polymer Science, 1959, Vol. 1, pp. 107-113.

Gent A.N., and Thomas A.G., "Mechanics of Foamed Elastic Materials," Rubber and Chemistry, 1963, Vol. 36, pp. 597-610.

Gibson L.J., and Ashby M., "The Mechanics of Three-Dimensional Cellular Solids," Philosophical Transactions of the Royal Society A: Mathematical, Physical and Engineering Sciences, 1982, Vol. A 382, pp. 43-59.

Gibson L.J., and Ashby, M. *Cellular Solids*, Elmsford, NY: Pergamon Press Inc., 1988, pp. 76-81, 241-256.

Gdoutos E.E. *Problems of Mixed Mode Crack Propagation*, The Hague, The Netherlands: Martinus Nijhoff Publishers, 1984, pp. 2.

Hoenig A., "Near Tip Behaviour of a Crack in a Plane Anisotropic Elastic Body," Engineering Fracture Mechanics, 1982, Vol. 16, pp. 393-403.

Huang J.S., and Gibson L.J., "Fracture Toughness of Brittle Honeycombs," Acta Metallurgica Materialia, 1991, Vol. 39, pp. 1617-1626.

Hussain M.A., Pu S.L., and Underwood J.H., "Strain Energy Release Rate for a Crack Under Combined Mode I and Mode II," Fracture Analysis ASTM STP, 1974, Vol. 560, pp. 2-28.

Hyer M.W. *Stress Analysis of Fiber-Reinforced Composite Materials*, New York: McGraw-Hill Inc., 1998, pp. 69-75.

Ingraffea A.R., and Manu C., "Stress Intensity Factor Computation in Three Dimensions with Quarter-Point Elements," International Journal for Numerical Methods in Engineering, 1980, Vol. 15, 1427-1445.

Irwin G.R., "Analysis of Stresses and Strains near the End of a Crack Traversing a Plate," Journal of Applied Mechanics, 1957, Vol. 24, pp. 361-364.

Irwin G.R., "Fracture Mechanics," In: Goodier J.N., and Hoff N.J., (editors), *Structural Mechanics*: *Proceedings of First Naval Symposium*, Pergamon Press, 1960, pp.557.

Ishikawa H., "A Finite Element Analysis of Stress Intensity Factors for Combined Tensile and Shear Loading by Only a Virtual Crack Extension," International Journal of Fracture, 1980, Vol. 16, pp. 243-246.

Ko W.L., "Deformations of Foamed Elastomers," Journal of Cellular Plastics, 1965, Vol.1, pp. 45-50.

Kuo M.G., and Bogy D.B., "Plane Solutions for the Displacement and Traction-Displacement Problem for Anisotropic Elastic Wedges," Journal of Applied Mechanics, 1974, Vol. 41, pp. 197-203.

Kreyszig E. *Advanced Engineering Mathematics*, New York: John Wiley and Sons Inc., 1962, pp. 105-105, 136.

Lekhnitskii S.G. *Theory of Elasticity of an Anisotropic Body*, San Francisco: Holden-Day, Inc., 1963, pp. 3, 104-110, 117-119, 122-123.

Li F.Z., Shih C.F., and Needleman A., "A Comparison of Methods for Calculating Energy Release Rates," Engineering Fracture Mechanics, 1985, Vol. 21, pp. 405-421.

Logan D.L. *A First Course in the Finite Element Method*, Pacific Grove, CA: Wadsworth Group, 2002, pp. 413-414, 433-434.

Maccagno T.M., and Knott J.F., "The Fracture Behaviour of PMMA in Mixed Modes I and II," Engineering Fracture Mechanics, 1989, Vol. 34, pp. 65-86.

Maccagno, T.M., and Knott J.F, "The Low Temperature Brittle Fracture Behaviour of Steel in Mixed Modes I and II," Engineering Fracture Mechanics, 1992, Vol. 38, pp. 111-128.

Maiti, S.K., Ashby M.F., and Gibson L.J., "Fracture Toughness of Brittle Cellular Solids," Scripta Mettalurgica, 1984, Vol. 18, pp. 213-217.

Man K.W., Aliabadi M.H., and Rooke D.P., "BEM Frictional Contact Analysis: Modeling Considerations," Engineering Analysis with Boundary Elements, 1993, Vol. 11, pp. 77-85.

McIntyre A., and Anderton G.E., "Fracture Properties of a Rigid Polyurethane Foam Over a Range of Densities," Polymer, 1979, Vol. 20, pp. 247-253.

Moran B., and Shih C.F., "A General Treatment of Crack-Tip Contour Integrals," International Journal of Fracture, 1987, Vol. 35, pp. 295-310.

Morgan J.S., Wood J.L., and Bradt R.C., "Cell Size Effects on the Strength of Foamed Glass," Materials Science and Engineering, 1981, Vol. 47, pp. 37-42.

Nobile L., and Carloni C., "Fracture Analysis for Orthotropic Cracked Plates," Journal of Composite Structures, 2005, Vol. 68, pp. 285-293.

Patel M.R., and Finnie I., "Structural Features and Mechanical Properties of Rigid Cellular Plastics," Journal of Materials, 1970, Vol.5, pp. 909-932.

Pettit R., "Crack Turning and Arrest in Integrally Stiffened Aircraft Structures," Ph. D Thesis, Cornell University, 2000.

Rice J.R., "A Path Independent Integral and the Approximate Analysis of Strain Concentration by Notches and Cracks," Journal of Applied Mechanics, 1968, Vol. 35, pp. 379-386.

Rathod H.T., "A Study of Asymmetrically Loaded Griffith Crack in a Plane Anisotropic Elastic Body," Engineering Fracture Mechanics, 1979, Vol. 11, pp. 87-93.

Saouma V.E., and Sikiotis E.S., "Stress Intensity Factors in Anisotropic Bodies Using Singular Isoparametric Elements," Engineering Fracture Mechanics, 1986, Vol. 25, 00. 115-121.

Sih G.C., Paris P.C., and Irwin G.R., "On Cracks in Rectilinearly Anisotropic Bodies," Engineering Fracture Mechanics, 1965, Vo1. 1, pp. 189-203.

Sih G.C., "Strain Energy Density Factor Applied to Mixed Mode Crack Problems," International Journal of Fracture, 1974, Vol. 10, pp. 305-321.

Sneddon IN., "The Distribution of Stress in the Neighbourhood of a Crack in an Elastic Solid," Proceedings, Royal Society of London, 1946, Vol. A-187, pp. 229-260.

Tada, H., Paris, P., and Irwin, G. *The Stress Analysis of Cracks Handbook*, Hellerton, PA: Del Research Corp., 1973.

Ting T.C. *Anisotropic Elasticity: Theory and Applications*, Oxford: Oxford University Press, 1996, pp. 54-55, 118-133.

Timoshenko S.P., and Goodier J.N. *Theory of Elasticity*, Tokyo: McGraw-Hill, 1982, pp. 354-380.

Tupholme G.E., "A Study of Cracks in Orthotropic Crystals Using Dislocation Layers," Journal of Engineering Mathematics, 1974, Vol. 8, pp. 57-69.

Wells A., "Unstable Crack Propagation in Metals-Cleavage and Fracture," Cranfield Crack Propagation Symposium, 1961, Vol. 1, pp. 210.

Westergaard H.M., "Bearing Pressures on Cracks," Journal of Applied Mechancis, 1939, Vol. 6, pp. 49-53.

Williams M.L., "On the Stress Distribution at the Base of a Stationary Crack," Journal of Applied Mechanics, 1957, Vol. 24, pp. 109-114.

Yau J.F., Wang S.S., and Corten H.T., "A Mixed-Mode Crack Analysis of Isotropic Solids Using Conservation Laws of Elasticity," Transactions of the ASME, 1980, Vol. 47, pp. 335-341.

BIOGRAPHICAL SKETCH

Erik Knudsen was born in West Chester, PA, on February 18th, 1979. At the age of four his family moved to Naples, FL, where he spent the remainder of his childhood and graduated from Lely High School in 1997. He earned a B.S. in mechanical engineering from Villanova in the Spring of 2001 and returned to Florida for his graduate work. Under the tutelage of Dr. Nagaraj Arakere he earned a M.S. in mechanical engineering in the Fall of 2003 working on a NASA related project. Upon completion of the doctorate from the University of Florida, he would like to become a full-time teacher at the college level or perhaps retain a position in the aerospace industry.